KfK 2868
Oktober 1979

Annual Report

Teilinstitut Kernphysik des Instituts für Angewandte Kernphysik (July 1, 1978 - June 30, 1979)

Editors:
W. Kneis, G. Nowicki
Institut für Angewandte Kernphysik

Kernforschungszentrum Karlsruhe

KERNFORSCHUNGSZENTRUM KARLSRUHE

Institut für Angewandte Kernphysik

KfK 2868

ANNUAL REPORT

Teilinstitut Kernphysik

des Instituts für Angewandte Kernphysik

(July 1, 1978 - June 30, 1979)

Editors: W. Kneis and G. Nowicki

Kernforschungszentrum Karlsruhe GmbH, Karlsruhe

Als Manuskript vervielfältigt

Kernforschungszentrum Karlsruhe GmbH
ISSN 0303-4003
ISSN 0341-7611

Abstract

The activities of the Nuclear Physics Section of the Institute of Applied Nuclear Physics from mid 1978 to mid 1979 are surveyed. The research program comprises both contributions to fundamental and applied nuclear research. The activities on the application of nuclear methods mainly concentrate on the measurements of cross sections of neutron-induced nuclear reactions for the fast breeder project, the application of gamma-ray spectrometry to nuclear fuel assay problems, the development of a proton microbeam for elemental analysis, and the production of radioisotopes for medical application. The study of nuclear reactions induced by alpha particles, ^{6}Li ions and fast neutrons, and the measurement of optical hyperfine structure using high-resolution laser spectroscopy form the major part of the fundamental research work. In addition, the operation of the Karlsruhe Isochronous Cyclotron is briefly reviewed.

Zusammenfassung

Es wird über die Tätigkeit des Teilinstituts Kernphysik des Instituts für Angewandte Kernphysik von Mitte 1978 bis Mitte 1979 berichtet. Das Forschungsprogramm beinhaltet sowohl Anwendungen der Kernphysik auf Probleme der Kernenergie als auch grundlagenphysikalische Arbeiten. Schwerpunkte der angewandten Arbeiten bilden die Messungen von Neutronenwirkungsquerschnitten für das Projekt Schneller Brüter, die Anwendung gammaspektrometrischer Meßverfahren zur Spaltstoffbestimmung, die Entwicklung einer Protonenmikrosonde für die Elementanalyse sowie die Erzeugung von Radioisotopen für medizinische Anwendungen. Zu den grundlagenphysikalischen Arbeiten gehören Untersuchungen von Kernreaktionen mit Alpha-Teilchen, ^{6}Li-Ionen und schnellen Neutronen sowie die Messung der optischen Hyperfeinstruktur mittels hochauflösender Laserspektroskopie. Ferner wird der Betrieb des Karlsruher Isochronzyklotrons kurz geschildert.

The Institute of Applied Nuclear Physics of the Karlsruhe Nuclear Research Centre is engaged in research in fundamental nuclear physics and its applications to problems of nuclear energy, solid state physics, medicine, and analysis. This report gives a survey of the work of the Nuclear Physics Section from mid 1978 to mid 1979. Progress of the Nuclear Solid State Section is reported separately.

One of the main fields of research is the measurement of cross sections of nuclear reactions induced by neutrons. This work aims partly at providing data required for the design of fast breeder reactors and, on the other hand, at determining cross sections necessary for a detailed understanding of the astrophysical processes that led to the production of heavy elements in universe. In the latter field, first results on the keV neutron capture cross sections of krypton isotopes have been obtained, to the best of our knowledge the first measurements of this kind on noble gases. A second group of experiments aims at determining the neutron capture cross section of nuclei near ^{176}Lu. These data should allow an estimate of the time elapsed since the synthesis of the heavy elements in the solar system by the so-called s-process.

One of the main objects of the study of nuclear reactions at the Karlsruhe Isochronous Cyclotron continues to be the determination of the mass (i.e. neutron) distribution of nuclei. This problem was also discussed at a workshop held at the Karlsruhe Nuclear Research Centre at the beginning of May. About 50 participants from 10 different countries gathered in order to critically compare the different methods of measuring nuclear radii.

The application of gamma ray spectroscopy to problems of the nuclear fuel cycle represents another main field of research. The aim of these efforts is to develop methods and instruments for automatically measuring amount, concentration, and composition of nuclear fuel. This demands for a precision and reliability considerably higher than required for pure nuclear physics investigations.

The institute operates two accelerators. A 3.7 MV single stage Van de Graaff is primarily used for neutron time-of-flight experiments and solid state physics. The Karlsruhe Isochronous Cyclotron, a fixed frequency machine, provides beams of protons, deuterons, alpha particles, and ^{6}Li ions at 26 MeV/nucleon. In order to extend the range of particles to higher masses we decided in 1978 to build an electron cyclotron resonance ion source. This consists of a magnetic mirror system, as has been studied in plasma physics for quite some time, in which electrons are heated by microwaves. As had been shown by a French group this source should be able to provide completely stripped ions of the light elements up to oxygen or possibly neon. These ions then can be accelerated by our cyclotron. Work on this source proceeded in a very promising way so far and found strong interest with other German and foreign groups. We hope to be able to install this source at the cyclotron not later than 1981.

Gerd Schatz

Das Institut für Angewandte Kernphysik des Kernforschungszentrums Karlsruhe beschäftigt sich zu etwa gleichen Teilen mit Grundlagenuntersuchungen zur Kernphysik und ihrer Anwendung auf Probleme der Kernenergie, Festkörperphysik, Medizin und Analyse. Der vorliegende Bericht gibt einen Überblick über die Tätigkeit des Teilinstituts Kernphysik von Mitte 1978 bis Mitte 1979. Über die Tätigkeit des Teilinstituts Nukleare Festkörperphysik wird getrennt berichtet.

Einen Schwerpunkt der Arbeiten des Instituts bildet die Messung von Wirkungsquerschnitten neutroneninduzierter Kernreaktionen. Diese dienen einerseits der Gewinnung von Daten, die für die Auslegung schneller Brutreaktoren benötigt werden. Andererseits zielt ein Teil der Arbeiten auf Wirkungsquerschnitte, die zum detaillierten Verständnis der Prozesse erforderlich sind, die zur Synthese schwerer Elemente im Weltall führen. Hierzu liegen jetzt erste Ergebnisse über die Neutroneneinfangquerschnitte von Krypton-Isotopen im keV-Bereich vor - unseres Wissens die ersten Messungen dieser Art an Edelgasen überhaupt. Eine zweite Gruppe von Experimenten hat das Ziel, die Neutroneneinfangquerschnitte von Nukliden in der Nähe des Kerns ^{176}Lu zu bestimmen. Mit diesen Daten sollte es möglich sein, die Zeit abzuschätzen, die seit der Entstehung der schweren Elemente im Sonnensystem im sog. s-Prozeß vergangen ist.

Bei den Untersuchungen von Kernreaktionen am Karlsruher Isochronzyklotron war die Bestimmung der Massen-, d.h. der Neutronenverteilung, in Atomkernen weiterhin eine wichtige Fragestellung. Dieses Problem wurde hier im Kernforschungszentrum in einem dreitägigen Workshop Anfang Mai diskutiert, an dem etwa 50 auswärtige Gäste aus zehn Ländern teilnahmen. Hierbei wurden die verschiedenen Methoden der Kernradienbestimmung am Beispiel der Ca-Isotope vergleichend diskutiert.
Die Anwendung der Gamma-Spektroskopie auf Probleme des Kernbrennstoffzyklus stellt ein weiteres wichtiges Arbeitsgebiet des Instituts dar. Ziel dieser Arbeiten ist die Entwicklung von Methoden und Geräten zur automatischen Messung der Menge, Konzentration und Zusammensetzung von Kernbrennstoffen. Dabei

werden an die Genauigkeit und Zuverlässigkeit der Messung Anforderungen gestellt, die weit über das bei kernphysikalischen Untersuchungen übliche hinausgehen.

Dem Institut stehen für seine Arbeiten zwei Beschleuniger zur Verfügung. Ein einstufiger van-de-Graaff-Beschleuniger von 3,7 MV wird hauptsächlich für Neutronenflugzeit-Experimente und für die Festkörperphysik benutzt. Das Isochronzyklotron Karlsruhe, ein Festfrequenz-Zyklotron, liefert Strahlen von Protonen, Deuteronen, Alphateilchen und ^{6}-Li-Ionen von 26 MeV/Nukleon. Um den Bereich dieser Teilchen zu höheren Massen auszudehnen, wurde Mitte 1978 beschlossen, eine Ionenquelle nach dem Prinzip der Elektronenzyklotronresonanz zu bauen. Diese besteht aus einem magnetischen Spiegelfeld, wie es in der Plasmaphysik seit längerem benutzt wird, in dem Elektronen durch Mikrowellen aufgeheizt werden. Arbeiten einer französischen Gruppe hatten gezeigt, daß man auf diese Weise die leichten Elemente bis zum Sauerstoff und evtl. Neon vollständig ionisieren kann. In dieser Form wären die Ionen für die Beschleunigung in unserem Zyklotron geeignet. Die Arbeiten an dieser Quelle verliefen bisher sehr erfolgversprechend und haben auch international starke Resonanz gefunden. Wir hoffen, diese Quelle spätestens 1981 am Zyklotron einsetzen zu können.

Gerd Schatz

CONTENTS

Page

1. NEUTRON PHYSICS

1.1 FUNDAMENTAL RESEARCH

1.1.1 The Capture Cross Section of ^{58}Fe between 5 and 400 keV Neutron Energy

F. Käppeler, L.D. Hong

In the preceding progress report (1) we described the first measurement of the capture cross section of ^{58}Fe in the neutron energy range from 10 to 200 keV. However, the results showed rather large statistical uncertainties and therefore the measurement was repeated with an improved experimental setup. Instead of the 800 l liquid scintillator tank a C_6D_6-detector was used (see also ref. (2) and contribution 1.1.2 of this report). The main advantage was that with this fast detector system the same time resolution of 1.5 ns/m could be obtained at a three times shorter flight path of 60 cm and therefore the sensitivity was considerably better. Moreover, for the second measurement a sample with a higher enrichment of 73 % was made available by the US loan pool. As a result, we were able to extend the investigated neutron energy range to the region between 5 and 400 keV and to accumulate data with good statistical accuracy.

As this measurement on ^{58}Fe was the first one we performed with the C_6D_6-detector system, a variety of different runs were made with different samples and different neutron spectra in order to investigate carefully the background problems, especially in view of the neutron sensitivity of this detector.

It turned out that we could benefit from the same effect of discriminating prompt capture gamma rays and scattered neutrons by their respective time-of-flight from the sample to the detector, as is described in contribution 1.2.4 of this report. Although the ratio of the distance sample-detector versus primary neutron flight path was only 0.25 instead of 2, it was still sufficient to avoid background from scattered neutrons for almost all capture resonances in ^{58}Fe.

The data analysis is not yet completed but the preliminary evaluation of single runs shows that even for the lowest neutron energies, the background was sufficiently small to allow for a proper resonance analysis. Fig. 1 shows part of the cross section which is not yet corrected for multiple scattering and self-shielding effects. In this energy range three

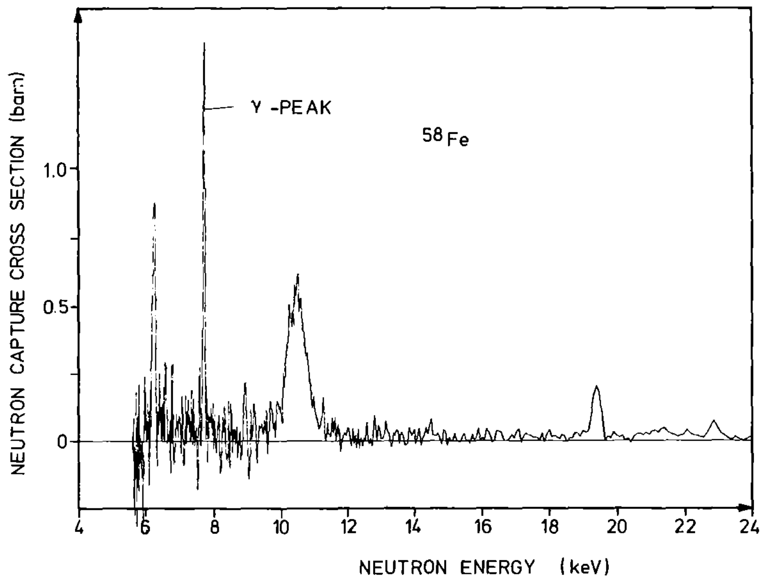

Fig. 1
Preliminary capture cross section of ^{58}Fe for a single run without corrections for multiple scattering and self-shielding effects. It demonstrates that the data allow for a reasonable resonance analysis even in the low energy range.

resonances of ^{58}Fe can be identified. That means that the assignment of a resonance with $\ell > 0$ at 18.7 keV in the first measurement was erroneous. The position of the s-wave resonance at 10.34 keV confirms the resonance energy determined in our total cross-section measurement (3) rather than the respective value of Garg et al. (4).

References

(1) L.D. Hong, H. Beer, F. Käppeler, KfK-Report 2686 (1978) 13.
(2) B. Leugers, KfK-Report 2686 (1978) 15.
(3) L.D. Hong, H. Beer, F. Käppeler, Nucl. Sci. Eng. 67 (1978) 184.
(4) J.B. Garg, S.J. Jain, J.A. Harvey, Phys. Rev. C18 (1978) 1141.

1.1.2 The Neutron Capture Cross Sections of the Stable Kr Isotopes between 3 and 250 keV

B. Leugers, F. Käppeler

For the investigation of the Kr isotopes the first setup of the C_6D_6-detector system for neutron capture cross section measurements was improved in the following points (see also ref. (1)):

1) The neutron shielding around the target was optimized by increasing the ^{6}Li-carbonate liner in the collimator part and by introducing a thick shield of boron resin.
2) The lead shielding around the detector was machined carefully in order to provide a thickness of 20 cm at least in any direction. In addition "white" lead was used to avoid background from the activation of antimony.
3) Instead of liquified Kr samples, high pressure gas samples were designed. Steel spheres 2 cm in diameter and of 0.5 mm wall thickness are able to withstand pressures up to 500 bar. In this way the same amount of Krypton could be enclosed in less canning material as compared to liquified samples.

With this improved setup measurements were made on samples of natural Krypton, on isotopically pure ^{84}Kr and on three other samples enriched in ^{83}Kr, ^{82}Kr and ^{80} Kr. Fig. 1 shows the cross sections obtained for natural krypton and ^{84}Kr. The error bars on the data points represent the statistical uncertainty which varies smoothly from $\sim$ 20 % at 10 keV to 3 % at 200 keV neutron energy. The resolution in neutron energy is 1.5 ns/m. This corresponds to a resolution of 200 eV at 30 keV neutron energy. In all measurements ^{197}Au was used as a standard. The improvement achieved with the new technique can be seen from a comparison of the present data on natural krypton with the results of Ref. (2).

As the krypton isotopes are of considerable interest to the astrophysical nucleosynthesis (see contributions 1.1.3 and 1.1.4),the differential cross sections have been averaged over a Maxwellian energy distribution for a thermal energy of kT = 30 keV to obtain he effective cross section for that particular temperature of $\sim 3.5 \times 10^{8}$ K.

For the average values the statistical uncertainty can be neglected. Thus, only a systematic uncertainty of 3-5 % must be assigned to the average cross sections for each of the samples. These values together with the isotopic compositions define a system of linear equations which can be solved to derive the Maxwellian averages of all stable Kr isotopes. Although not all corrections are accounted for completely (e.g. multiple scattering), a current best set of average cross sections for kT = 30 keV is included in Table 1. For ^{78}Kr and ^{86}Kr, which are quoted in parenthesis, a larger uncertainty of about 30 % and 100 % respectively, must be admitted.

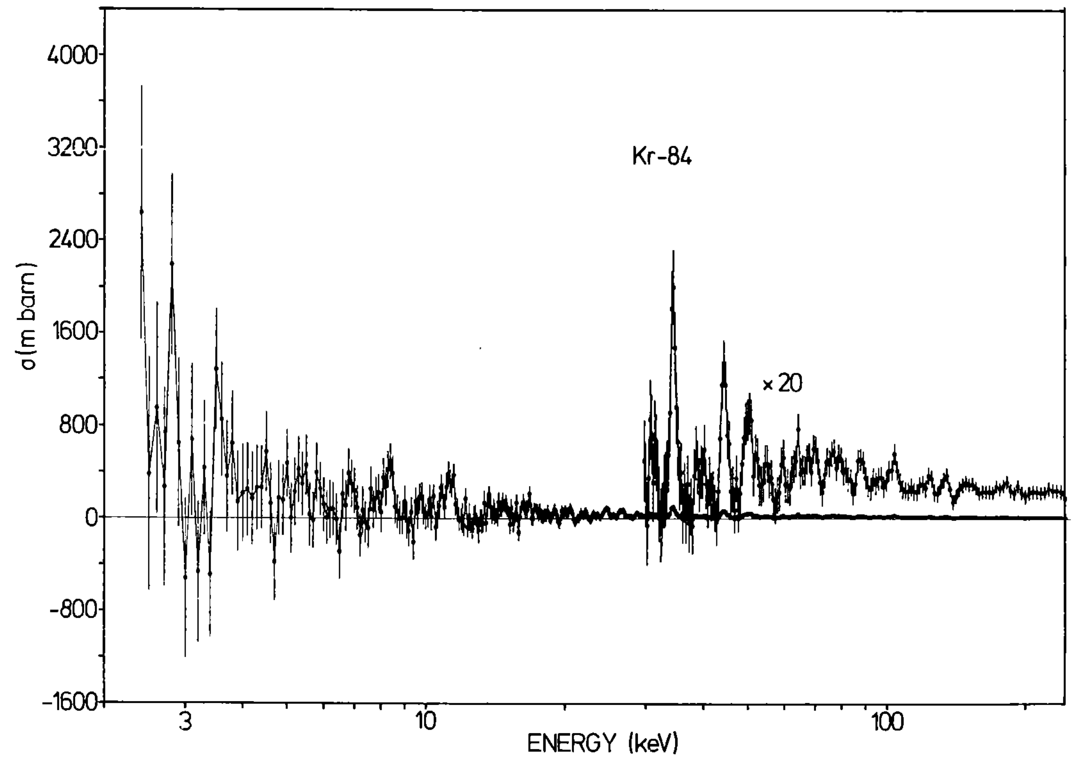

Fig. 1. The neutron capture cross section of ^{84}Kr between 3 and 250 keV

Table 1 Maxwellian averaged capture cross sections for the stable krypton isotopes (kT = 30 keV)

Isotope	78	80	82	83	84	86
<σ>(mb)	(450)	220	100	275	30	(∼1)

References

(1) B. Leugers, Report KfK 2686 (1978) 15.
(2) F. Hensley, F. Käppeler, KfK 2686 (1978) 14.

1.1.3 A Determination of the Solar Kr Abundance from s-Process Systematics

B. Leugers, F. Käppeler

In contribution 1.1.2 of this report we described the determination of Maxwellian averaged neutron capture cross sections of the stable Kr isotopes. The importance of krypton for the astrophysical s-process is based on the fact that ^{80}Kr and ^{82}Kr are of pure s-process origin because they are shielded against the r-process synthesis by their Se isobars. As can be seen from fig. 1, the synthesis path of the s-process recombines at ^{82}Kr after its split at ^{79}Se.

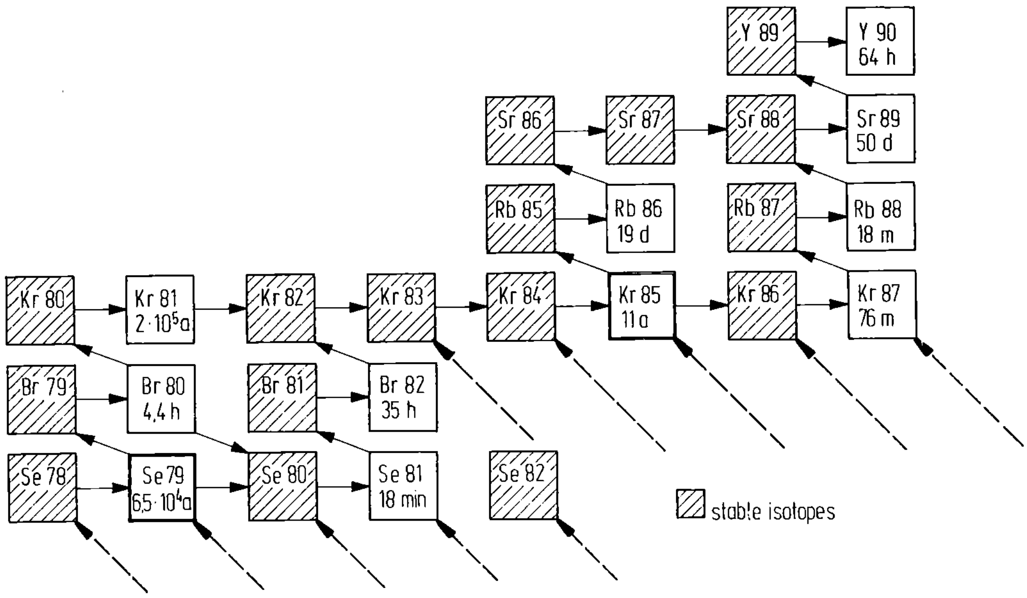

Fig. 1 The s-process path through the Se, Br, Kr-region (solid line). Possible r-process contributions are indicated by dashed arrows.

The s-process synthesis is characterized by the typical correlation between the isotopic abundances and the respective average neutron capture cross sections. This product N<σ> can be calculated as a function of mass number if the cross sections are known and if an assumption on the cosmic neutron flux distribution is accepted. Fig. 2 shows the calculated N<σ>-curve derived from an exponential flux distribution similar to the one reported by Ward and Newman (1).

The points in fig. 2 are the products of empirical solar abundances and average capture cross sections. Only the solid points which correspond to shielded s-process isotopes like ^{82}Kr are close to the calculated curve. The fact that the majority of isotopes show much larger values of N<σ> means that they were synthesized partly by other processes, e.g. by the e-process for A $\lesssim$ 65 and the r-process for higher mass numbers.

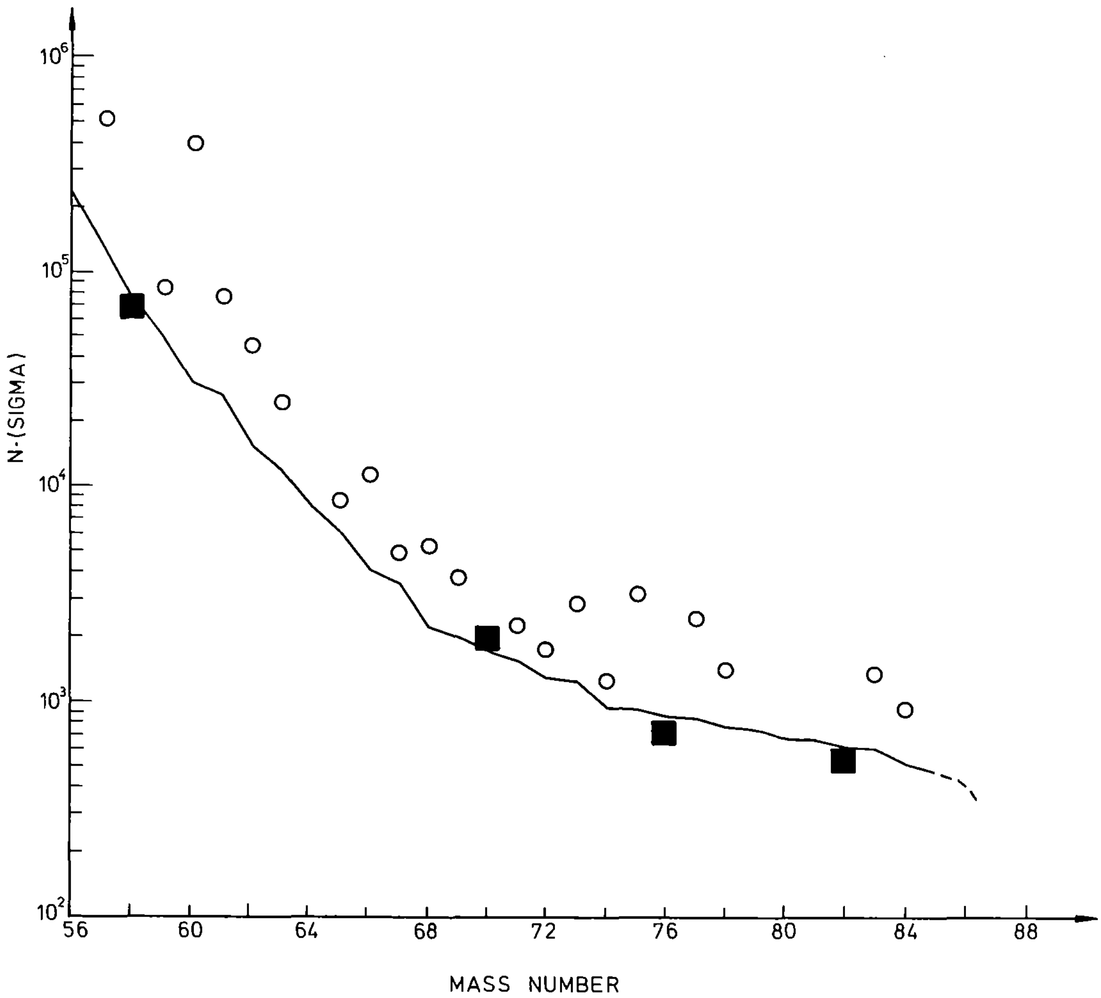

Fig. 2 The product of solar abundance times average capture cross section N<σ>, which is characteristic of the s-process synthesis.

From fig. 2 it is evident that accurate cross sections for the pure s-process isotopes are extremely important for the determination of the N<σ>-curve which in turn allows to derive e- and r-process abundances. For krypton, however, one deals with the problem that abundance determinations of noble gases are very difficult and show large systematic uncertainties because these elements are so volatile. In this case the N<σ>-systematics allow for an abundance determination from the calculated N<σ>-value for ^{82}Kr and the experimental average cross section.

As it was shown by H. Beer (2), the flux distribution used in fig. 2 reproduces also the N<σ>- values in the mass region up to A = 200 very precisely. Therefore the calculated value for ^{82}Kr should be accurate to 10 % at least. With an equal uncertainty from the preliminary capture cross section for ^{82}Kr ($\langle\sigma\rangle$ = 100 mb) we obtain the abundance of ^{82}Kr to 5.29 ± 15 % (Si = 10^6). This is close to the value of 5.41 reported by Cameron (3) which is the average of geometric interpolations between ^{80}Se, ^{84}Kr, ^{88}Sr and ^{81}Br, ^{83}Kr, ^{85}Rb. Earlier estimates of this type reported ^{82}Kr abundances of 7.43 (4) and 5.83 (5). With the final cross section the new abundance determination can certainly be given with an accuracy of 10 %. Then, it will be also of great interest to determine the r-process contributions of ^{83}Kr and ^{84}Kr.

References

(1) R.A. Ward, M.J. Newman, Report OAP-486 (1977)

(2) H. Beer, private communication.

(3) A.G.W. Cameron, in "Explosive Nucleosynthesis", p. 1, eds. D.N. Schramm, W.D. Arnett, Univ. of Texas Press, Austin and London (1973).

(4) A.G.W. Cameron in "Origin and Distribution of the Elements", p. 125, eds. L.H. Ahrens, Pergamon Press, New York (1968).

(5) H. Suess, H. Urey, Rev. Mod. Phys. 28 (1956) 53.

1.1.4 The s-Process Branch at ^{79}Se

B. Leugers, F. Käppeler, F. Fabbri⁺, and G. Reffo⁺

In fig. 1 of contribution 1.1.3 it was shown that there is a branch in the s-process path at ^{79}Se. This branch is of particular interest because the beta decay half life of ^{79}Se shows a strong temperature dependence. This is due to the fact that the beta decay probability is enhanced with increasing temperature by the population of excited states in ^{79}Se. For typical temperatures of the s-process environment the half life of ^{79}Se is short enough that neutron capture and beta decay proceed at comparable rates of $\sim \frac{1}{20}\, a^{-1}$. Thus, an analysis of this branch provides a possibility to determine the effective s-process temperature. This is illustrated in fig. 1 which shows the ^{79}Se half life as a function of

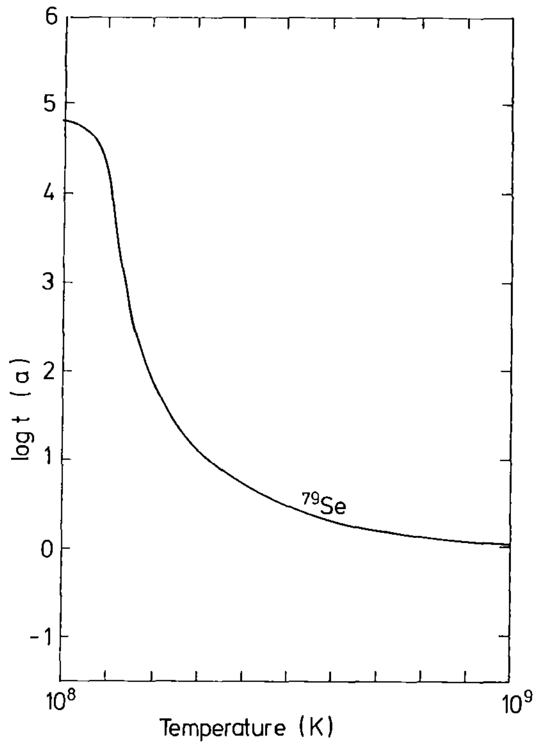

Fig. 1 The beta decay half life of ^{79}Se as a function of temperature as taken from ref. (1). The temperature is given in units of 10^8 K.

temperature (1).

Accepting the smoothness of the N<σ>-curve around ^{79}Se (see fig. 2 of contribution 1.1.3) the branching ratio

$$B_{ß-} = \frac{\lambda_{ß}^{-}}{\lambda_{ß}^{-}+\lambda_{n}} \tag{1}$$

can be determined via the N<σ>-values of ^{80}Kr and ^{82}Kr:

$$B_{ß}^{-} = |N\langle\sigma\rangle|^{80}Kr/|N\langle\sigma\rangle|^{82}Kr \tag{2}$$

One complication of the ^{79}Se branch comes from the decay of ^{80}Br. Whereas Conrad (2) estimates that at high temperature the strong ionization hampers electron capture (EC practically negligible), Ward et al. (1) obtained a drastic enhancement of the electron capture rate from continuum capture due to the high densities involved. From our analysis we find evidence that the second assumption is correct. Consequently, eqn. (2) has to be modified to correct for this additional branching at ^{80}Br.

Then the beta decay rate λ_{β^-} can be calculated from eqn. (1) if the neutron capture rate

$$\lambda_n = \Phi_n \langle\sigma\rangle_{^{79}Se}$$

is known. As at present no neutron capture cross section for the radioactive nucleus ^{79}Se is measured, extensive calculations of theoretical capture cross sections for a total of 13 s-process isotopes in the Se, Br, Kr-region were performed. Using the usual Hauser-Feshbach statistical model formalism including width fluctuation corrections (3,4,5,6) particular care was devoted to the determination of the relevant model parameters which critically determine the accuracy of the results (7), e.g. level densities and radioactive decay widths.

With the s-process neutron flux from ref. (1) $\phi_n = 3.8 \times 10^{15}\ cm^{-2}s^{-1}$ we finally obtain the beta decay rate for ^{79}Se

$$\lambda_{\beta^-} = 1.0 \times 10^{-9}\ s^{-1}$$

This leads to a beta decay half life of ^{79}Se under s-process conditions of $T^*_{1/2} = (22 \pm 7)$ a. The s-process temperature follows then from fig. 1:

$$T = (2.7\ ^{+0.3}_{-0.2}) \times 10^8\ K \text{ or } kT = (23\ ^{+2.2}_{-1.8})\ keV.$$

This result is somewhat lower compared to the value of 26 keV given in ref. (1) but one still has to keep in mind the preliminary nature of the experimental cross sections. In addition there are uncertainties associated with the neutron flux ϕ_n and with the effective decay scheme of ^{80}Br which are not included in the quoted errors. Nevertheless, the improved information on the involved capture cross section indicates a trend to a somewhat lower s-process temperature.

References

(1) R.A. Ward, M.J. Newman, D.D. Clayton, The Astrophysical Journal Supp. Series 31 (1976) 33.

(2) J.H. Conrad, thesis, Univ. of Heidelberg (1976).

(3) F. Fabbri, G. Reffo: CNEN Report RT/FI (74) 36.

(4) G. Gruppelaar, G. Reffo: Nucl. Sci. Eng. 62, 756 (1977).

(5) G. Reffo, F. Fabbri, H. Gruppelaar: Nuovo Cimento Letters 17, 1 (1976).

(6) G. Reffo, F. Fabbri: Nucl. Sci. Eng. 66, 251 (1978).

(7) G. Reffo: CNEN Report RT/FI (78) 11 (1978) and IAEA Winter Courses on Nuclear Physics and Reactors, Trieste (February 1978).

+Comitato Nazionale Energia Nucleare, Divisione Fisica, Bologna, Italy

1.1.5 The Neutron Capture Cross Section of Natural Xenon between 3 and 250 keV

B. Leugers

In addition to the measurements on different krypton isotopes (1.1.4) a measurement of the neutron capture cross section of natural Xenon was performed. As described in contribution 1.1.2, a high pressure gas target and the total energy detector method were employed in this measurement. The pulse height weighting technique in this case leads to a difficult problem, as the effective binding energy E_B of the isotopic mixture is required for the calculation of the cross section. This binding energy can be calculated as a weighted mean value by the equation

$$E_B = \frac{\sum_{i=1}^{n} \sigma_i H_i E_i}{\sum_{i=1}^{n} \sigma_i H_i} \qquad (1)$$

H_i: ance of isotope i

E_i: neutron binding energy for isotope i

Neglecting the energy dependence of the capture cross section σ_i the binding energy E_B was determined by using calculated values of σ_i for E_n = 30 keV (1). This approximation leads to a systematic error of ∿ 15 %. Preliminary results are given in fig. 1. From these data a

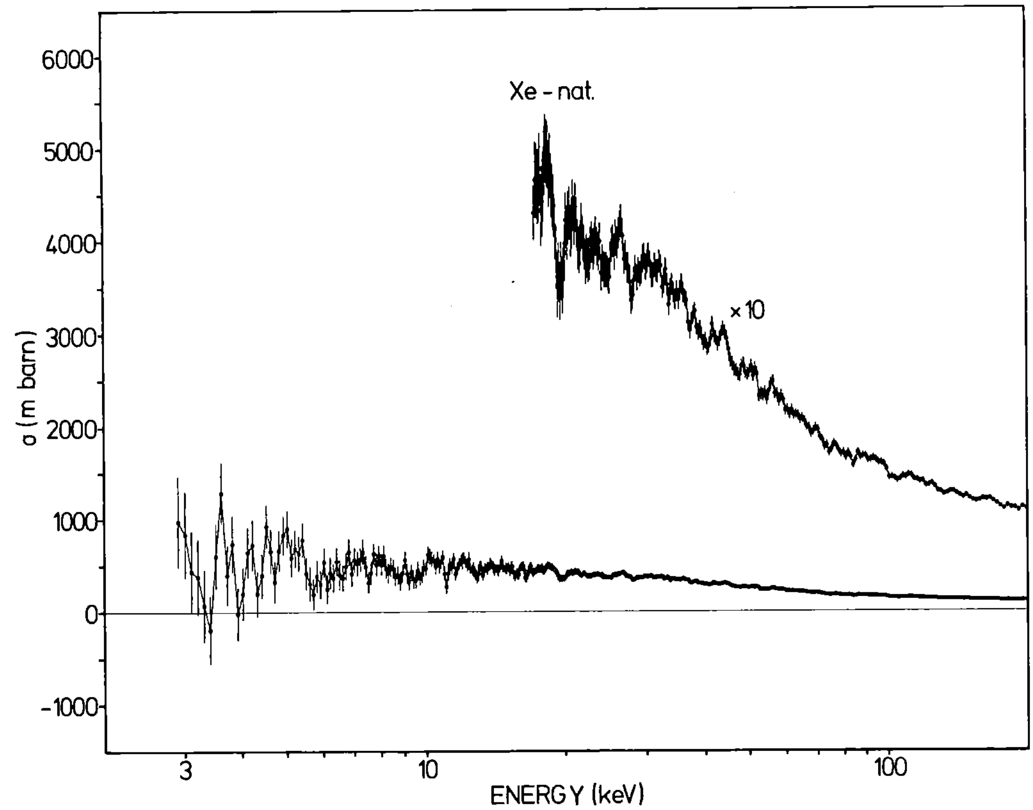

Fig. 1 The neutron capture cross section of natural xenon between 3 and 250 keV.

Maxwellian averaged cross section for kT = 30 keV was calculated to 330 ± 1.3 mb where the systematic uncertainties are not yet included.

In the measurement an additional time-of-flight spectrum of coincident events between the two C_6D_6-detectors was accumulated. By means of this spectrum it was possible to calculate the average multiplicity in the gamma-cascade after neutron capture. The average gamma-energy could be determined from the weighted analogue spectra of the C_6D_6-detectors. This leads to another method for the calculation of the capture cross section, without using the pulse height weighting technique. From this method the Maxwellian-averaged cross section was calculated to 336.3 ± 2.9 mb which agrees well with the first result within the systematic uncertainties.

1.1.6 Activation Measurements for the ^{176}Lu Cosmochronometer

H. Beer and F. Käppeler

^{176}Lu is the only nucleus of pure s-process origin which has a sufficiently long half life (3.3 x 10^{10} a) to allow for an age determination of the s-process elements. In theoretical studies of the ^{176}Lu cosmochronometer the importance of accurate experimental capture cross sections at thermal energies around kT = 20 to 30 keV has been emphasized (1,2,3). Especially the population of the 3.68 h isomeric state in ^{176}Lu via neutron capture in ^{175}Lu has to be determined. This is responsible for a branching of the s-process path which has to be corrected for.

In view of these requests neutron capture cross section measurements with the activation technique have been performed at our 3 MV Van de Graaff accelerator. The neutrons were generated via the ^{7}Li(p,n) reaction with proton energies close to the reaction threshold. This gives a neutron flux in forward direction which is similar to a Maxwellian distribution corresponding to a thermal energy around kT = 23 to 24 keV. During the activations the Van de Graaff accelerator was operated in the dc mode to obtain beam currents of 50 to 100 μA. The activation foil and a gold foil which served as a standard were placed in a back-to-back arrangement immediately at the neutron target. Throughout the irradiation the neutron flux was recorded continuously as a function of time by a ^{6}Li glass detector. After irradiation the activated foils were analyzed by a calibrated high resolution Ge(Li) detector.

In table 1 the results of the measurements are summarized. Except for ^{175}Lu(n,γ)^{176m}Lu where no information about the energy dependence was available, our results were extrapolated to kT = 30 keV using theoretical work (4). In the last column the cross sections from previous measurements are given. This comparison demonstrates that with our technique a considerable improvement in accuracy is achieved.

Table 1 The Maxwellian Averaged Capture Cross Sections

Reaction	Thermal Energy kT (keV)	$\frac{<\sigma v>}{v_T}$ (mb) present work	other work
$^{138}Ba(n,\gamma)^{139}Ba$	30	4.22 ± 0.25	8 ± 2[a] 11 ± 1.5[b] 5.7 ± 0.9[c] 3.9 ± 0.8[c]
$^{140}Ce(n,\gamma)^{141}Ce$	30	11.52 ± 0.57	23 ± 4[b] 3 ± 3[a] 7.7 ± 0.9[c]
$^{175}Lu(n,\gamma)^{176m}Lu$	24	906 ± 54	
$^{176}Lu(n,\gamma)^{177}Lu$	30	1718 ± 85	2250 ± 200[a]

[a]Ref. 5 [b]Ref. 6 [c]Ref. 7

References

(1) J. Audouze, W.A. Fowler, D.N. Schramm, Nature Physical Sci. 238, 8 (1972).

(2) M. Arnould, Astron. & Astrophys. 22, 311 (1973).

(3) R.A. Ward, M.J. Newman, Astrophys. J. 219, 195 (1978).

(4) V. Benzi, R. d'Orazi, G. Reffo, M. Vaccari, C.N.E.N.-Report RT/F1 (72) 6.

(5) B.J. Allen, J.H. Gibbons, R.L. Macklin, Adv. in Nucl. Phys., 4, 205 (1971).

(6) K. Siddappa, M.S. Murty, J. Rao, Nuovo Cimento 18A, 48 (1973).

(7) A.R. de L. Musgrove, B.J. Allen, J.W. Boldeman, Nucl. Phys. A252, 301 (1975) and private communication.

1.1.7 Neutron Capture Cross Sections of Natural Yb, ^{170}Yb, ^{175}Lu, and ^{184}W for the Investigation of the ^{176}Lu Cosmochronometer

H. Beer, K. Wisshak, F. Käppeler

For the calculation of the age of our chemical elements via the ^{176}Lu clock the capture cross sections of pure s-process nuclei like ^{170}Yb of nuclei with large s-process contributions like ^{184}W are important normalization points in the vicinity of ^{176}Lu (1,2). In addition, an accurate value of the total capture cross section of ^{175}Lu is required for the analysis of the s-process branching at ^{176}Lu.

Differential capture cross section measurements on these nuclei have been carried out in the relevant neutron energy range between 5 and 200 keV. The experimental technique was described in detail recently (3). A kinematically collimated neutron beam was produced via the ^{7}Li(p,n) and the T(p,n)-reaction with the proton energy just above the reaction threshold. Neutron energy determination was achieved by the time-of-flight technique with a resolution of $\sim$ 20 ns/m at a flight path of only 6 cm. The prompt capture gamma rays were detected by a Moxon-Rae system.

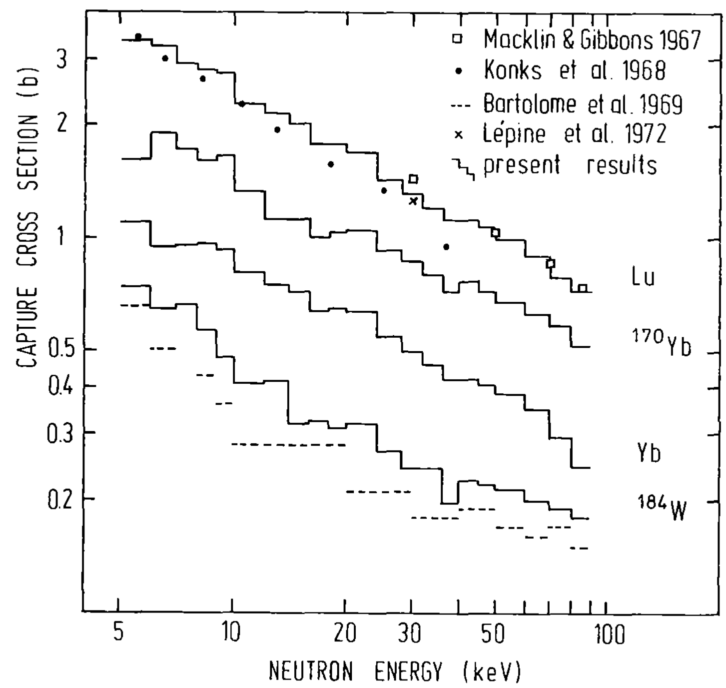

Fig. 1. The neutron capture cross sections of natural Lu, ^{170}Yb, natural Yb and ^{184}W

The results of our measurements in the 5 to 90 keV energy range are shown in fig. 1. For Lu the agreement with other measurements is satisfactory, whereas for ^{184}W our result was found to be 10 to 20 % higher than the previous one of Bartolome et al. (4).

References

(1) J. Audouze, W.A. Fowler, D.N. Schramm, Nature Phys. Sci. 238, 8 (1972).
(2) M.T. McCulloch, J.R. de Laeter, K.J.R. Rosman, Earth and Planetary Sci. Lett. 28, 308 (1976).
(3) K. Wisshak, F. Käppeler, Nucl. Sci. Eng. 66, 363 (1978), 69, 39 (1979).
(4) Z.M. Bartolome, R.W. Hockenbury, W.R. Moyer, J.R. Tatarczuk, R.C. Block, Nucl. Sci. Eng. 37, 137 (1969).
(5) R.L. Macklin, J.H. Gibbons, Phys. Rev. 159, 1007 (1967).
(6) V.A. Konks, Yu. P. Popov, Yu. I. Fenin, Sov. J. of Nucl. Phys. 7, 310 (1968).
(7) J.R.D. Lépine, R.A. Douglas, Nucl. Phys. A196, 83 (1972).

1.1.8 The Inelastic Scattering Cross Section of ^{187}Os Near 30 keV Neutron Energy

R.R. Winters[+], F. Käppeler, K. Wisshak, and B.L. Berman[++]

The very long half life of 5×10^{10} a makes ^{187}Re a possible cosmic clock which is associated exclusively with the r-process. This clock can be evaluated by a comparison of the $N\langle\sigma\rangle$-values of the pure s-process nuclei ^{186}Os and ^{187}Os. From s-process systematics one would expect practically equal values for $N\langle\sigma\rangle$ because in this mass region the $N\langle\sigma\rangle$-curve is very flat. Hence it is possible to determine how much ^{187}Os has been created by the decay of ^{187}Re and this in turn gives a measure for the age of ^{187}Re (1,2).

However, this straight-forward procedure is complicated by the fact that ^{187}Os has a low lying level at 9.8 keV. At the high temperature of the s-process this level is excited to a considerable degree so that the neutron capture cross section of the nucleus in this state must be known, too.

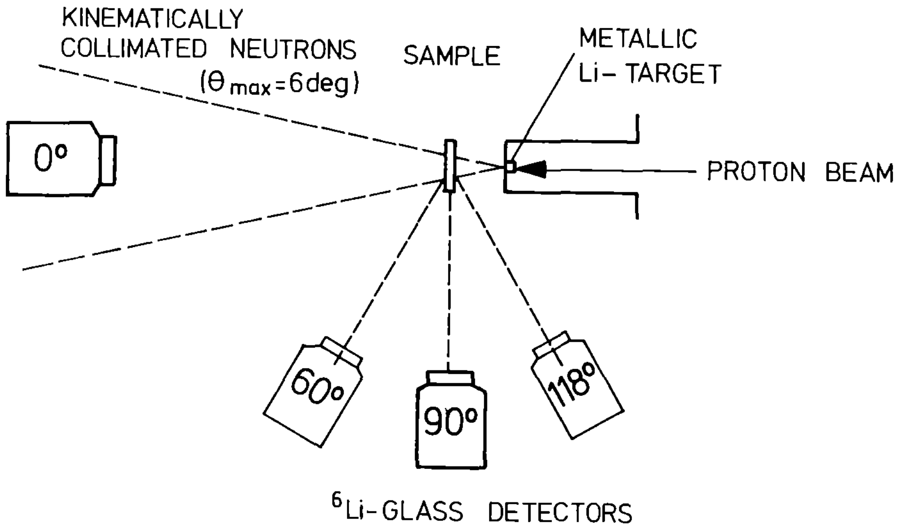

Fig. 1
Schematic sketch of the experimental setup.

As the reliability of nuclear model calculations is rather limited, one possibility for an experimental check is to determine the inelastic scattering cross section of ^{187}Os for neutron energies which are typical for the s-process distribution. With this information the model calculations can be refined or normalized.

The experiment was performed at the Karlsruhe pulsed 3 MV Van de Graaff. Fig. 2 shows the schematic setup. With the proton energy only 0.5 keV above the threshold of the $^7Li(p,n)$ reaction,a kinematically collimated neutron beam with an opening angle of $\pm$ 6 deg and an energy spread of 30 $\pm$ 5 keV was produced.

The samples were mounted on a sample changer perpendicular to the plane of fig. 1. With the fast pulsing system of our accelerator (pulse width $\sim$ 500 ps), very short flight paths could be used between neutron target and samples (10 mm) as well as between samples and detectors (0 deg detector 640 mm, scattering detectors 100 mm). At the position of the samples the neutron cone had a diameter of $\sim$ 5 mm which was considerably less than the sample diameter of 10 mm. Beside ^{187}Os also ^{188}Os and natural lead samples were used in the experiment. In addition an empty sample position served for background determination.

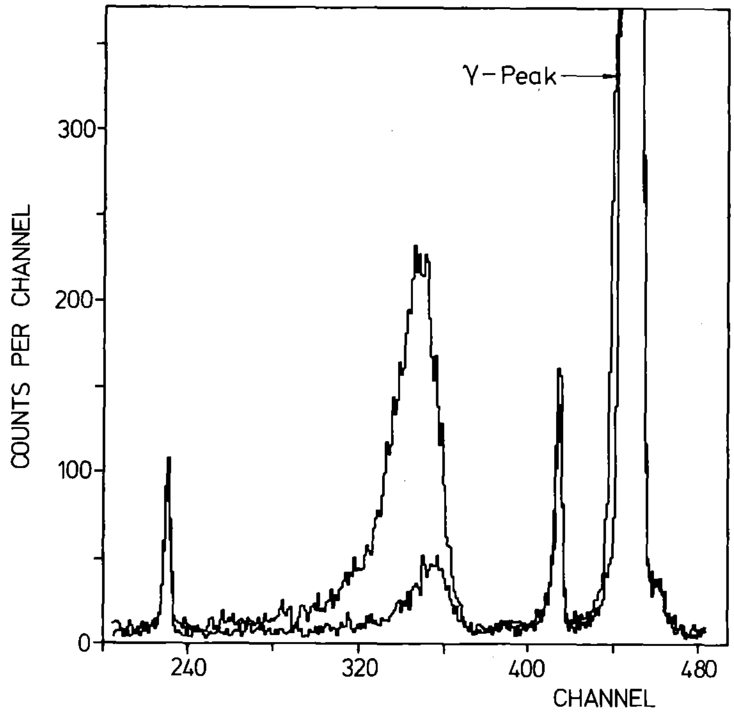

Fig. 2 Typical time-of-flight spectrum for scattered neutrons from the ^{187}Os sample and the respective background.
The background peak around channel 415 is due to neutrons scattered in the Ta baking of the Li-target

A typical time-of-flight spectrum with the scattered neutrons detected under 60 deg is shown in Fig. 2 for the ^{187}Os sample together with the background spectrum.

At present the data analysis is under way.

References

(1) J. Browne, B.L. Berman, Nature 262 (1976) 197.
(2) R.R. Wintes, R.L. Macklin, J. Halperin, to be published.

+ Oak Ridge National Laboratory, Nuclear Physics Division, Oak Ridge, Tenn. 37830, U.S.A.
++ Lawrence Livermore Laboratory, University of California, P.O.B. 808, Livermore, Calif. 94550, U.S.A.

1.1.9 Results from a 4-Parameter Experiment: Mass Distributions, Kinetic Energy Distributions and the Number of Prompt Fission Neutrons ν(A) for Fast Neutron Induced Fission of ^{237}Np

A.A. Naqvi, F. Käppeler, and R. Müller[+]

The 4-parameter measurements on correlated fragments in the fission of ^{235}U and ^{237}Np with fast neutrons were described in the preceding reports

(1). This contribution summarizes briefly the preliminary results on ^{237}Np. For this isotope measurements have been made at 0.8 and 5.5 MeV neutron energy corresponding to excitation energies of 0.1 and 4.8 MeV at the saddle point deformation.

The data analysis is based on the fragment kinetic energies and velocities which were determined in the experiments. While the fragment velocities were derived directly from the time-of-flight, the kinetic energies were obtained using a pulse height calibration scheme which was slightly modified compared to that reported by Schmitt et al. (2).

Fig. 1 shows the fragment velocity distributions which were determined at flight paths of 275 and 375 mm with an overall time resolution of ∿800 ps. The upper part of the figure gives the difference between the two distributions to illustrate the influence of excitation energy. At higher excitation there is clearly a pronounced decrease in velocity for the mass

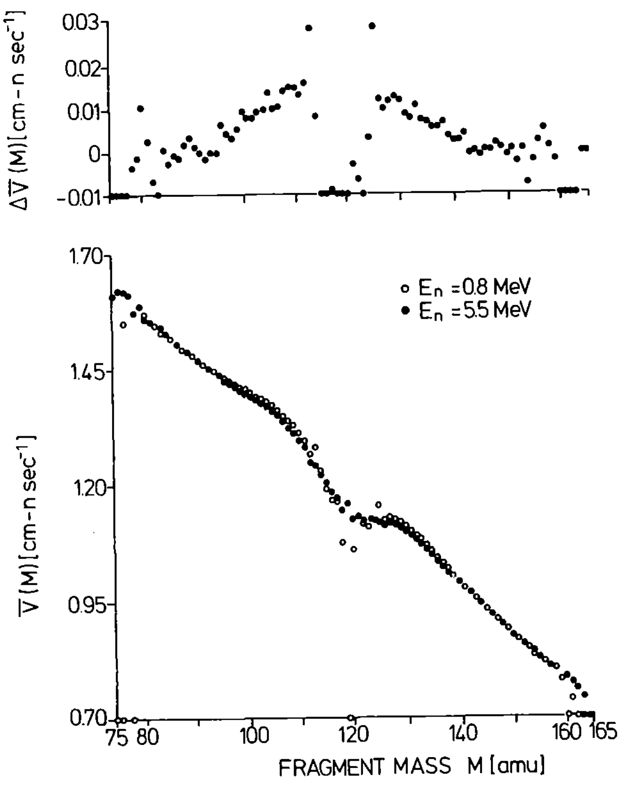

Fig. 1: The distributions of fragment velocities for E_n=0.8 (•) and E_n = 5.5 MeV neutron energy. On top of the figure the difference between the two distributions is given in an enlarged scale.

region 125 < A < 135 and also for the corresponding light fragments. This can be explained by the common picture that with increasing excitation energy dissipation effects cause an increasing deformation of the fissioning system. Therefore the Coulomb energies and hence the total kinetic energies are lowered accordingly. Obviously the near magic fragments around mass number 132 are most affected by this behaviour whereas additional deformations do not cause much changes at very large fragment masses. From the fragment velocities the primary mass distributions $N(M^{*})$ can be calculated with significantly better resolution than it is possible if only the fragment energies are used. In fig. 2 the fragment mass yields are shown for both excitation energies.

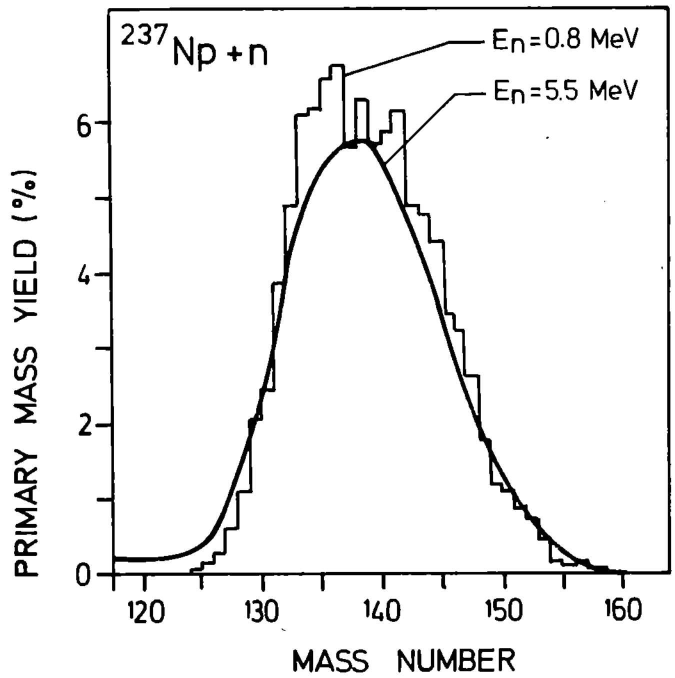

Fig. 2:
Primary mass yields in fast neutron induced fission of ^{237}Np

The distribution obtained close to the fission barrier at 0.8 MeV exhibits indications of a fine structure with a period of ∿3 mass units which reflects the enhancement due to pairing and shell effects. The peak-to-valley ratio in the mass distribution changes from 600 at 0.8 MeV to 35 for E_n = 5.5 MeV.

References

(1) R. Müller, A.A. Naqvi, F. Käppeler, KfK-Report 2686 (1978) also KfK-Report 2504 (1977).

(2) H.W. Schmitt, W.E. Kiker, C.W. Williams, Phys. Rev. 137 (1965) B 837.

(3) G. Andritsopoulos, Nucl. Phys. A 94 (1967) 537.

1.1.10 Investigation of the Validity of the Valence Model for Neutron Capture in the Mass Range $40 < A < 70$*

H. Beer

For a large number of nuclei in the 3s giant resonance region ($40 < A < 70$) studied experimentally at the Karlsruhe pulsed 3 MV Van de Graaff accelerator, total radiation widths have been calculated by means of the valence capture model and compared with the experimental results. Systematic trends of the validity of this model have been investigated. It was found that valence capture plays only a limited role in the mass region $40 < A < 70$.

*J. de Physique 40, 339 (1979)

1.1.11 Capture-to-fission Ratio of ^{235}U in the Neutron Energy Range from 10 to 500 keV*

H. Beer and F. Käppeler

The capture-to-fission ratio $\alpha = \sigma_c/\sigma_f$ of ^{235}U has been determined in the neutron energy range from 10 to 500 keV with an accuracy of typically 8 to 10 %. The measurement was carried out on a 3 MV pulsed Van de Graaff accelerator using an 800 l liquid scintillator tank for the detection of capture and fission gamma rays. A fission neutron counter in coincidence with the tank served to distinguish between capture and fission events. With the good energy resolution of 2 nsec/m achieved in this experiment, intermediate structure in the capture-to-fission ratio could be resolved up to 50 keV neutron energy. Interpreted in terms of the double humped fission barrier, the experimental average level spacing $D_{II} = 1000 \pm 30$ eV led to an energy difference between the first and second well of $E_{II} = 3.26 \pm 0.14$ MeV.

*Phys. Rev. C 20, 201 (1979).

1.2 NUCLEAR DATA

1.2.1 The Total Neutron Cross Section of Boron-10 between 90 and 420 keV*

H. Beer and R.R. Spencer+

The neutron total cross section of ^{10}B has been determined between 90 and 420 keV neutron energy by means of a transmission measurement on a boron sample enriched in ^{10}B. Deviations in shape from other measurements are within the statistical accuracy of the present measurement and are smaller than 1.5 %. In the measured energy region, no indication of narrow resonance structure was found, and the deviation of the total cross section from an $E^{-1/2}$ energy dependence above 100 keV was confirmed. An analysis using the R-matrix formalism showed that this deviation can be associated with the $7/2^+$ s-wave resonance at 370 keV.

+Present address: Oak Ridge National Laboratory, Oak Ridge, Tenn., 37830,USA
*Nuclear Science & Engineering 70, 98-101 (1979).

1.2.2 A Precise Determination of the Neutron Capture Width of the 27.7 keV s-wave Resonance in ^{56}Fe

K. Wisshak and F. Käppeler

The capture widths of broad s-wave resonances in structural materials are of special interest for fast reactor calculations because these resonances contribute a significant part to a spectrum averaged cross section. Especially for the strong 27.7 keV resonance in ^{56}Fe the existing data for the capture width vary between 0.9 and 1.6 eV.

Therefore a new measurement was carried out using an experimental setup completely different from previous work (1).

Kinematically collimated neutrons in the energy range from 10 to 60 keV were obtained from a pulsed Van de Graaff accelerator using the

Li(p,n) reaction just above the reaction threshold. An enriched (99.97 %) metallic sample was positioned at a flight path of only 8 cm and a ^{197}Au sample served as a standard. A Moxon-Rae detector was used for the detection of capture gamma rays. The distance between sample and detector was twice as long as the flight path of the primary neutrons.

With this setup two of the main difficulties of previous measurements could be avoided:

1) The high neutron flux at the sample position allowed to use very thin samples (0.6, 0.3, 0.15 mm). Consequently, the corrections for multiple scattering and self-shielding are low (∿ 8 % for the thinnest sample).

2) Background due to neutrons scattered in the resonance and then captured in the detector or the surrounding materials appears delayed in the time of flight spectra and does not contribute to the area of the 27.7 keV resonance. Therefore no correction for the neutron sensitivity of the detector is required.

The overall time resolution of 1.2 nsec was sufficient, even with the short flight path of only 8 cm, to resolve the resonance unambiguously from the neighbouring p-wave resonances. This is demonstrated in the experimental TOF spectrum shown in fig. 1.

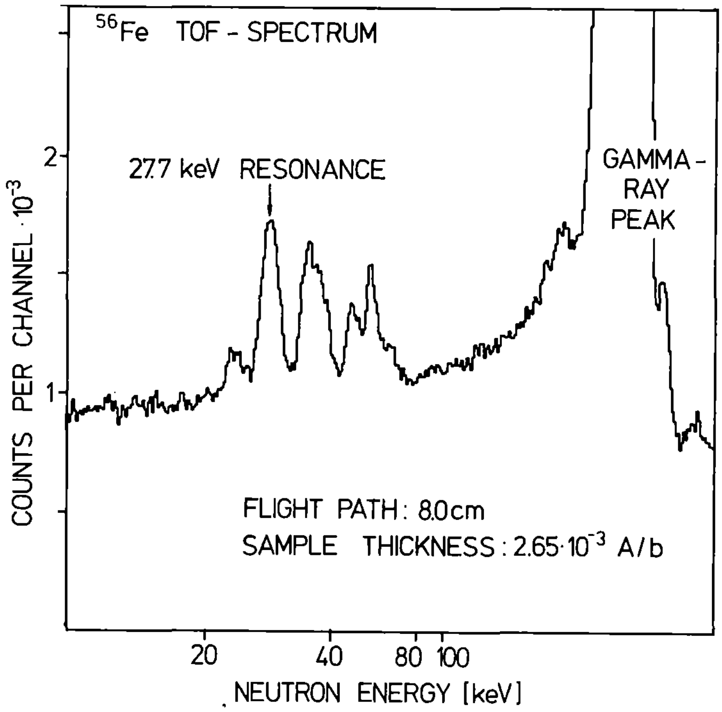

Fig. 1
Experimental TOF spectrum obtained with a sample of 0.3 mm thickness.

To obtain the capture width for the 27.7 keV resonance we performed a shape fit to the experimental capture yield with the FANAC-code of F. Fröhner (2). Except the resonance energies only the capture width of the 27.7 keV resonance was taken as a free parameter. In the calculations all other parameters were taken as fixed values from literature (2,3). An example of an actual fit is shown in fig. 2.

Up to now the data measured with the samples of 0.15 and 0.3 mm thickness have been analyzed and a mean value of 1.03 eV has been obtained for the width. The statistical accuracy is ∿ 2 %. The analysis of systematic uncertainties is not yet completed so that the above value has to be taken as preliminary.

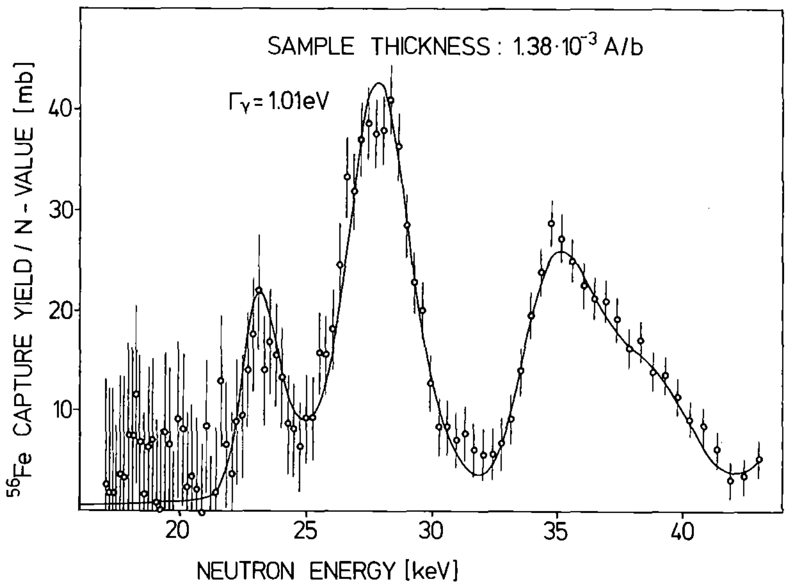

Fig. 2. FANAC fit to the 27.7 keV s-wave resonance in ^{56}Fe

References

(1) F. Käppeler, Report KfK 2686 (1978) 24.

(2) F.H. Fröhner, Report KfK 2145 (1977).

(3) F.G. Perey, G.F. Chapman, W.E. Kinney, and C.M. Perey, Proc. of a Conference on Neutron Data of Structural Materials for Fast Reactors, Geel (5-8 December, 1977) p. 530.

1.2.3 A Technique to Determine the Isomeric Ratio in ^{242}Am Following Neutron Capture in ^{241}Am

K. Wisshak, J. Wickenhauser, and F. Käppeler

Measurements of the isomeric ratio in neutron capture of ^{241}Am are urgently requested for keV neutron energies (1). This ratio determines essentially the amount of ^{242}Cm produced in a reactor during burnup, and the spontaneous fission of this nucleus dominates the neutron radiation of spent fuel. Whereas for thermal neutrons a measurement has been performed already (2), no data are available until now in the keV range which is of interest for fast reactors.

A proposal to measure this ratio at an energy of ∿ 30 keV has been given already in ref. 3. The measurements of the total capture cross section of ^{241}Am are now completed (see contribution 1.2.4). The partial capture cross section for the population of the groundstate of ^{242}Am will be measured by activating a thin (∿ 1 mg/cm^2) ^{241}Am sample in a neutron flux of about 10^9 n/sec at our Van de Graaff accelerator. The decay of the ^{242}Am nuclei into the groundstate will then be detected via the electrons emitted in the β^- decay to ^{242}Cm. The separation of the electrons from the intense γ and α background in the ^{241}Am sample is accomplished with a "mini orange spectrometer" (4) consisting of a filter of permanent magnets and an Si(Li)- detector for energy analysis. A transmission curve of the spectrometer is shown in fig. 1. The transmission was determined by using conversion electrons from Th(B+C+C")-, ^{207}Bi- and ^{137}Cs-sources and from the continuous spectrum of a ^{90}Y-source. The figure demonstrates that the upper part (E_β > 400 keV) of the ß-spectrum of ^{242g}Am which has an end point energy of 660 keV can be observed with an efficiency of 1-3 %. The low energy background e.g. from conversion electrons of the 60 keV transition in ^{237}Np is suppressed by several orders of magnitude. In addition the transmission is adjusted such that the β^- spectrum of ^{198}Au (endpoint energy 963 keV) which is used as a reference in the cross section determination, can be observed with sufficient accuracy, too. Measurements with the ^{241}Am samples have just been started.

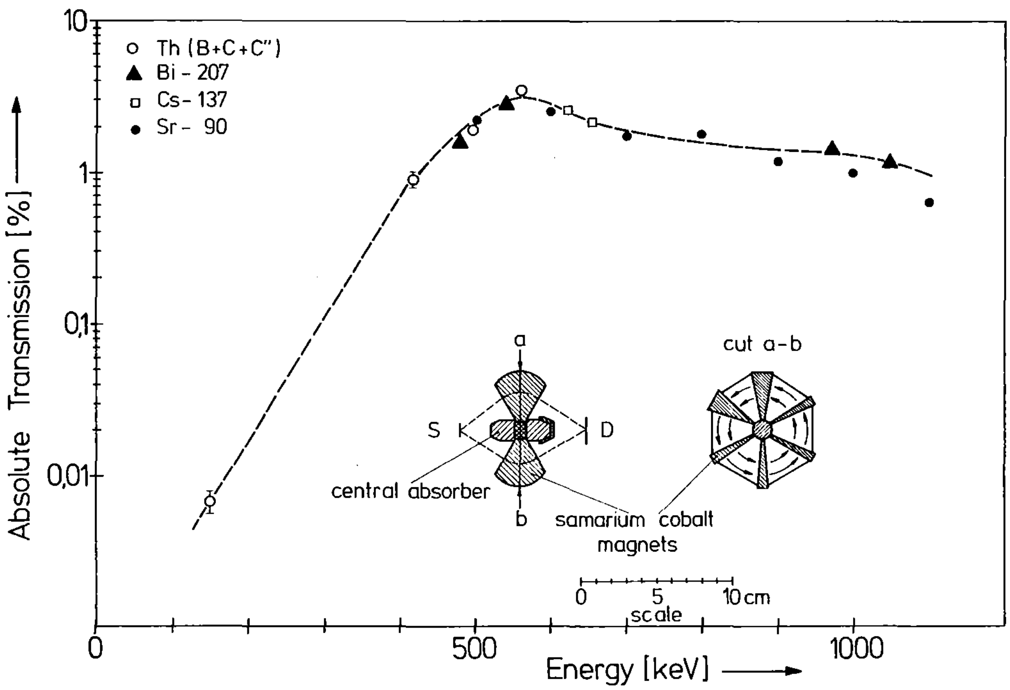

Fig. 1 Transmission curve of the "mini-orange-spectrometer". A schematic drawing of the magnet configuration is given in the inset.

As a first step we intend to remeasure the isomeric ratio at thermal energies. Then the samples will be activated in a neutron spectrum of 30 $\pm$ 10 keV FWHM obtained from the ^{7}Li(p,n) reaction at proton energies $\sim$ 40 keV above threshold.

References

(1) R.M. Lessler, Ed. "World Request List for Nuclear Data", INDC(SEC)-55/URSF, International Atomic Energy Agency, Vienna (1976).

(2) R.M. Harbour, K.W. MacMurdo, and F.J. McCrossen, Nucl. Sci. Eng. 50 (1973) 364.

(3) K. Wisshak and F. Käppeler, Report KfK 2504 (1977) 29.

(4) J. van Klinken and K. Wisshak, Nucl. Instr. Meth. 98, (1972) 1.
J. van Klinken, S.J. Feenstra, and G. Dumont, Nucl. Instr. Methods 151 (1978) 433.

1.2.4 The Neutron Capture and Fission Cross Section of ^{241}Am in the Energy Range from 10 to 250 keV*

K. Wisshak and F. Käppeler

The neutron capture and subthreshold fission cross sections of ^{241}Am were measured in the energy range from 10 to 250 keV, using ^{197}Au and ^{235}U as the respective standards. Neutrons were produced via the ^{7}Li(p,n) and the T(p,n) reaction with the Karlsruhe 3 MV pulsed Van de Graaff accelerator. Capture events were detected by a Moxon-Rae detector and fission events by an NE-213 liquid scintillator with pulse shape discrimination equipment. Flight paths as short as 50-66 mm were used to obtain optimum signal to background ratios. The capture cross section could be determined with a total statistical and systematic uncertainty of 4-10 % while the respective values are 13-2o % for the fission cross section. The results are compared with recent results of other authors which in some cases are severely discrepant.

*Submitted for publication in Nucl. Sci. Eng.

1.2.5 High Precision Time-of-Flight Measurements of Neutron Resonance Energies in Carbon and Oxygen between 3 and 30 MeV*

S. Cierjacks, F. Hinterberger+, G. Schmalz, D. Erbe,
P. v. Rossen+, and B. Leugers

An essentially improved time-of-flight device has been set up at the Karlsruhe Isochronous Cyclotron. Transmission measurements on carbon and oxygen in the energy range from 3 to 30 MeV with a spectrometer resolution of 5.5 psec/m allowed to determine neutron resonance energies of some narrow resonances with an accuracy of 1.2×10^{-5}. The present results are in many cases by more than two orders of magnitude more accurate than previously published values. Above 10 MeV, measured excitation energies of various T = 3/2 states in ^{17}O have an order of magnitude higher accuracy than the most precise determinations from charged particle reactions. Resonance energies of narrow neutron resonances are presented and two sets of data suitable as high precision energy standards are proposed. For the ^{16}O+n system, energies and total widths of five T = 3/2 states in the range $7 \leq E_n \leq 11$ MeV are given.

*to be submitted for publication in Nucl. Instr. Meth.
+Institut für Strahlen- und Kernphysik der Universität Bonn,
Nußallee 14-16, 5300 Bonn, Germany

1.2.6 Neutron Induced Fission Cross Sections of ^{239}Pu, ^{240}Pu and ^{235}U between 0.5 and 20 MeV*

Part I. Measurement of Fission Cross Section Ratios ^{239}Pu:^{235}U and ^{240}Pu:^{235}U

K. Kari+, S. Cierjacks

The fission cross section ratios ^{239}Pu:^{235}U and ^{240}Pu:^{235}U were determined in the energy range between 0.5 and 20 MeV using gas scintillation counters and the time-of-flight technique at the Karlsruhe Isochronous Cyclotron. Fission events were measured requiring fast coincidences from both fission fragments. The high neutron flux available at the 12 m flight path allowed to measure the ratios with statistical accuracies between 0.2 and 1 % with a spectrometer resolution of 0.3 nsec/m. Total uncertainties of measured ratios range between 2.1 and 2.3 % for ^{239}Pu:^{235}U and between 2.5 and 2.7 % for ^{240}Pu:^{235}U. The present cross section ratio determinations deviate in some energy intervals significantly from those presently recommended for fast reactor calculations.

*to be submitted for publication in Nucl.Sci. Eng.
+Present address: Siemens-Entwicklungslaboratorium, Wittelsbacher Platz 2, D-8000 München, Germany

1.2.7 Neutron Induced Fission Cross Sections of ^{239}Pu, ^{240}Pu and ^{235}U between 0.5 and 20 MeV*

Part II. Measurement of Absolute Fission Cross Sections of ^{239}Pu, ^{240}Pu and ^{235}U

S. Cierjacks and K. Kari+

Absolute fission cross sections of ^{239}Pu, ^{240}Pu and ^{235}U were measured simultaneously with fission cross section ratios described in part I using the same fission device. Absolute neutron fluxes between 0.5 and 20 MeV were determined by means of a telescope-like proton recoil device employing solid radiators and gas scintillation counting. For ^{235}U two different sets of data were obtained from samples of 0.4 and 0.8 mg/cm² areal densities. Absolute fission cross sections for the three isotopes were measured with a total uncertainty of 2.0 - 2.5 % for ^{239}Pu and ^{235}U and of 2.2 - 2.7 % for ^{240}Pu.

*to be submitted for publication in Nucl. Sci. Eng.
+Present address: Siemens Entwicklungslaboratorium, Wittelsbacher Platz 2, D-8000 München, Germany

1.2.8 A Fast Spherical Avalanche Fission Detector with Intrinsic Alpha-Discrimination*

M.A. Kazerouni and F. Käppeler

A spherical avalanche type fission detector is described for fission cross section measurements on highly alpha-active isotopes. It combines good alpha-suppression (discrimination factor better than 10^{-10}) and fast timing properties ($\Delta t \lesssim 0.2$ nsec FWHM). The detector works with almost 100 % efficiency so that only μg-amounts of sample material are required.

*Nucl. Instr. Meth. 164 (1979) 439

2. CHARGED PARTICLE REACTIONS AND NUCLEAR SPECTROSCOPY

2.1 ALPHA-AND ^{6}Li- PARTICLE REACTIONS

2.1.1 ^{48}Ca-^{40}Ca Radius Difference from Elastic Scattering of 104 MeV Alpha-Particles*

E. Friedman[+], H.J. Gils, H. Rebel, and Z. Majka[++]

Elastic scattering of 104 MeV alpha-particles from ^{48,40}Ca was measured between 3^{o} and 110^{o}. Optical-model fits were made using a Fourier-Bessel description of the real potential and also using density-dependent folding models. The average result for the difference between nuclear-matter rms radii is $r_m(^{48}Ca) - r_m(^{40}Ca) = 0.12 \pm 0.06$ fm. Comparisons are made with results obtained by other methods.

* Phys. Rev. Lett. 41 (1978) 1220

\+ The Racah Institute of Physics, The Hebrew University, Jerusalem, Israel

++ Permanent address: Institute of Physics, Jagellonian University, Cracow, Poland

2.1.2 Nuclear Sizes of ^{40,42,44,48}Ca from Elastic Scattering of 104 MeV Alpha-Particles

H.J. Gils, E. Friedman[+], H. Rebel, J. Buschmann, Z. Majka[++], S. Zagromski, H. Klewe-Nebenius[+++], B. Neumann, R. Pesl, and G. Bechtold

The alpha-particle scattering studies of the radial shape of Ca nuclei have been continued . Additionally to ^{40,48}Ca the differential cross sections for elastic scattering of 104 MeV alpha-particles from ^{42,44}Ca have been measured with high angular accuracy ($\Delta\Theta \leq 0.10^{o}$) over a wide angular range ($3^{o} \leq \Theta_{CM} \leq 110^{o}$) in order to determine differences between the sizes and shapes of the nucleon density distributions of these nuclei. The experimental results are displayed in fig. 1.

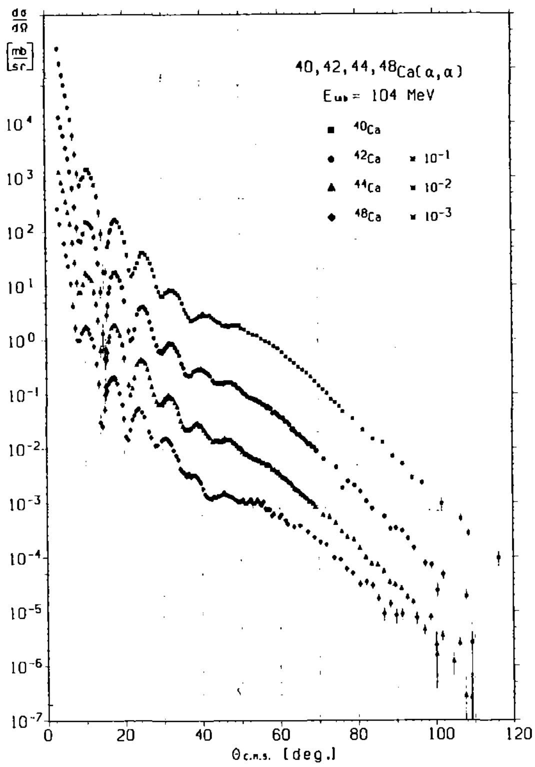

Fig. 1 Differential cross sections for elastic alpha-particle scattering from $^{40,42,44,48}Ca$

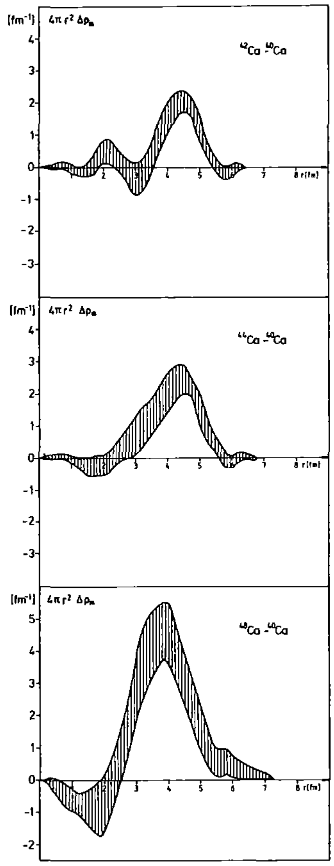

Fig. 2 Differences between nucleon density distributions obtained from density dependent folding model analysis using Fourier-Bessel description of the densities.

Due to the "nuclear rainbow criterion" (1) these data enable to determine the alpha particle-nucleus potential with a high degree of uniqueness even at small radii. For the analysis two different approaches have been used for the real optical potential

(i) phenomenological Fourier-Bessel series (2) potential
(ii) single folding potential including a saturation term which respects the density dependence of the alpha-nucleon interaction.

The shape of the nucleon density distributions used in the folding model (ii) have also been described by a Fourier-Bessel series (2). Thereby the model dependence of the extracted shape as well as of integral quantities of the real potential (rms-radius, volume integral) and of the densities, respectively, are drastically reduced as compared to simple functional forms as e.g. a Saxon-Woods form. Moreover, significantly better reproductions of the experimental results are obtained (2) and realistic estimates of the uncertainties of the various extracted quantities are provided.

In fig. 2 the differences between the nucleon density distributions resulting from the density dependent folding model analysis are shown. It is clearly indicated that the additional neutrons of $^{42,44,48}Ca$ are predominantly located in a shell of radius $r \sim 3.5 - 4.5$ fm. The corresponding rms radii of proton, neutron and total matter densities are quoted in table 1.

A	R_p	ΔR_p (A-40)	R_n	ΔR_n (A-40)	R_m	ΔR_m (A-40)	ΔR_{n-p}
40	3.386		3.335		(3.361)		(-0.051)
42	3.422	0.036	3.420	0.085	3.421±0.03	0.060	-0.002
44	3.439	0.053	3.476	0.141	3.459±0.03	0.098	+0.037
48	3.407	0.021	3.633	0.298	3.541±0.03	0.180	+0.226

Table 1: Rms Radii of Ca-Isotopes

$\langle r_p^2 \rangle^{1/2} = R_p$: Rms-radii of proton-distributions; from Ref. 3

$\langle r_m^2 \rangle^{1/2} = R_m$: Rms-radii of total matter-distributions; from present work

$|1/N\ (A\langle r_m^2 \rangle - Z\ \langle r_p^2 \rangle)^{1/2}| = R_n$: Rms-radii of neutron distributions (in fm)

References

(1) D.A. Goldberg and S.M. Smith, Phys. Rev. Lett. 29 (1972) 500.

(2) E. Friedman and C.J. Batty; Phys. Rev. C 17 (1978) 34.
E. Friedman, H.J. Gils, H. Rebel, and Z. Majka; Phys. Rev. Lett. 41 (1978) 1220.

(3) H.D. Wohlfahrt et al., Phys. Lett. 73B (1978) 131.

+ The Racah Institute of Physics, The Hebrew University of Jerusalem, Israel

++ Institute of Physics, Jagellonian University, Cracow, Poland

+++ Kernforschungszentrum Karlsruhe, Institut für Radiochemie

2.1.3 Saturation Effect and Determination of Nuclear Matter Density Distribution from Alpha-Ca Optical Potentials

Z. Majka[+], H.J. Gils, and H. Rebel

Optical model fits (1) to the elastic scattering data of 104 MeV alpha-particles from $^{48,40}Ca$ using a Fourier Bessel description of the real potential show that the rms radius of the α-^{48}Ca potential is larger than the α-^{40}Ca one by an amount of $\langle r^2 \rangle^{1/2}_{Pot(48)} - \langle r^2 \rangle^{1/2}_{Pot(40)} = 0.13 \pm 0.04$ fm. Moreover, the volume integrals per nucleon pair for both potentials agree within the experimental error of $\pm$ 3 MeV.fm^3.

The question arises whether the rms difference reflects merely the density dependence of the nucleon-nucleon interaction or whether it uniquely implies a difference between the rms radii of the corresponding nuclear density distributions. We have studied this question on the basis of a refined double folding model (2) which includes exchange effects and the density dependence of the effective nucleon-nucleon interaction.

The model has been shown to describe 104 MeV alpha-particle scattering also in the "rainbow" region and results in reasonable values of the potential volume integral per nucleon pair. For calculating the real part of the α-^{48}Ca optical potential, the following assumptions for the matter density distribution $\rho_m(48)$ in ^{48}Ca have been examined:

a. $\rho_m(48) = \frac{48}{20}\,\rho_p(48)$ where an experimentally deduced proton distribution ρ_p (48) (three parameter Fermi form) has been used. This model requires a considerable increase of the central density in the ^{48}Ca nucleus

b. Adopting the same value of the central density in ^{48}Ca as for the ^{40}Ca nucleus and adjusting the shape of ρ_m so that the rms radius equals that of the proton distribution used in case (a).

The calculations demonstrate that these assumptions do not reproduce the experimentally determined difference between the rms radii of the α-^{40}Ca and α-^{48}Ca optical potentials and that an additional assumption of an increased size of the neutron distribution in ^{48}Ca is necessary.

References

(1) E. Friedman, H.J. Gils, H. Rebel, and Z. Majka, Phys. Rev. Lett. 41 (1978) 1220 - H.J. Gils, E. Friedman, H. Rebel, J. Buschmann, S. Zagromski, H. Klewe-Nebenius, B. Neumann, R. Pesl, and G. Bechtold, to be published.

(2) Z. Majka, H.J. Gils, and H. Rebel, Z. Physik A 288 (1978) 139.

+ Institute of Physics, Jagellonian University, Cracow, Poland

2.1.4 104 MeV Alpha-Particle and 156 MeV ^{6}Li Scattering and the Validity of Refined Folding Model Approaches for Light Complex Projectile Scattering*

Z. Majka+, H.J. Gils, and H. Rebel

The real parts of the optical model potentials for 104 MeV alpha-particle and 156 MeV ^{6}Li-ion scattering from ^{40,48}Ca are calculated in terms of folding model approaches. The validity of different procedures is tested by comparing the differential cross section predictions with experimental data measured with high angular accuracy. It is found that a refined folding potential accounting for density dependence of an effective nucleon-nucleon interaction is appropriate for alpha-particle scattering without any parameter adjustment. However, for ^{6}Li-ion scattering renormalization of the depth of the real potential is necessary.

*Z. Physik A 288 (1978), 139

+Permanent address: Institute of Physics, Jagellonian University, Cracow, Poland

2.1.5 Optical Potentials for the Scattering of Alpha-Particles and ^{6}Li-Ions from ^{12}C

H.J. Gils and H. Rebel

The real part of the alpha-particle nucleus optical potential can be determined with a high degree of uniqueness if the energy of the scattered alpha-particle is high enough ($\gtrsim$ 80 MeV) and if large angle data beyond the "nuclear rainbow-angle" are included in the analysis(1). For high energy ^{6}Li scattering from ^{12}C (E_{Lab} = 156 MeV) a similar behaviour was observed (2). Hence, it is possible to compare details of the α-^{12}C and ^{6}Li-^{12}C interaction potential e.g. for the same projectile velocity. However, the conventional parametrizations of the potential like the Saxon-Woods form (SW) or the SW form squared are unable to describe the experimental data of elastic alpha-particle and ^{6}Li scattering from ^{12}C reasonably well presumably due to the unsuitable coupling of the interior part of the potential with the outermore tail given by these functional forms.

In order to remove this deficiency we applied the flexible Fourier-Bessel method (3) to the analysis of elastic scattering of 104 MeV alpha-particles and 156 MeV ^{6}Li-ions from ^{12}C. Besides the nearly "model independent" determination of the potential form this enables to estimate realistic errors at each radial point of the potential revealing interesting additional information for the comparison of the alpha-particle and ^{6}Li scattering optical potentials.

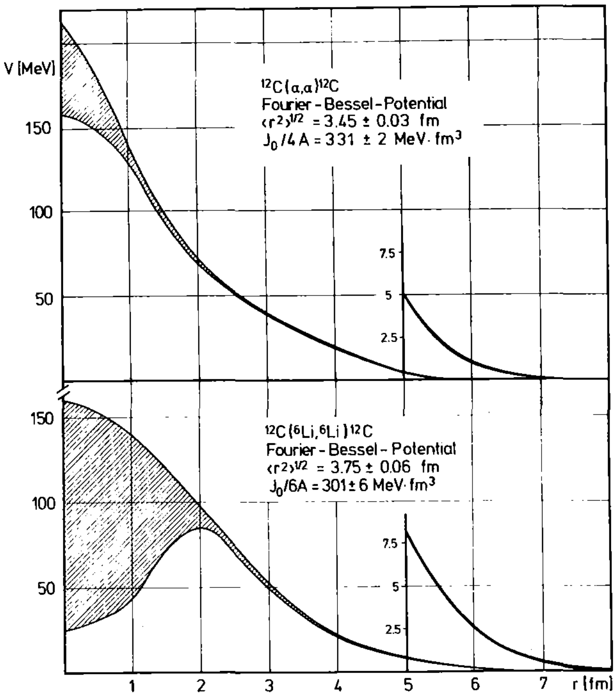

Fig. 1: Optical potentials for alpha-particle and ^{6}Li scattering from ^{12}C with error bands.

In fig. 1 the real potentials including their respective error bands (hatched areas) are displayed. It is clearly indicated, that the alpha-particle-^{12}C potential is well determined even at very small radii ($r \lesssim 2$ fm) whereas the ^{6}Li-^{12}C potential is well determined only at radii $r > 2$ fm. The inner part of the real optical potential reflects the transparency of target nucleus central density of the probing particle. Therefore, from Fig. 1 one concludes that the ^{12}C-nucleus in less transparent for ^{6}Li than for alpha-particles, certainly due to the strong break-up probability of the ^{6}Li projectile in the nuclear field (4).

These findings are in contrast to previous investigations of ^{6}Li scattering from ^{12}C at lower energies which reveal sensitivity also to the interior of the optical potential (5). The form of the optical potential found by the FB-method significantly deviates from the conventional best fit potential forms (6) (SW or SW^2) (in particular for alpha-particle scattering) explaining why these forms are unable to give reasonable descriptions of the experimental cross sections. Some integral quantities of conventional and FB-potentials and the χ^2-values per degree of freedom are compared in table 1 underlining the differences between the α-^{12}C and ^{6}Li-^{12}C optical potentials as already observed in fig. 1.

Table 1

a) α-^{12}C

Potential	χ^2/F	$-J_V/4A$	$<r_v^2>^{1/2}$	$-J_W/4A$	$<r_w^2>^{1/2}$
		$\lvert MeV.fm^3\rvert$	$\lvert fm\rvert$	$\lvert MeV.fm^3\rvert$	$\lvert fm\rvert$
SW	10.1	390	3.646	123.1	3.744
SW^2	6.2	385	3.539	126.8	3.677
FB	1.2	331	3.45 ± 0.03	117.4	3.894
b) ^6Li-^{12}C		$-J_V/6A$		$-J_W/6A$	
SW	6.9	291	3.795	154.9	4.282
SW^2	6.9	280	3.699	163.6	4.215
FB	4.5	301±6	3.75 ± 0.06	173.3	4.072

References

(1) D.A. Goldberg and S.M. Smith; Phys. Rev. Lett. 29 (1972) 500.

(2) H.J. Gils, J. Buschmann, H. Klewe-Nebenius, B. Neumann, H. Rebel, and S. Zagromski; Proc. Intern. Summer School on Nuclear Physics, Predeal, Romania (1978).

(3) E. Friedman and C.J. Batty; Phys. Rev. C 17 (1978) 34.

(4) B. Neumann, J. Buschmann, H. Klewe-Nebenius, H. Rebel, and H.J. Gils, KfK-Report 2819 (1979).

(5) E. Norbeck, M.D. Strathman, and D.A. Fox; Phys. Rev. C 18, 1275 (1978).

(6) H.J. Gils, Z. Majka, and H. Rebel, in preparation.

2.1.6. Transfer of ^6Li Break-Up Fragments

B. Neumann, J. Buschmann, H. Klewe-Nebenius[+], H. Rebel, and H.J. Gils

The dominating reaction channel in nuclear reactions which are induced by ^6Li-particles is the break-up of ^6Li into various fragments, in particular into an alpha-particle and a deuteron. The extremely high break-up probability suggests that the dissociation processes strongly interfere with other reaction channels and may lead to peculiar types of reaction mechanisms, for example

transfer of one of the break-up fragments into the target nucleus.
We have investigated break-up fragment capture reactions considering the case $^{6}Li + {}^{208}Pb$ in the energy range E_{Li} = 60-156 MeV (1). The experiments are based on the observation of the target residues, in particular ^{211m}Po and on measurements of the recoil energies of residual nuclei produced by charged particle bombardment. Looking for the production of ^{211m}Po, there are two dominating reaction paths leading to the same residual nucleus. Considering the case: ^{6}Li on ^{208}Pb the residual nucleus ^{211m}Po may be produced by the reaction $^{6}Li + {}^{208}Pb \rightarrow {}^{214*}At \rightarrow {}^{211m}Po + 2n + p$ (I).

This compound nucleus formation competes with the mechanism under consideration: break-up of the ^{6}Li-projectile followed by capture of the beam velocity alpha-particle

$$(\alpha + {}^{208}Pb) \rightarrow {}^{211*}Po \rightarrow {}^{211m}Po + n$$

^{6}Li (II)

d-spectator

The experimental discrimination between these processes is possible due to different recoil energies of the residual nucleus ^{211m}Po. The recoil energies were determined by measuring the penetration depths of the recoils in carbon catcher foils. This experimental method was tested by two cases of pure precompound-compound nuclear reactions of type I

$^{208}Pb\ (^{6}Li,\ 13\ n)^{201}At$ (at E_{Li} = 156 MeV)
$^{208}Pb\ (\alpha,n)\ ^{211m}Po$ (at E_{α} = 104 MeV)

The calculated recoil energies of the compound nuclei correspond to penetration depths of 220 and 100 $\mu g/cm^2$ carbon. Fig. 1 displays the results. The open symbols show the integral distributions of the implanted recoils from type I reactions with upper edge of the ramp at expected catcher thickness. For cases where both paths are possible (closed symbols) one immediately recognizes that the yield curves of ^{6}Li induced reaction follow rather closely that of the alpha-particle induced reactions. These results convicingly demonstrate the break-up fragment capture reaction to be the prevailing mechanism. Fu-thermore one measures a remarkable agree-

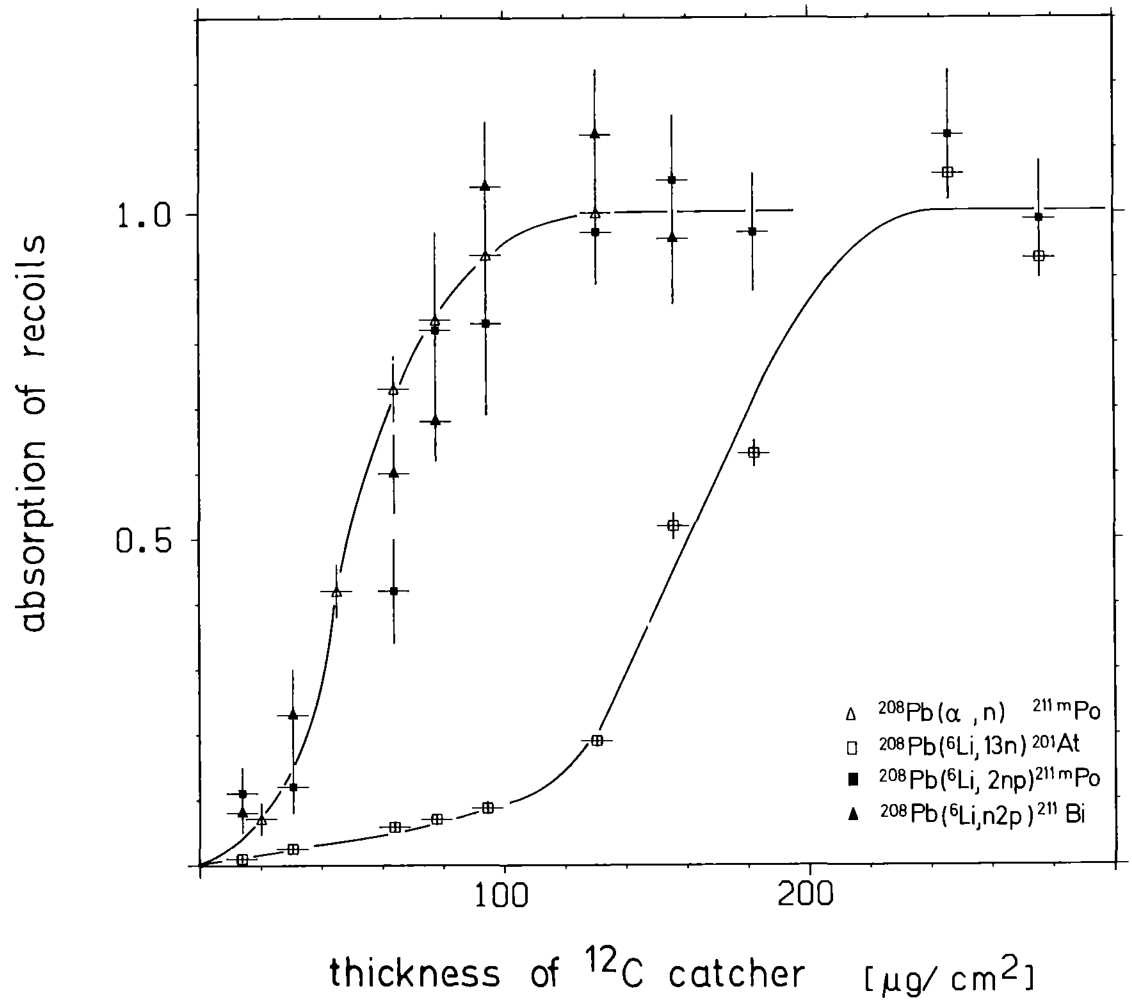

Fig. 1: Yield of recoil nuclei in carbon catcher foils versus thickness of the foils for alpha-particle and ^{6}Li induced nuclear reactions at E_{α} = 104 MeV and E_{Li} = 156 MeV.

ment of the cross sections of ^{6}Li and corresponding alpha-particle induced reactions at E_{Li} = 156 MeV and E_{α} = 104 MeV. By measuring excitation functions of ^{6}Li induced processes and comparing them with corresponding alpha-particle induced reactions one can see that (^{6}Li,xn + yp) reactions behave remarkably similar to (α,xn) processes, in particular in the high energy tail of the excitation function and that the transfer mechanism dominates also in the lower part of the excitation function.

References

(1) B. Neumann, J. Buschmann, H. Klewe-Nebenius, H. Rebel, H.J. Gils, KfK-Report 2819 (1979).

+Institut für Radiochemie, Kernforschungszentrum Karlsruhe, Germany

2.1.7 Continuum Particle Spectra from ^{6}Li Bombardment at E_{Li} = 156 MeV

B. Neumann, J. Buschmann, H.J. Gils, H. Klewe-Nebenius[+],
H. Rebel, S. Zagromski, H. Faust[++], J. Rieder[+++]

We have started systematic experimental studies of continuum spectra of outgoing particles in ^{6}Li induced nuclear reactions with 156 MeV ^{6}Li particles on various target nuclei (^{12}C, ^{60}Ni, ^{90}Zr, ^{120}Sn, ^{208}Pb). From the pronounced cluster structure of the ^{6}Li projectile strong contributions due to the break-up of the ^{6}Li projectile are expected. With increasing ^{6}Li energy the pure Coulomb break-up is competed by the break-up in the nuclear field. Simultaneously the reaction mechanism dominated by the sequential break-up near the Coulomb barrier changes to immediate fragmentation of the ^{6}Li nucleus into continuum states. Fig. 1 displays energy spectra of light outgoing particles when bombarding ^{208}Pb by 156 MeV ^{6}Li-ions. The broad bumps centered at the beam velocity reflect the importance of the break-up channels. At higher energies, in addition to the familiar (α + d) component the dissociation of $^{6}Li \rightarrow {}^{3}He + t$ (Q = −15.8 MeV) is clearly observed. Three particle break-up processes $^{6}Li \rightarrow p + n + \alpha$ and secondary deuteron break-up may explain the proton bump observed at $E \sim 1/6\ E_{Li}$. Similarly the triton spectrum may have a component from the secondary break-up of excited alpha-particles. The beam-velocity alpha-particles and deuterons roughly fulfill the kinematically founded optimum Q-value criterion (1) (closest approach distance matching) which has been schown to govern the transfer probabilities in heavy ion reactions at lower energies.

Our measurements aim at the determination of the "bump" cross sections, their angular distributions and A dependence. Charged particle spectra were measured by ΔE-E telescopes. For the high energy light particles a 20 mm thick high purity Ge-detector cooled by liquid nitrogen has been used. The discussion of the reaction mechanisms reflected by the measured spectra and an analysis on the basis of a direct break-up model are in progress.

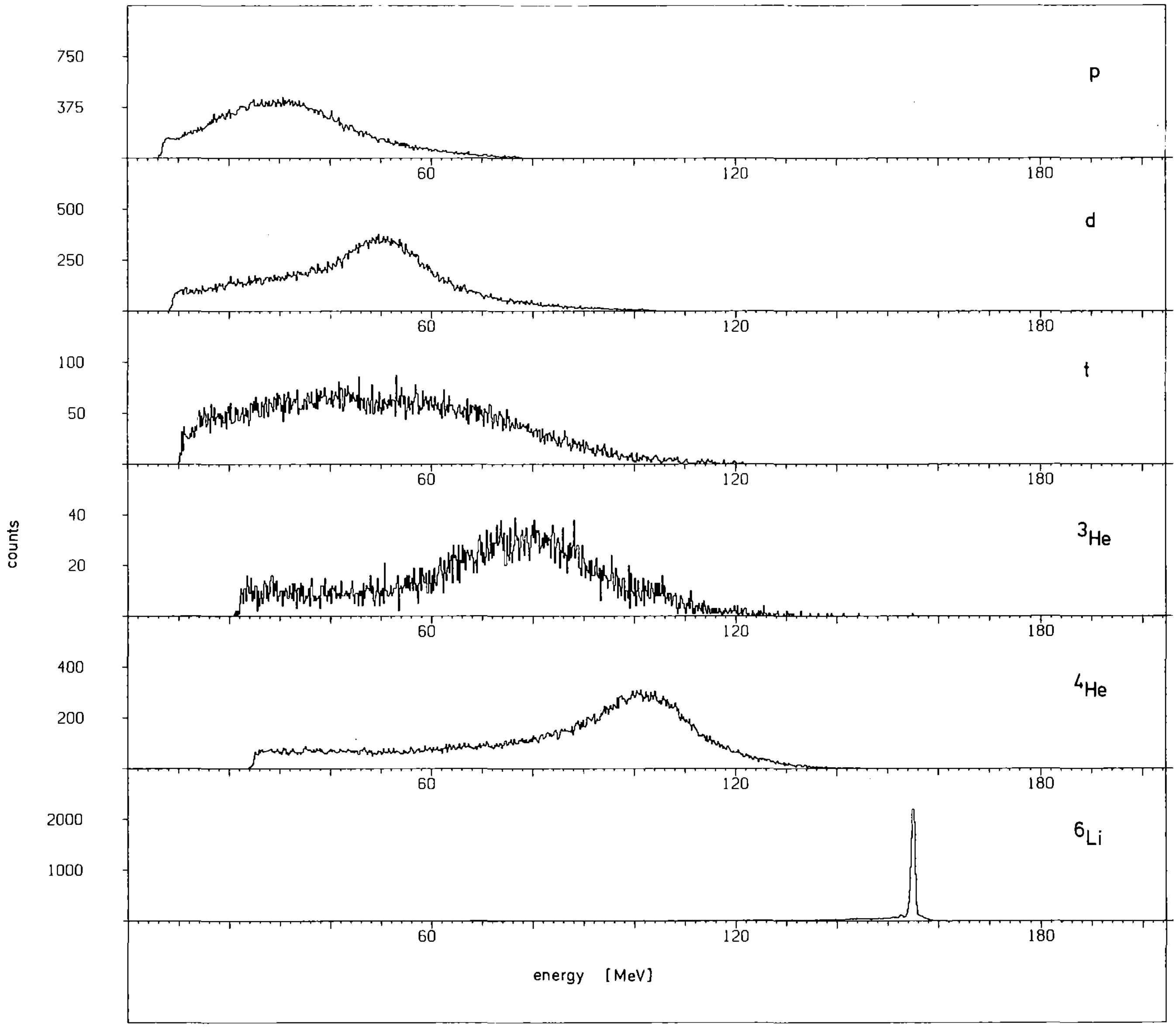

Fig. 1: Energy spectra of outgoing light charged particles when bombarding ^{208}Pb by 156 MeV ^{6}Li-ions ($\Theta = 18^{o}$).

References

(1) P.J.A. Buttle and L.J.B. Goldfarb, Nucl. Phys. A 176 (1971) 299.

+ Institut für Radiochemie, Kernforschungszentrum Karlsruhe, Germany

++ Present address: Institute Laue-Langevin, Grenoble, France

+++ Physikalisches Institut der Universität Heidelberg, Germany

2.2 POLARIZED DEUTERON REACTIONS

2.2.1 Elastic Scattering of Vector-Polarized Deuterons on ^{28}Si, ^{58}Ni, ^{90}Zr, and ^{197}Au

V. Bechtold, L. Friedrich, K.T. Knöpfle+, G. Mairle+, H. Müller+, H. Riedesel+, K. Schindler+, and G.J. Wagner+

The DWBA description of one- and two-particle transfer reactions like $(\vec{d},\tau)$, (d,t) and $(\vec{d},\alpha)$ requires a detailed knowledge of the deuteron-nucleus optical potential. In earlier measurements (1) we used unpolarized 52 MeV deuterons and were, therefore, not sensitive to the spin-orbit potential. Measurement of the analyzing power of elastically scattered deuterons on a number of selected nuclei should give the missing information. The observed analyzing powers for ^{28}Si, ^{58}Ni, ^{90}Zr and ^{197}Au (fig. 1) show typical and pronounced structures ($|iT_{11}| < 0.7$). The optical model analysis of cross sections (1) and analyzing powers was performed with the use of the code MAGALI. It was the aim to get "average parameters", which are characterized by the same geometrical quantities (radius parameter and diffuseness) for all the nuclei. Their individual properties are then contained in the potential depths, which show a simple dependence on mass number A and charge Z. Best results are obtained with a real radius parameter of 1.20 fm. Surface absorption could be applied in the complete mass region; volume absorption gave reasonable results only for light nuclei. The spin-orbit potential $r^{-1}dV(r)/dr$ shows a typical mass dependence: for light nuclei it decreases monotonically ($a_{s.o.} > r_{s.o.}$), whereas for heavy nuclei ($a_{s.o.} < r_{s.o.}$) a typical maximum occurs. The well depths of the real potential V and the surface absorbent imaginary potential W have the following mass and charge dependence:

$$V(A,Z) = (1.36\ Z\cdot A^{-1/3} + 68.2)\ \text{MeV}$$
$$W(A) = (1.82\ A^{1/3} + 5.7)\ \text{MeV}$$

Reference

(1) F. Hinterberger, G. Mairle, U. Schmidt-Rohr, G.J. Wagner, and P. Turek, Nucl. Phys. A 111 (1968) 265.

+Max-Planck-Institut für Kernphysik, Heidelberg, Germany

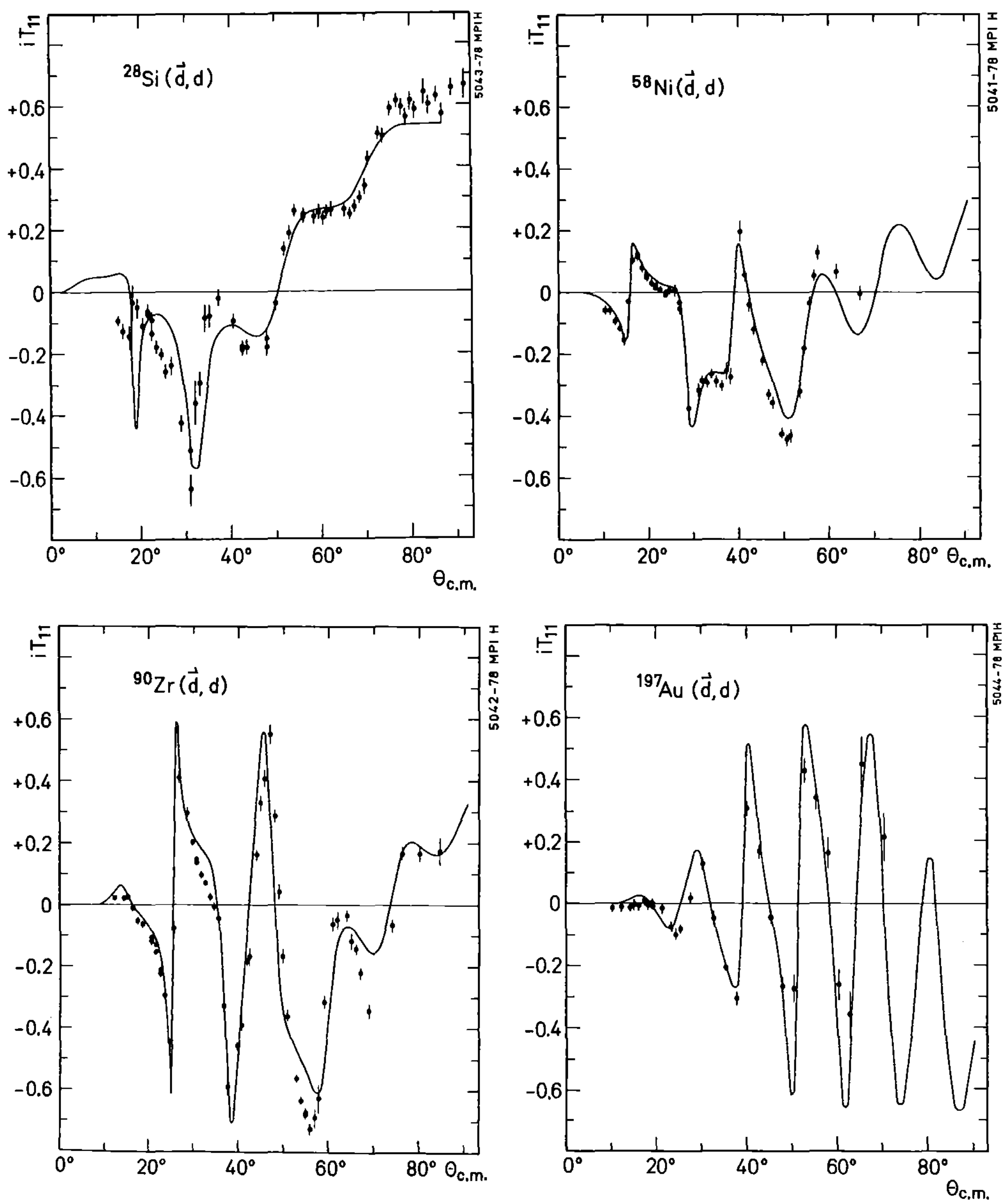

Fig. 1: Comparison of optical model calculations (average parameters) to measurements of analyzing powers for elastic scattering of 52 MeV deuterons.

2.2.2 Simultaneous Measurement of the $(\vec{d},t)$ and $(\vec{d},{}^3He)$ Reactions on ^{17}O

V. Bechtold, L. Friedrich, K.T. Knöpfle+, G. Mairle+, H. Müller+, H. Riedesel+, K. Schindler+, and G.J. Wagner+

Pick-up reactions on ^{17}O excite $1d_{5/2} \cdot 1p_{1/2}^{-1}$ ($J = 2^-, 3^-$) and $1d_{5/2} \cdot 1p_{3/2}^{-1}$ ($J = 1^-, 2^-, 3^-, 4^-$) configurations in $^{16}O(T = 0,1)$ and $^{16}N(T = 1)$. To determine particle-hole matrix elements the relative contributions of $1p_{1/2}$ and $1p_{3/2}$ strengths leading to 2^- and 3^- states need to be known. From a measurement of analyzing powers of these reactions we conclude that only the 2^- states at 8.87 MeV and 12.97 MeV contain noticeable $1p_{3/2}$ admixtures. States above E_x = 17 MeV turned out to contain pure $d_{5/2}\ p_{3/2}^{-1}$ configurations in agreement with previous assumptions (1,2).

References

(1) S.T. Hsieh, K.T. Knöpfle, G. Mairle, and G.J. Wagner, Nucl. Phys. A 234 (1975) 380.

(2) G. Mairle, G.J. Wagner, P. Doll, K.T. Knöpfle, and H. Breuer, Nucl. Phys. A 299 (1978) 39.

+Max-Planck-Institut für Kernphysik, Heidelberg, Germany

2.2.3 Spin Determination of 1p Hole States with Isospin $T = 3/2$ in ^{17}N, ^{17}O, ^{21}F and ^{21}Ne

V. Bechtold, L. Friedrich, K.T. Knöpfle+, G. Mairle+, H. Müller+, H. Riedesel+, K. Schindler+, and G.J. Wagner+

Angular distributions of the $(d,{}^3He)$ reactions on ^{18}O and ^{22}Ne with unpolarized deuterons of 52 MeV have been published previously (1,2). We have now measured analyzing powers of these reactions (for ^{18}O see fig. 1). They show a pronounced j-dependence and a weak mass and Q-value dependence (3) in agreement with DWBA calculations. Interestingly, volume absorption is required

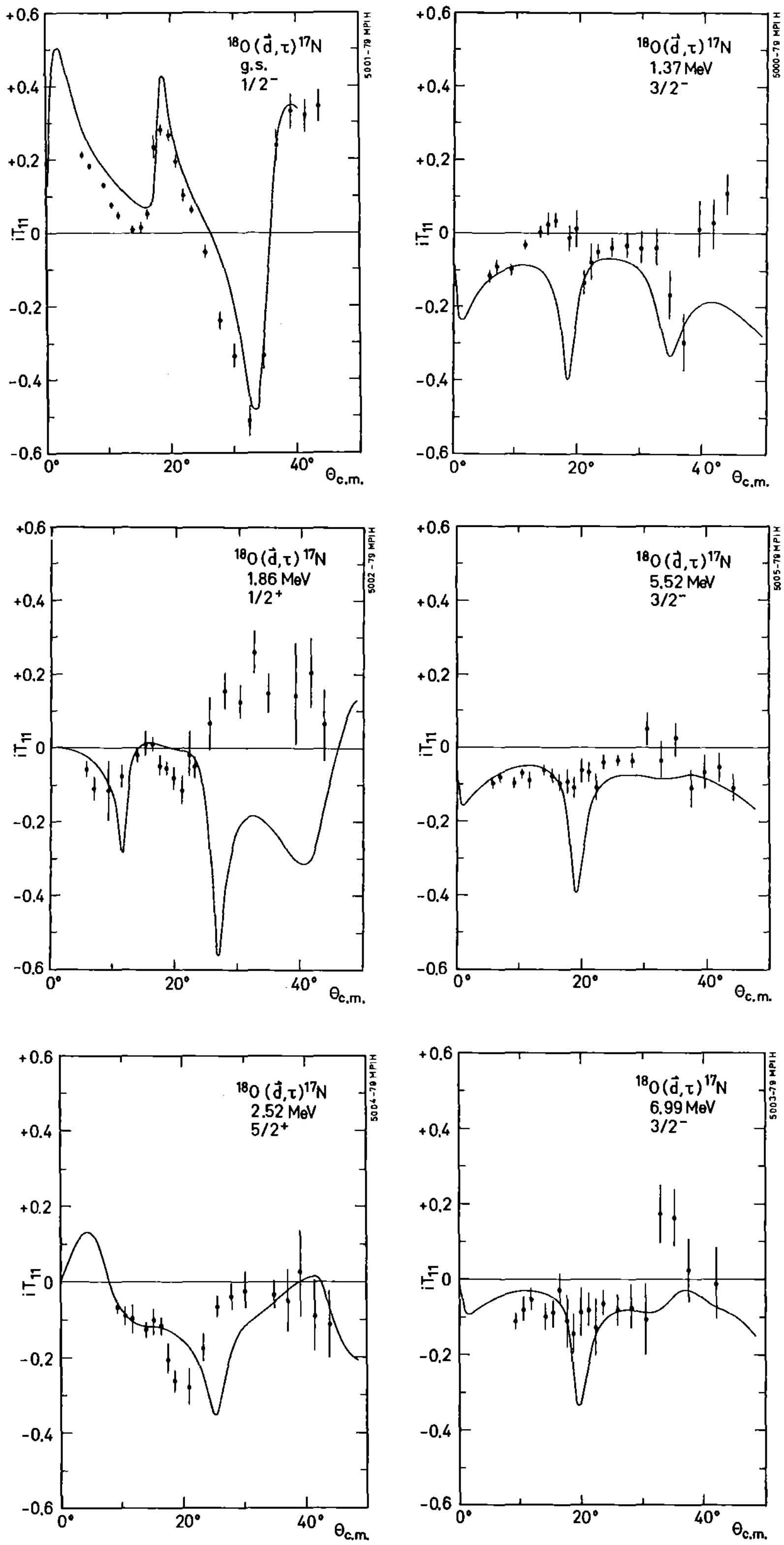

Fig. 1 Analyzing powers from the $^{18}O(\vec{d},\tau)^{17}N$ reaction with DWBA calculations

A_Z	E_x(MeV)	J^π
^{17}N	5.52	$3/2^-$
	6.99	$3/2^-$
^{17}O	16.58	$3/2^-$
	18.14	$3/2^-$
^{21}F	1.10	$1/2^-$
	2.05	$3/2^-$
	5.05	$3/2^-$
	7.65	$3/2^-$
^{21}Ne	9.96	$1/2^-$
	10.90	$3/2^-$
	13.88	$3/2^-$

Table 1
Newly determined spins of 1p hole states with T = 3/2.

in the $\vec{d}$ optical model potential to get a fit in the first maximum of the angular distribution. Spin determination of 1p hole states resulting from our data are given in table 1. Those for analog states in ^{17}O and ^{21}Ne are based on the mirror relationship established by a simultaneous (d,t) and (d,^{3}He) measurements.

References

(1) G. Mairle, K.T. Knöpfle, P. Doll, H. Breuer, and G.J. Wagner, Nucl. Phys. A 280 (1977) 97.
(2) G. Th. Kaschl, G.J. Wagner, G. Mairle, U. Schmidt-Rohr, and P. Turek, Nucl. Phys. A 155 (1970) 417.
(3) V. Bechtold, L. Friedrich, P. Doll, K.T. Knöpfle, G. Mairle, and G.J. Wagner, Phys. Lett. 72B (1977) 169.

+Max-Planck-Institut für Kernphysik, Heidelberg, Germany

2.2.4 Investigation of Nuclear Shape-Effects in the Scattering of Tensor Polarized Deuterons

W. Kretschmer⁺, H. Löh⁺, H. Rebel, W. Stach⁺, P. Urbainsky⁺, and M.B. Wango⁺

The interaction of tensor polarized deuterons with the nuclear field of target nuclei may be understood in analogy to the hyperfine interaction of a non-spherical charge distribution with the electric field gradient. From this, in the case of inelastic scattering of tensor polarized deuterons on $J^{\pi} = 2^{+}$ states a shape effect is expected and the tensor analzying power should be affected by the sign and the magnitude of the quadrupole moment of the target nucleus. We have started experimental studies looking for such effects in the scattering of 10 MeV tensor polarized deuterons on ^{46}Ti (deformed nucleus) and on ^{50}Ti (spherical nucleus) by using the tensor polarized deuteron beam of the Erlangen Lambshift source at the EN-Tandem accelerator. The target current was about 60 - 80 nA with a tensor polarization t_{20} =-.46 (corresponding P_{zz} = -.65). The three tensor analyzing powers T_{20}, T_{21}, T_{22} were measured simultaneously at two scattering angles in 4 π geometry (1) (left, right, up, down with respect to the beam axis). The particle identification was performed with ΔE-E telescopes. The polarization of the beam was monitored in a ^{3}He polarimeter behind the 4 π -chamber. The preliminary results of the 3 tensor analzying powers are shown in fig. 1 for elastic and in fig. 2 for inelastic scattering on both target nuclei ^{46}Ti (open dots) and ^{50}Ti (dots). It should be mentioned that the experiment is still in progress and that further measurements are planned to increase the statistical accuracy of the data.

Reference

(1) G.G. Ohlsen and P.W. Keaton, Jr., Nucl. Instr. and Meth. 109 (1973) 41.

⁺Physikalisches Institut der Universität Erlangen-Nürnberg, Germany

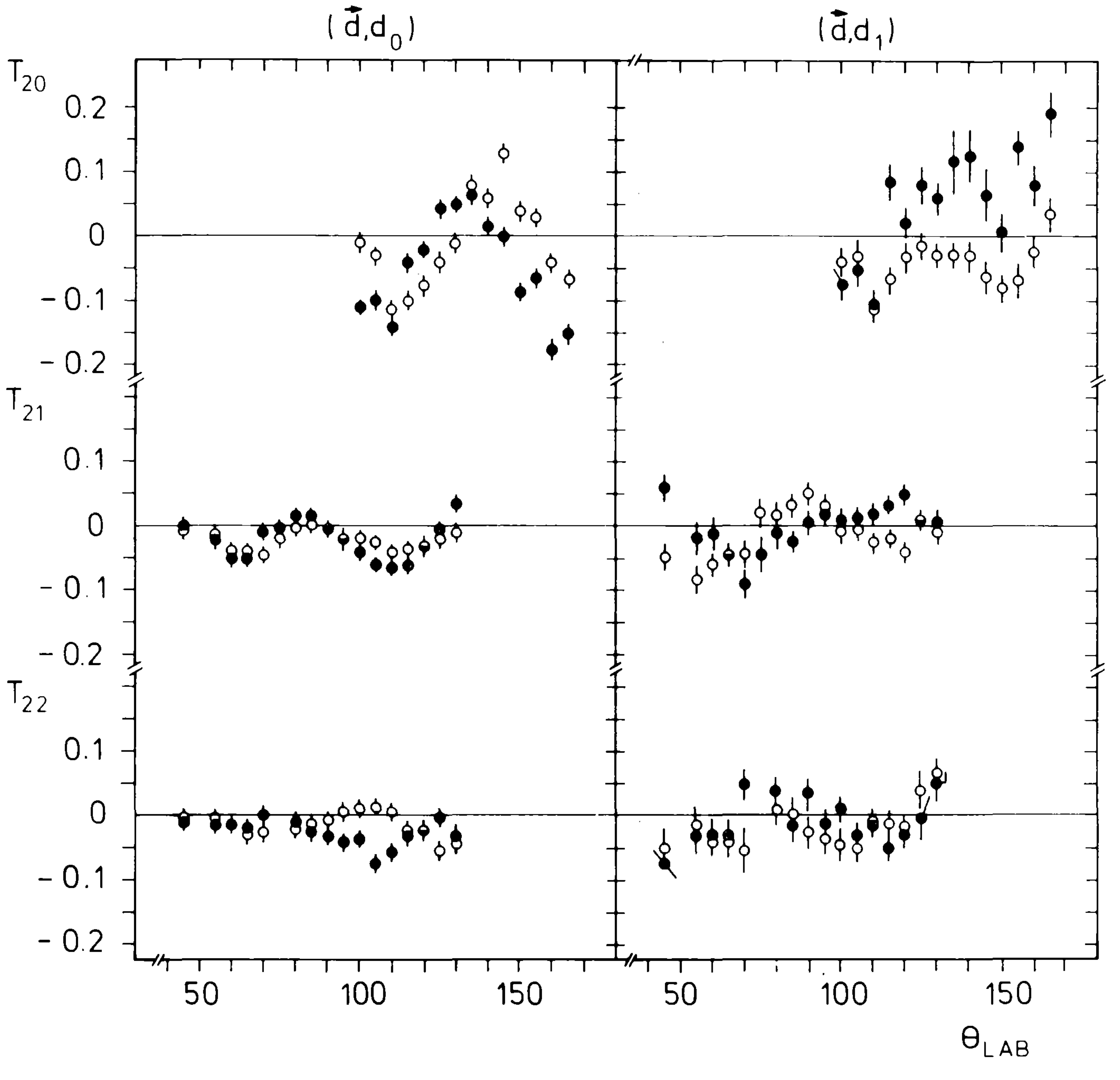

Fig. 1: Tensor analzying power for elastic scattering of 10 MeV deuterons on ^{46}Ti) ( ) and on ^{50}Ti ( ).

Fig. 2: Tensor analyzing power for inelastic scattering (to the first 2^+) of 10 MeV deuterons on ^{46}Ti ( ) and on ^{50}Ti ( ).

2.3 NUCLEAR SPECTROSCOPY

2.3.1 Study of the Giant Resonances in ^{40}Ca by Inelastic Scattering of 104 MeV Alpha-Particles at Forward Angles

W. Eyrich+, A. Hofmann+, H. Rost+, U. Scheib+, S. Schneider+, F. Vogler+, and H. Rebel

A sensitive method to obtain information on giant resonances especially on the giant monopole resonance is the measurement of hadron scattering at extreme forward angles. We applied this method to ^{40}Ca using the 104 MeV alpha-beam of the Karlsruhe Cyclotron. The angular range of $\Theta_{Lab}=4°-16°$ measured in this experiment covers the region of the characteristic minimum of the E0 excitation (1), situated at about $\Theta_{Lab} = 5°$.

In fig. 1 an alpha-scattering spectrum measured at $\Theta_{Lab}=5°$ is shown for the giant resonance region. We analyzed the excitation region between 13.3 MeV and 21.8 MeV. In the giant resonance region of ^{40}Ca besides the known E2 strength around 18 MeV from various experiments indication was found for strength of other multipolarities: $J^{\pi} = 0^{+}$ at 14.2 MeV (2), $J^{\pi} = 0+$ at 20.6 MeV (3) and $J^{\pi} = 3^{-}$ at 16.7 MeV (2). Following the natural structure of the spectra the energy region of interest can be divided into four areas around 14.3 MeV, 16.0 MeV, 18.5 MeV and 21.0 MeV excitation energy as indicated in fig. 1. The subtracted background drawn nearly from minimum to minimum between the bumps of interest is represented by the full curve in fig. 1. The angular distributions of the different bumps were analyzed in the framework of DWBA. The optical potential was taken from ref. (4), the β_L values were adjusted to the experiment by least square fits.

Using this procedure we found an E2-strength of about 35 % of the energy weighted sum rule (EWSR), mostly concentrated in the bump around 18.5 MeV ($\sim$ 25 %) in good agreement with other scattering experiments (4). Practically neither monopole strength could be found around 14.3 MeV nor octupole strength around 16.7 MeV in contradiction to the results of ref. (2). Monopole strength of roughly 12 % of the EWSR was found however around 21 MeV where also a π-scattering experiment (3) gave some evidence for a "breathing mode".

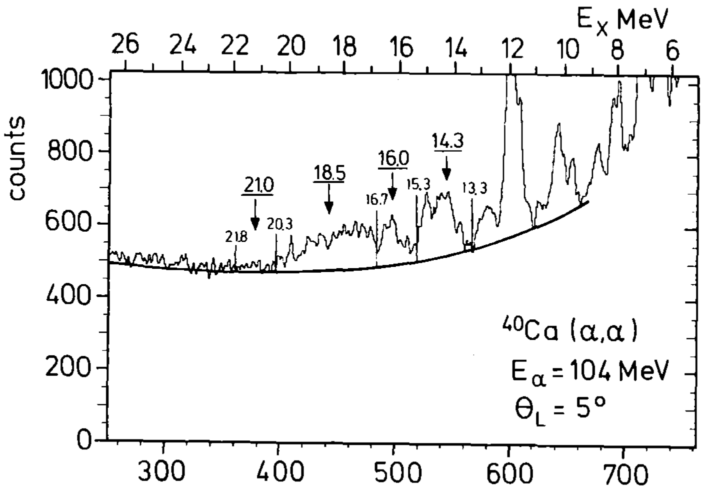

Fig. 1: Alpha particle spectrum at $\Theta_{Lab} = 5^{o}$. The analyzed energy region and the subtracted background are indicated.

The angular distributions of the bumps around 14.3 MeV and 16.0 MeV show steep slopes at extreme forward angles. In the framework of the conventional DWBA this behaviour can only be described by including a considerable dipole strength. A satisfying explanation of this phenomenon could not be found till now, though ,from a (α,γ)-capture experiment (5) there is some evidence of L = 1, T = 0 strength in this energy region. These modes can also be excited by alpha-scattering (cf. ref. (6)).

References

(1) D.H. Youngblood, C.M. Rosza, J.M. Moss, D.R. Brown, J.D. Bronson, Phys. Rev. Lett. 39 (1977) 1188.

(2) T. Yamagata et al., Phys. Rev. Lett. 40 (1978) 1628.

(3) J. Arvieux, J.P. Albanese, M. Buenerd, D. Lebrun, E. Boschitz, and C.H.Q. Ingram, Phys. Rev. Lett. 42 (1979) 753.

(4) D.H. Youngblood, J.M. Ross, C.M. Rosza, J.D. Bronson, A.D. Bacher, and D.R. Brown, Phys. Rev. C13 (1976) 994.

(5) E.M. Diener, J.F. Amann, P. Paul, Phys. Rev. C7 (1973) 695.

(6) G.R. Satchler, Nucl. Phys. A 100 (1967) 481.

+Physikalisches Institut der Universität Erlangen-Nürnberg, Germany

2.3.2 A Study of the Decay of the Giant Resonances in ^{208}Pb via α-γ Angular Correlation Measurements

W. Eyrich[+], A. Hofmann[+], H. Rost[+], U. Scheib[+], S. Schneider[+], F. Vogler[+], and H. Rebel

The investigation of the decay of the giant resonances in ^{208}Pb via (α,γ)-angular correlation measurements of the reaction $^{208}Pb(\alpha,\alpha')^{208}Pb^{GR}(n)$ $^{207}Pb^{*}(\gamma)^{207}Pb$ has been continued. In the preceding annual report (1) we showed that the GR's around 10.9 MeV (GR1) and 13.7 MeV (GR2) decay by nearly 100 % into the lowest states of ^{207}Pb. In the meantime we completed the analysis of the in-plane (α,γ)-angular correlations between the alpha-particles scattered from the GR region and the gamma-quanta belonging to the n-decay into the first and second excited states of ^{207}Pb with subsequent decay into the groundstate, respectively.

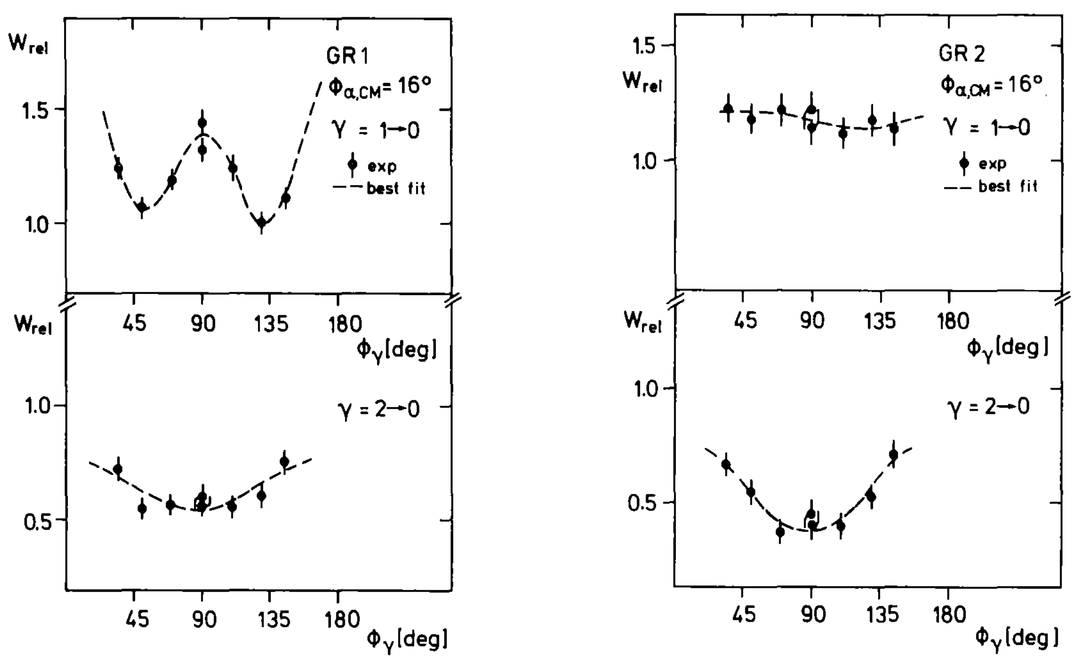

(a) (b)

Fig. 1: Experimental angular correlation functions of the decay of GR1 (a) and GR2 (b) into the first (upper part) and second (lower part) excited state of ^{207}Pb, respectively. The dashed curves are best fits corresponding to the assumption of (a) an E2-mode of GR1 and (b) an excitation mode higher than E0 of GR2, respectively.

The pattern of the angular correlation functions of GR1 (Fig. 1 (a)) confirm the assumption of an E2 mode for this resonance, which was identified as the giant quadrupole resonance from the angular distribution of different scattering experiments (2,3).

In fig. 1(b) the angular correlation functions of GR2 are shown. The correlation function of the decay into the second excited state (lower part), however, shows a significant anisotropic pattern in contradiction to the assumption of pure E0-strength. Consequently there must be considerable strength of higher multipolarities in this resonance. From the fact that an anisotropy occurs at least in one decay channel and from the degree of this anisotropy compared to the correlation function of GR1, we roughly estimate 30 % - 40 % strength of higher multipolarities in the region of GR2.

Another important result can be obtained from the particle spectra coincident to the gamma-quanta of the observed transitions in ^{207}Pb. The GR-bump, which in contrast to the singles spectra appears nearly free of background, shows significant fine structure . More details of the experiment including analyses in the framework of different models for the n-decay will be given in a forthcoming paper.

References

(1) W. Eyrich, A. Hofmann, H. Rost, U. Scheib, S. Schneider, F. Vogler, and H. Rebel, Annual Report, KfK 2686 (1978) 43.

(2) M.N. Harakeh, K. van der Borg, T. Ishimatsu, H.P. Morsch, A. van der Woude, and F.E. Bertrand, Phys. Rev. Lett. 38 (1977) 676.

(3) D.H. Youngblood, C.M. Rosza, J.M. Moss, D.R. Brown, and J.D. Bronson, Phys. Rev. Lett. 39 (1977) 1188.

+Physikalisches Institut der Universität Erlangen-Nürnberg, Germany

2.3.3 Test Measurement for the Investigation of the Neutron Decay of the Giant Resonances in ^{208}Pb

W. Eyrich+, A. Hofmann+, U. Scheib+, R. Stamminger+, H. Steuer+, F. Vogler+, and H. Rebel

In the preceding contribution we reported on a (α,γ)-angular correlation experiment on ^{208}Pb,where the n-decay of the giant resonances (GR) was studied indirectly by observation of the subsequent gamma-decay in the residual nucleus ^{207}Pb. It is a disadvantage of such an (α,γ)-experiment that the n-decay into the groundstate and into isomericstate can not be observed.
The structures of the giant resonances in the region between 9 and 15 MeV have a width of about 3 MeV. Therefore it is also impossible to identify neutrons from the decay of the GR's into the different states in ^{207}Pb in singles spectra. In (α,n)-coincidence experiments without discrimination of the n-energy, however, only very inclusive information can be obtained. We have now started an (α,n)-coincidence experiment where the n-decay to the individual states in ^{207}Pb can be observed. For this purpose an energy resolution of about 300 keV in the n-spectra is necessary. In order to achieve this requirement we use time of flight technique where the start signal is taken from the high frequency supply of the cyclotron and the stop signal from a plastic scintillator (type KL 236 (1)) which detects the neutrons from the target after a flight path of about 2 m. In fig. 1 a neutron time of flight spectrum is shown obtained in a test experiment. The neutron bump coming from the target is indicated.

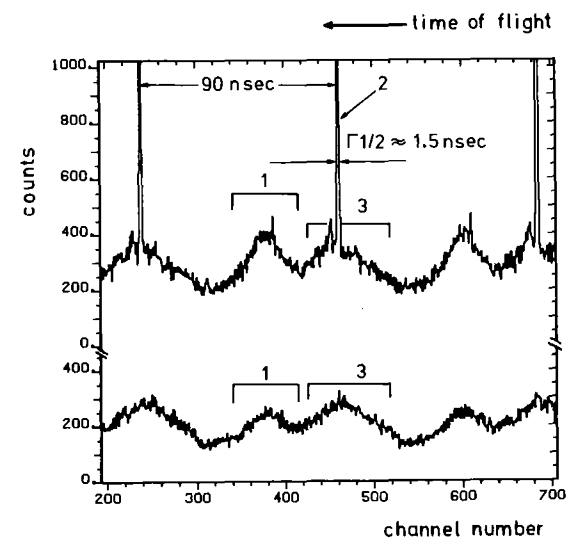

Fig. 1: The time of flight spectrum(high frequency of the cyclotron - plastic scintillator)
1: neutron bump from the target
2: gamma peak from the target
3: neutron bump from the analyzing slits.

From the width of the gamma-peak a time resolution of about 1.5 nsec can be estimated. In our experimental arrangement this corresponds to an energy resolution of 250-300 keV for the neutrons of interest. From the lower part of fig. 1 it can be seen that the gamma background especially that originating from the target can be suppressed nearly quantitatively. The neutron background due to reactions in the slits of the analyzing magnet and in the beam stop could be suppressed sufficiently by shielding with concrete, lead, and paraffin. In a first coincidence run of 10 h neutrons from the decay of the giant resonance region in ^{208}Pb to different states in ^{207}Pb could be identified. The statistical errors, however, are still too large for more quantitative statements.

Reference

(1) R. Stolle, Diplomarbeit 1973, Erlangen, unpublished.

+Physikalisches Institut der Universität Erlangen-Nürnberg, Germany

2.3.4 Tables of Gamma-Rays Observed After Thermal Neutron Capture in ^{99}Tc*

D. Heck and J.A. Pinston+

These tables reproduce the energies and intensities of gamma rays, observed after thermal neutron capture in ^{99}Tc with different setups used at the High Flux Reactor in Grenoble and at the Karlsruhe Research Reactor FR2.

*KfK 2693

+Institut Laue-Langevin, Grenoble , France
Present address: Centre d'Etudes Nucléaires de Grenoble
Department de Recherche Fondamental/CPN, France

2.3.5 Level Structure of ^{100}Tc*

J.A. Pinston[+], W. Mampe[+], R. Roussille[+], K. Schrenkenbach[+],
D. Heck, H.G. Börner[++], H.R. Koch[++], S. André[+++], and D. Barnéoud[+++]

Gamma- and electron-spectra following thermal neutron capture on ^{99}Tc have been studied with a bent-crystal spectrometer Ge(Li)- and Si(Li)-detectors and a magnetic spectrometer. Prompt and delayed gamma-gamma coincidences with Ge(Li)-detectors have been performed. A level scheme is proposed for ^{100}Tc comprising 21 excited states up to 640 keV. The binding energy of the last neutron in ^{100}Tc was deduced. For most levels, spin and parity values were assigned. Two isomeric transitions of respective half-lives 10.2 and 4.6 µs have been identified using the $^{100}Mo(d,2n)^{100}Tc$ reaction with a pulsed beam of deuterons. From the comparison of the present (n,γ) study and the collaborative study of the $^{99}Tc(d,p)$ reaction, several members of the multiplets $\pi g_{9/2}\nu g_{7/2}$, $\pi g_{9/2}\nu d_{5/2}$, $\pi g_{9/2}\nu s_{1/2}$ and $\pi p_{1/2}\nu d_{5/2}$ have been identified.

*Nucl. Phys. A 321, 25 (1979).

[+] Institut Laue-Langevin, Grenoble, France
[++] Institut für Kernphysik, Kernforschungsanlage Jülich, Jülich, Germany
[+++] Institut des Science Nucléaires(IN2P3), Grenoble, France

2.3.6 Delbrück Scattering of 2.75 MeV Photons by Plutonium

M. Schumacher[+], P. Rullhusen[+], F. Smend[+], A. Hanser,
and H. Rebel

One of the most obvious consequences of vacuum polarization is the scattering of photons by the Coulomb field of nuclei, viz. Delbrück (D) scattering. The absorptive part of D-scattering is the shadow scattering process connected with pair production. This part is well known from experiments at very high photon energies (>100 MeV), where it is the dominant scattering process at small angles. The dispersive part may be viewed as being due to a refractive index of the vacuum. This part has been observed for the first time in 1975 at an energy of 2.75 MeV (1).

At energies of a few MeV, D-scattering is a dominant elastic scattering process. Its amplitudes are much larger than those of Rayleigh and nuclear resonance scattering and of the same size as those of nuclear Thomson scattering. This means, that D-scattering is one of the rare cases where QED does not merely modify the process by a small amount, but is responsible for a large fraction of the total process. This makes D-scattering an ideal case for testing the predictions of QED.

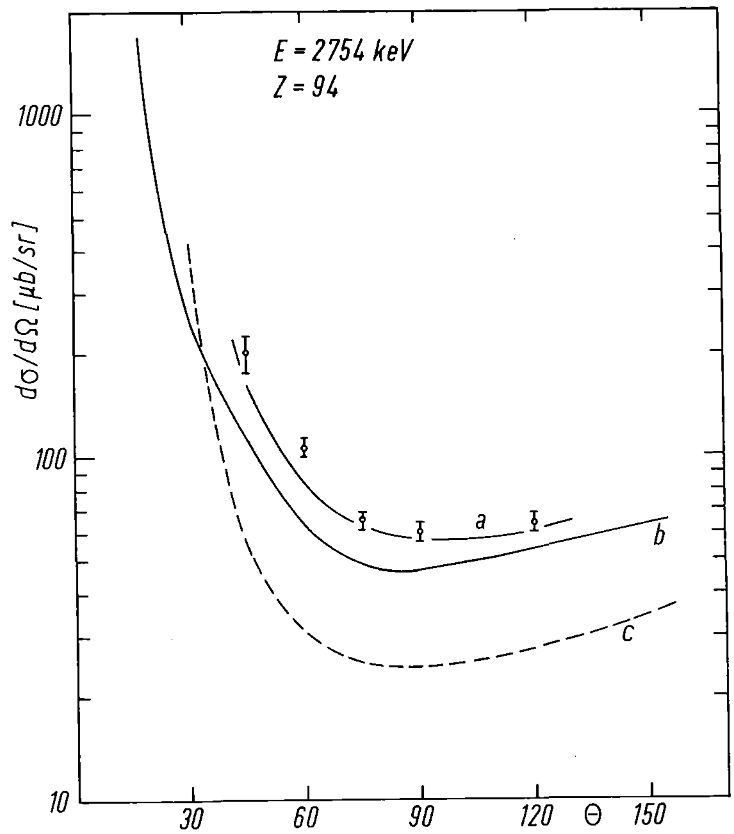

In D-scattering the incident photon creates an electron-positron pair, which in lowest order exchanges two photons with the nucleus. Thus ,the scattering amplitudes are proportional to $(Z\alpha)^2$. Only this lowest-order term, corresponding to a plane-wave approximation for the electron-positron pair, has been calculated up to now. But in principle also higher-order or Coulomb correction terms are possible, the amplitudes of which are expected to be proportional to $(Z\alpha)^4$, $(Z\alpha)^6$ etc. For a complete understanding of D-scattering the knowledge of these Coulomb correction terms is of basic importance.

Previous investigations have revealed large discrepancies between experiment and lowest-order D-theory (2). These discrepancies have been removed (2) by introducing an empirical $(Z\alpha)^4$-Coulomb correction term, except for the very large charge numbers Z = 90 and 92. These remaining discrepancies could not be explained by introducing a $(Z\alpha)^6$-Coulomb correction term, but the comparison of the data at Z = 82 and Z=92 leads to terms with orders of up to $(Z\alpha)^{20}$. Because of these large orders,it has been speculated that part of the discrepancies at Z = 92 might be due to nuclear structure effects.

The presence of Coulomb correction terms with very large orders in Z will lead to a drastic increase of the discrepancies between the lowest-order D-theory and experiment for transuranium elements. On the other hand nuclear strucutre effects are not expected to show a smooth variation with charge number at these energies. Therefore, a further clarification was expected by the present experiment carried out at Z = 94. The results are shown in the figure where the experimental differential cross sections are compared with the lowest-order D-theory (curve b) and with calculations including the empirical $(Z\alpha)^4$-Coulomb correction term (curve a). Curve c has been calculated without including D-amplitudes. In agreement with the observations at Z = 92, the experimental data are in general larger than the predictions including the empirical Coulomb correction term (curve a). However, these discrepancies are smaller in the case of Z = 94 as compared to 92. This means that there is in fact a trend towards the existence of Coulomb correction terms of higher order than $(Z\alpha)^4$, but for a definite statement about the order, data with improved accuracy are required for Z = 92 and below.

References

(1) M. Schumacher et al., Phys. Lett. 59B (1975) 134.
(2) P. Rullhusen et al., Nucl. Phys. A 313 (1979) 307, Phys. Lett. in press.

+II. Physikalisches Institut der Universität Göttingen, Germany

3. LASERSPECTROSCOPY

3.1 Nuclear Charge Radii and Nuclear Moments of Neutron Deficient Ba Isotopes from High Resolution Laser Spectroscopy*

G. Nowicki, K. Bekk, S. Göring, A. Hanser, H. Rebel, and G. Schatz

Isotope shifts and hyperfine structure of the BaI $6s^2\ ^1S_o - 6s6p\ ^1P_1$ transitions (λ = 553.6 nm) in neutron deficient Ba nuclides (N < 82) have been investigated by observing the resonance fluorescence in a well collimated atomic beam with a high resolution tunable CW dye laser. The experiments aimed at information on nuclear charge radii and on nuclear moments. Results are presented for the radioactive isotopes and isomers $^{133}Ba^g$, $^{133}Ba^m$, ^{131}Ba, ^{128}Ba, in addition to remeasurements of all stable Ba nuclides. The extracted values of $\delta\langle r^2\rangle$,the observed odd-even staggering and the nuclear moments are discussed in the light of other theoretical and experimental nuclear structure studies of the region $50 \leq (Z,N) \leq 82$.

*Phys. Rev. C 18 (1978) 2369

3.2 Laserspectroscopic Studies of Collective Properties of Neutron Deficient Ba Nuclei*

K. Bekk, A. Andl, S. Göring, A. Hanser, G. Nowicki, H. Rebel, and G. Schatz

Isotope shifts and hyperfine structure of the BaI resonance line (λ = 553.6 nm) have been measured by dye laser induced resonance fluorescence on an atomic beam for $^{135m,129g,129m,126}Ba$ thus extending previous high resolution measurements of neutron deficient Ba nuclides (N < 82). The experimental results, now available for 16 Ba isotopes and isomers with A=140-126, are used to deduce differences of rms charge radii, magnetic dipole and electric quadrupole moments. While the groundstates display a pronounced odd-even staggering the h 11/2$^-$ isomers ^{135m}Ba and ^{133m}Ba show a decreased staggering. Conspicuously the isomer shift of the g 7/2$^+$ isomer ^{129m}Ba proves to be negative. The nuclear structure information is discussed in the context of gamma-spectroscopic studies of transitional nuclei with $50 \leq N,Z < 82$ and on the basis of a quasi-particle-plus-triaxial rotor model. The isotope shift discrepancy observed is fairly well described by the droplet model.

*Z. Physik A 291 (1979) 219.

3.3 Isotope Shift Measurement for ^{124}Ba

A. Andl, K. Bekk, B. Feurer, S. Göring, A. Hanser, and G. Nowicki

The interest for a further extension of our laserspectroscopic investigation of isotope shifts to lighter and shorter living Ba isotopes arose from the expected sudden change of the intrinsic deformation for nuclei around ^{126}Ba. Kumar and Baranger predicted such a transition from prolate to oblate shape in their extensive studies of nuclei in the Barium mass region on the basis of a pairing plus quadrupole model (1). Dynamic calculations of collective states in even- even Ba and Xe isotopes support this finding (2).

We continued our experiments, measuring the isotope shift of ^{124}Ba. The small production rate of the reaction ^{124}Xe$(\alpha,4n)$^{124}Ba and the short half life of 11.9 min, resulted in a sample of only 10 pg of ^{124}Ba, present in the atomic beam oven at the beginning of the measurements.

Heating at 1550 K provided an atomic beam which was intense enough to study the decrease of the fluorescence spectra in three half lives.

We estimated from the fluorescence intensity to have about 500 atoms/sec of ^{124}Ba in the collimated atomic beam at the beginning of the measurements.

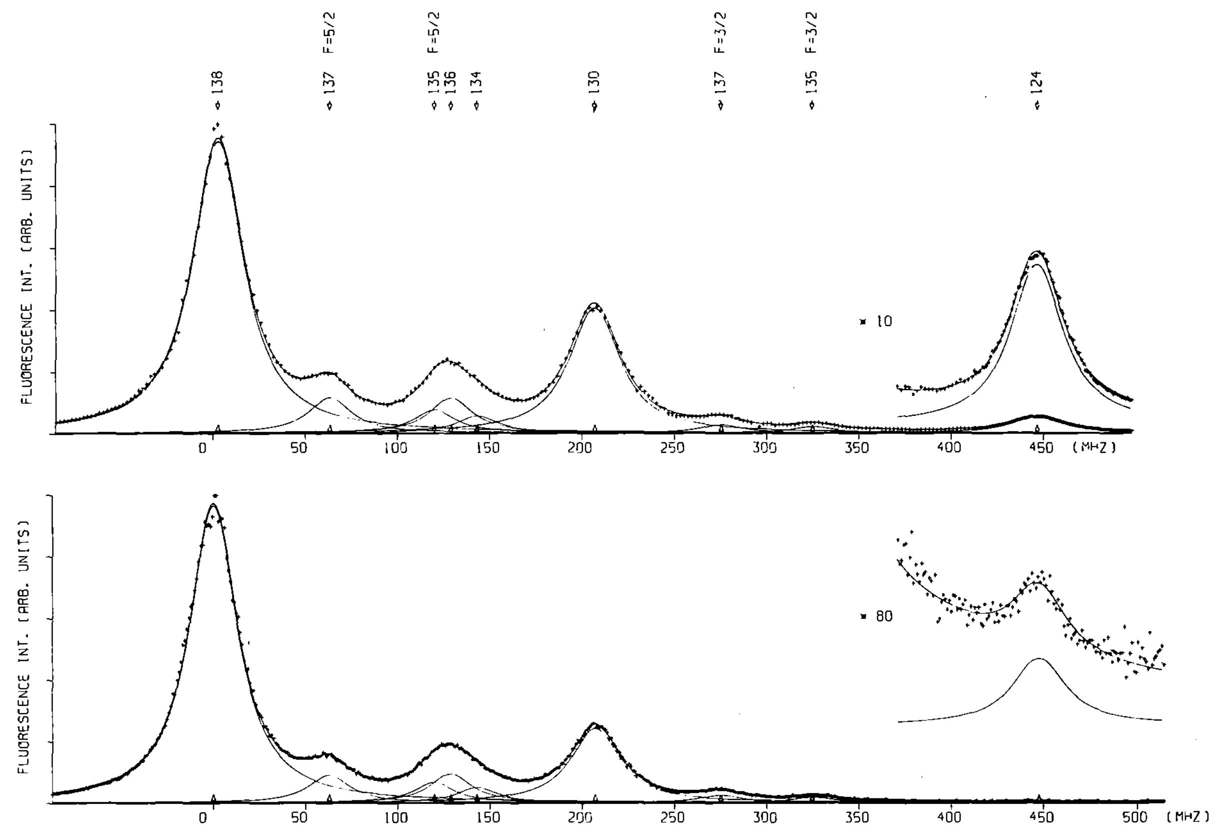

Fig. 1: Two fluorescence spectra taken from a sample of ^{124}Ba. The lower spectrum was measured 35 min later than the upper one.

The measured isotope shift is $(\nu(^{124}Ba) - \nu(^{138}Ba)) = 447\ (1)$ MHz. Using the procedure described in previous papers (3), we extracted the difference of the rms charge radii $\delta\langle r^2\rangle(^{124-138}Ba) = -1.75\ (62) \times 10^{-1}\ fm^2$. As can be seen in fig. 2, this value fits well into the systematic behaviour of the rms charge radii of the heavier isotopes studied before. Calculating the A-dependence of the charge radius from the droplet model, we get a steadily increasing deformation with decreasing neutron number without any hint to a shape transition.

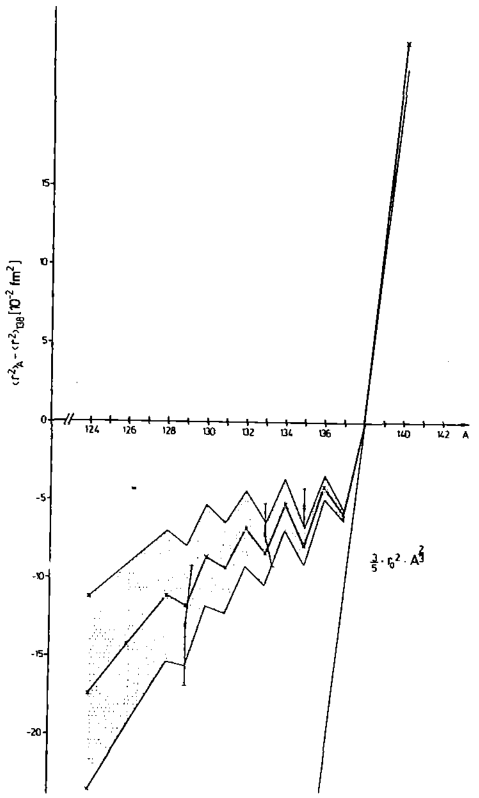

Fig. 2:
Differences of rms charge radii of Barium isotopes. The straight line represents the A dependence expected for the standard homogeneous sphere with r_o = 1.2 fm.

References

(1) K. Kumar and M. Baranger, Phys. Rev. Lett. 12 (1967) 73.

(2) J. Dobaczewski, S.G. Rohozinski, and J. Srebrny, Z. Phys. A 282 (1977) 203.

(3) K. Bekk, A. Andl, S. Göring, A. Hanser, G. Nowicki, H. Rebel, and G. Schatz, Z. Physik A 291 (1979) 219.

3.4 Design of a Jet-Stream Dye Laser

A. Andl, K. Bekk, and G. Nowicki

The dye lasers we used so far in our barium experiments (1) are not suitable for operation with dyes like Stilben needing uv pump light. The high uv power density may cause color centers in the windows of the dye flow cell and high quality laser mirrors coated for such a large wave length range (335 nm - 450 nm), as it would be necessary for the combined pump and folding mirror, are not available. Needing a reference laser for an optical heterodyning experiment (1) at a wave length of 423 nm, we therefore designed a dye laser with folded resonator (2) having a dye jet as active element and a separated pump mirror.

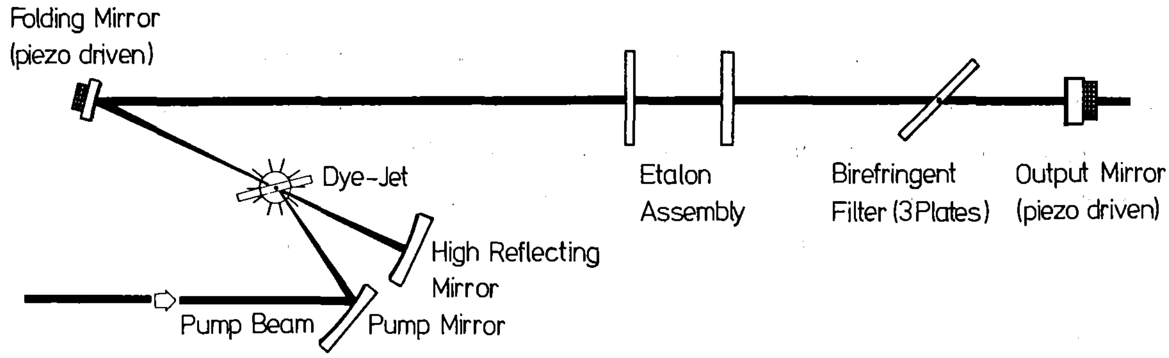

Fig. 1: Optical schematic of the dye laser resonator

The principal layout of this design (fig. 1) is similar to that of commercially available dye lasers. As we don't need a large tuning range, we could optimize this laser for high free running stability and easy and precise adjustment.

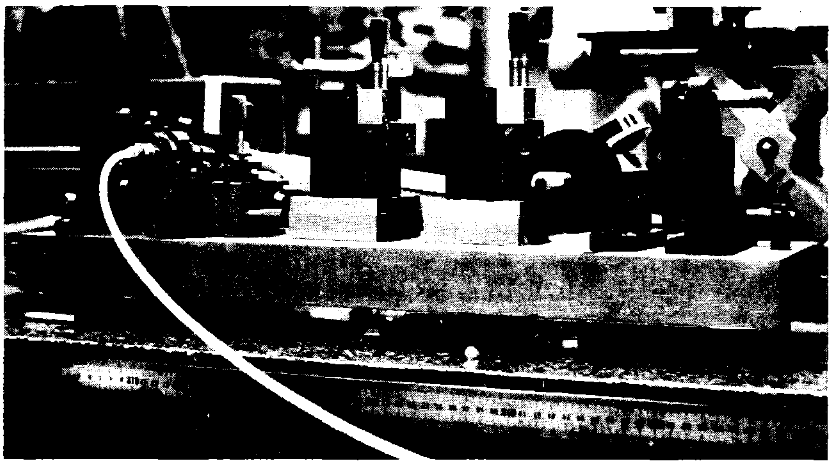

Fig. 2:
Photograph of the dye laser

The optical elements of the resonator are mounted on a large solid invar plate (fig. 2). All these elements including the dye jet are adjustable in position as well as in direction by means of micrometer screws. Coarse frequency selection is achieved by a three elements birefringent filter. Two solid etalons, one of 4 mm thickness coated to 35 % reflection and one uncoated with either 3 mm or 0.6 mm thickness, are sufficient to get single mode operation.

As first results, we achieved the following performance with Stilben 3 pumped by the uv lines of an Ar^{+}-laser: threshold: 500 mW, tuning range: 414-465 nm, multimode power at 453 nm with 3.5 W pump power: 330 mW, single mode power at the same conditions: 70 mW, multimode power at 423 nm: 100 mW, single mode power at 423 nm: 30 mW.

References

(1) G. Nowicki, K. Bekk, S. Göring, A. Hanser, H. Rebel, and G. Schatz, Phys. Rev. C18 (1978) 2369.

(2) H.W. Kogelnik, E.J. Ippen, A. Dienes and C.V. Shank, IEEE J. Quant. Electr. QE8 (1972) 373.

3.5 Atomic Beam Laser Spectroscopy of Radioactive Ba Atoms*

G. Schatz

Experiments to measure hyperfine structures and isotopic shifts on ng to pg amounts of radioactive Ba atoms are described, and a table of the results on 16 stable and unstable nuclides are given. The achieved sensitivity of the applied method and its probable improvements are discussed.

*Proc. of the Fourth International Conference on Laser Spectroscopy, Rottach-Egern, Germany, June 11-15, 1979, to be published.

4. THEORY

4.1 Description of Asymptotic Scattering States in the Generator Coordinate (GC) Method

R. Beck

We consider the scattering of two complex nuclei (mass numbers A and B, proton numbers Z_A and Z_B) and study the connection between channel wave functions as defined by Lane and Thomas (1) and the asymptotic wave functions used in a GC formulation of reaction theory (2).

Let us denote by ψ the solution of the Schrödinger equation in the channel region

$$(\tilde{H} - E)\ \psi = 0 \tag{1}$$

The channel Hamiltonian $\tilde{H}$ is the sum of four parts

$$\tilde{H} = H_o + H_c + H_A + H_B$$

where

$$H_o = - \frac{h^2}{2M} \nabla_R^2$$

$$H_c = - \frac{h^2}{2\mu} \nabla_r^2 + \frac{Z_A Z_B e^2}{r}$$

are the Hamiltonians of the center of mass and relative motion of the two colliding nuclei and H_A and H_B denote the Hamiltonians of internal degrees of freedom of nucleus A and B.

It is shown that eq. (1), when projected onto the space of generator coordinate functions $\psi = \int d^3s\ f\ (\underline{s})\ \phi\ (\underline{s})$, where $\phi\ (\underline{s})$ is a two-center shell model wave function and $\underline{s}$ denotes the vector connecting the centers of the two potential wells, is equivalent to the asymptotic Hill-Wheeler equation

$$\int d^3s'\ \langle\phi\ (\underline{s})\ |H - E|\ \phi\ (\underline{s}')\rangle\ f\ (\underline{s}) = 0 \tag{2}$$

The Hamiltonian H in eq. (2) is given by

$$H = T + V_A^N + V_B^N + V^c ,$$

where $T = - \frac{h^2}{2m} \sum_{i=1}^{A+B} \nabla_i^2$ is the kinetic energy operator,

$$V_A^N = \sum_{r=1}^{2} (-V_r) \sum_{i=j\neq 1}^{A} e^{-(\underline{x}_i-\underline{x}_j)^2/\alpha_r^2} (1-m+mP_{ij}^x) \quad \text{and}$$

$$V_B^N = \sum_{r=1}^{2} (-V_r) \sum_{i\neq j=A+1}^{A+B} e^{-(\underline{x}_i-\underline{x}_j)^2/\alpha_r^2} (1-m+mP_{ij}^x)$$

are the nuclear interactions within nucleus A and B in the parameterization introduced by Volkov (3) and

$$V_c = \sum_{i=j=1}^{A+B} \frac{e^2}{|\underline{x}_i - \underline{x}_j|} \; |1 + \tau_3\,(i)|\; |1 + \tau_3\,(j)|/4$$

is the Coulomb interaction. In calculating the kernels in the asymptotic Hill-Wheeler equation (2) we neglect the nuclear interaction and exchange effects between nucleons belonging to different nuclei.

If we restrict ourselves to two-center shell model wave functions which are built from s-wave single particle functions, the integral kernels in eq. (2) have the form

$$\langle\phi\;(\underline{s})|\phi\;(\underline{s}')\rangle = \exp\left[-\frac{ß}{4}\left(\frac{A\,B}{A+B}\right)(\underline{s}-\underline{s}')^2\right] \tag{3}$$

$$\begin{aligned}\langle\phi\;(\underline{s})|H|\phi\;(\underline{s}')\rangle = {} & \left(\frac{\hbar^2 ß}{2m}\right)\left[\frac{3}{2}(A+B) - \frac{ß}{4}\left(\frac{A\,B}{A+B}\right)(\underline{s}-\underline{s}')^2\right] \\ & + \left[\binom{A}{2} + \binom{B}{2}\right] \sum_{r=1}^{2} (-V_r)\left(1 + \frac{2}{\alpha_r^2\,ß}\right)^{-3/2} \\ & + \left[\binom{Z_A}{2} + \binom{Z_A}{2}\right] e^2\sqrt{\frac{2ß}{\pi}} \\ & + \frac{2Z_A\,Z_B\,e^2}{|\underline{s}+\underline{s}'|}\;\mathrm{erf}\left(\frac{\sqrt{ß'}}{2}\;|s+s'|\right)\langle\phi\;(\underline{s})|\phi\;(\underline{s}')\rangle\end{aligned} \tag{4}$$

where ß is the oscillator parameter of the single particle s-wave and $ß' = ß\,\frac{A\,B}{A+B}$. Using the kernels (3) and (4) in the integral equation (2), we obtain the GC amplitude

$$f_{\ell m}\;(\underline{s}) = Y_{\ell m}\;(\hat{s})\;\frac{1}{2}\exp\left[\frac{k^2}{2ß'}\left(1-\frac{2\eta}{ks}\right)\right]\left\{W_\ell(ks) + \left(\frac{k^2}{ß'}\right)^2 \frac{\eta}{2(ks)^3}\left[\frac{W_\ell\;(ks)}{ks} - W_\ell'(ks)\right]\right\} \tag{5}$$

where $\eta = Z_A Z_B e^2\;\mu/\hbar^2 k$ is the Sommerfeld parameter, $k = \sqrt{2mE}/\hbar$ is the wave number and W_ℓ denotes the solutions of the radial Schrödinger equation of the Coulomb field $$\left[\frac{d^2}{d\rho^2}+1-\frac{2\eta}{\rho}-\frac{\ell(\ell+1)}{\rho 2}\right] W_\ell\ (\rho) = 0.$$

In eq. (5) we neglected higher than quadratic powers in $(\frac{k^2}{\beta\tau})$.

The application of the above result, i.e. the equivalence of the Hill-Wheeler equation with asymptotic kernels and the Schrödinger equation in the channel region, to the calculation of the K-matrix in a GC formulation of scattering theory leads to considerable simplifications.

References
(1) A.M. Lane and R.G. Thomas, Rev. Mod. Phys. 30 (1958) 251
(2) M.V. Mihailović, L.J.B. Goldfarb and M.A. Nagarajan, Nucl. Phys. A273 (1976) 207
(3) A.B. Volkov, Nucl. Phys. 74 (1965) 33

4.2 A Theory for the Transition to Self-Trapping in Spin-Phonon Systems*

R. Beck, W. Götze[+] and P. Prelovsek[++]

The dynamical correlations and thermodynamic functions for a single spin 1/2 experiencing a static external field and a linear interaction with phonons in a direction perpendicular to the field are discussed as a function of the spin-phonon coupling in order to study the abrupt transition from a nearly free spin system to an almost self-trapped situation. The theory is based on a mode-coupling approximation allowing to express the relaxation kernels for the dynamical spin susceptibilities in terms of convolution integrals over the spin excitation spectra. The thermodynamic functions are obtained from transcendental equations expressing the consistency of the static response with the relaxation dynamics. The relevance of the theory for a description of paraelectric impurities is indicated.

* Phys. Rev. (in press)

+ Physik-Department der Technischen Universität München und Max Planck-Institut für Physik, D-8000 München, Germany

++ Department of Physics, University of Ljubljana, 6100 Ljubljana, Yugoslavia

4.3 Hartree-Fock-Bogoliubov-Techniques in the Theory of Nuclear Deformation

F. Dickmann

The experimental evidence on the conservation of nucleon-pairing in low-energy fission (1) accentuates the need for a treatment of this process by means of time-dependent or constrained HFB-theory. Even formal theoretical work, however, is mostly restricted to the HF-approach in order to avoid the clumsiness of the more powerful HFB-treatment. We have thought of some developments of the formalism and notation which simplify the derivation of known and new results and facilitate the task to check formulae. The quasi-particle creation-operator α_m^+ is denoted by $\alpha_{m'}$. Thus, instead of using the conventional sign for Hermitian conjugation, we add a prime to the label m of the one-quasiparticle (1qp) state. A greek label μ can be either m or m' (note that $m'' \equiv m$). This allows to write the most general 1qp-operator $\hat{S}$ in the compact form

$$\hat{S} = S_o + \frac{1}{2} \sum_{\mu\nu} S_{\mu\nu} \alpha_{\mu'} \alpha_{\nu} , \qquad (1)$$

where by convention

$$S_{\mu'\nu'} = - S_{\nu\mu}. \qquad (2)$$

The factor 1/2 in front of the sum avoids double counting, since μ and ν run over twice as many values as usual. A general unitary HFB-transformation from a given qp-basis α to a new basis ß can be expressed by means of an Hermitian 1qp-operator $\hat{S}$:

$$ß_{\mu} = e^{i\hat{S}} \alpha_{\mu} e^{-i\hat{S}}. \qquad (3)$$

One can prove that

$$ß_{\mu} = \sum_{\nu} \left(e^{-iS}\right)_{\mu\nu} \alpha_{\nu} = \sum_{\nu} \alpha_{\nu} \left(e^{iS}\right)_{\nu'\mu'} , \qquad (3)$$

where the matrix S has the elements $S_{\mu\nu}$. The matrix exp (-iS) is unitary. Special cases of the general transformation are

(i) the HF-transformation, for which $S^{(1)}_{m\,n'} = 0$, (4a)

(ii) the BCS-transformation, for which $S^{(2)}_{\mu\,\nu} = S^{(2)}_{\mu\bar{\mu}'} \, \delta_{\nu\bar{\mu}'}$. (4b)

The bar above the state-label indicates time-reversal as usual. For the quasiparticle-vacua associated with the bases α and ß the following relation holds:

$$\text{If} \quad \alpha_m \,|0\rangle = 0, \text{ then } \beta_m \,(e^{i\hat{S}}\,|0\rangle) = 0 \tag{5}$$

The form in which the ß-vacuum is written reminds of Thouless' theorem. However, since the qp-transformation (eq. (3)) is unitary the α - and ß - vacua have the same norm and can even be orthogonal. The conditions of stationarity and stability for the mean value $\langle 0\,|\hat{G}|\,0\rangle$ of the constrained Hamiltonian $\hat{G}$ have the same formal appearance as for the HF-case. Also special results that have no equivalent in HF-theory are easily derived. Exploiting e.g. the theorem of Bloch and Messiah (2) the condition of stationarity can be written as

$$\text{Trace}\left(S^{(1)}\, e^{iF}\,[R,g]\, e^{-iF}\right) = 0, \tag{6a}$$

$$\text{Trace}\left(S^{(2)}\, e^{iF}\,[R,g]\, e^{-iF}\right) = 0 \tag{6b}$$

for arbitrary Hermitian matrices $S^{(j)}$ subject to the conditions given in eqs. (4). The unitary HF-matrix exp (iF) transforms the density R to the normal form of Ref. (2) and g denotes the 1qp-matrix obtained by normal ordering the constrained Hamiltonian with respect to the state $|0\rangle$. The form of eqs (6) for the condition of stationarity is especially suitable for the study of the decrease of pairing-correlations that occur when a nucleus deforms non-adiabatically.

References

(1) H. Nifenecker, I. Blachot, J.P. Boquet, R. Brissot, J. Crancon, C. Hamelin, G. Mariolopoulos and Ch. Ristori
Proceedings of the 4th Symposium on Physics and Chemistry of Fission, Jülich 1979, paper F1

(2) C. Bloch and A. Messiah, Nucl. Phys. 39 (1962) 95

5. APPLIED NUCLEAR PHYSICS

5.1 NUCLEAR FUEL ANALYSIS

5.1.1 Results from Test Measurements on ^{235}U Enrichment Prototype Samples

H. Eberle and P. Matussek

The European Safeguards Research and Development Association, in collaboration with the National Bureau of Standards, USA, has started a program to provide the users of the gammaspectrometric ^{235}U enrichment analysis technique with suitable physical calibration standards. In the course of this program 20 prototype standards have been prepared by CBNM Geel. They consist of U_2O_8 powder sealed in specially designed aluminium containers. The samples are circulated to four different laboratories for independent measurements: CBNM Geel, JRC Ispra, NBS Washington and KfK Karlsruhe. It is the aim of these measurements

i) to verify that the production of the physical standards with tightly specified tolerance limits is possible

ii) to study in particular the effect of variable powder density on the enrichment measurement.

The following 4 subset of samples were included in the 20 prototype standards distributed for comparison measurements: i) 4 identical samples with enriched (2.95 % ^{225}U) uranium, ii) 5 samples of identical enrichment (2.95 %) but variable powder density, iii) 6 identical samples with natural uranium, iv) 5 identical samples with depleted (0.298 %) uranium. The enrichment values, total U_3O_8 mass and mean powder density were given by CBNM. The bottom thickness of the containers has been measured independently at KfK by means of an ultrasonic gauge with an accuracy of less than 5 μ. The gamma measurements were performed by placing the samples directly on a cylindrical lead collimator (diameter 4 cm, depth 2 cm) above a Ge(Li) detector. We used a 13 ccm coaxial Ge(Li) detector with an energy resolution of 830 eV at 185 keV and a digitally stabilized multichannel analyzer. Typical measuring times were 20 000 to 400 000 seconds per sample depending on the enrichment value. The net peak count rate of the 185 keV gamma line from ^{235}U was determined by the channel summation method within the energy interval from 184.0 to 187.4 keV after subtraction of a smooth step-like background line below the peak (1).

The reproduceability of the 185 keV peak count rate, which is exactly proportional to the ^{235}U enrichment for thick samples, was tested for each set separately. Some samples were measured repeatedly at different times, others were replaced or turned around after each measurement to check for the influence of sample positioning and operational stability of detector and electronics. The results of all measurements are given in Fig. 1, which shows the relative deviation from the mean value of the 185 keV peak count rate for each subset. The precisions calculated from counting statistics vary between 0.02 % and 0.07 % for a single measurement. This compares well with the measured standard deviations which range from 0.05 % to 0.08 % for the different subsets. The latter values include counting statistics as well as sample-to-sample variations and instabilities of the experimental setup.

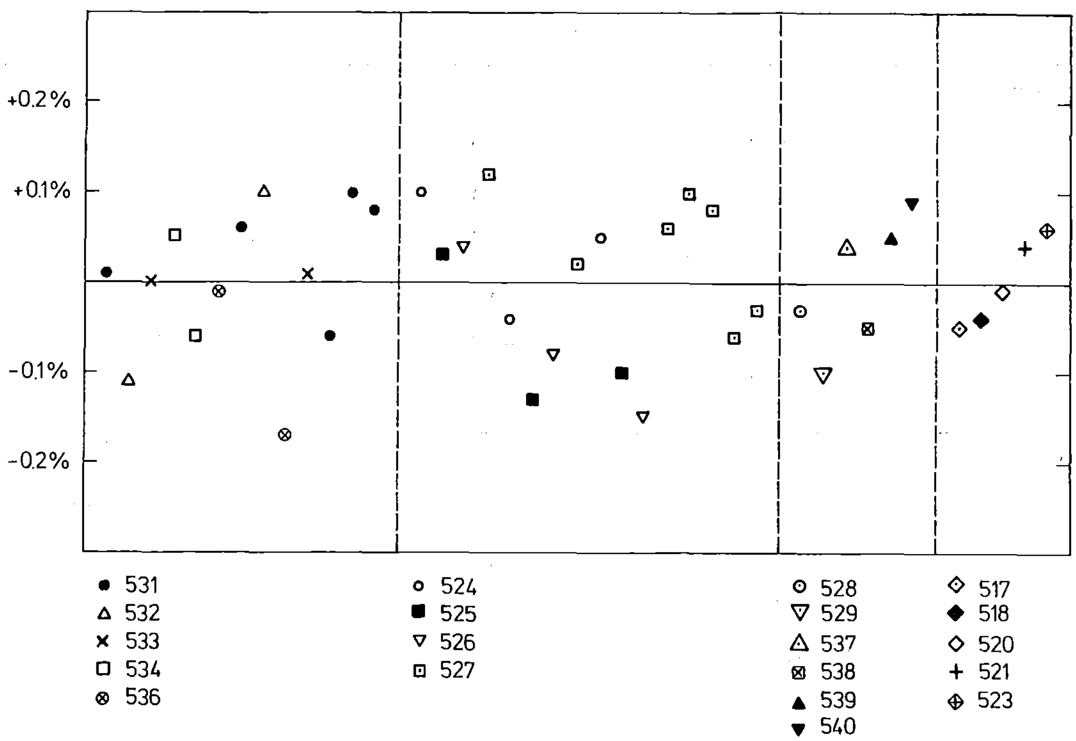

Fig. 1. Relative deviations from mean values of the 185 keV peak count rates for the 4 different sets of prototype samples.

Table 1 Characteristic parameters of the ^{235}U Enrichment Prototype Samples

Sample No. (nominal $^{235}U/U$ atom ratio)	Mass U_3O_8 (± 0.15 g) (g)	Mean Density (calculated) (g/cm^3)	Mean bottom thickness and stand. deviation (mm)
Enriched (0.030)			
531	200.4	1.99	1.994 ± 0.007
532	200.1	2.00	1.989 ± 0.005
533	200.3	2.24	1.997 ± 0.003
534	200.2	2.24	2.009 ± 0.004
536	200.3	2.70	2.010 ± 0.002
524	200.2	2.48	2.038 ± 0.008
525	199.7	2.50	2.035 ± 0.006
526	200.0	2.55	2.045 ± 0.010
527	200.2	2.48	2.035 ± 0.007
Natural (0.0072)			
528	200.0	2.5	2.024 ± 0.010
529	199.8	2.5	2.035 ± 0.010
537	200.1	2.5	2.013 ± 0.007
538	205.2	2.5	2.014 ± 0.011
539	195.3	2.5	1.986 ± 0.012
540	200.2	2.5	2.005 ± 0.007
Depleted (0.0030)			
517	-	2.5	2.004 ± 0.008
518	202.7	2.36	2.027 ± 0.005
520	199.9	2.46	2.002 ± 0.006
521	200.0	2.48	2.016 ± 0.008
523	200.2	2.46	2.026 ± 0.005

The experiment has demonstrated the validity of the fabrication concept for the final calibration standards. The present results show that the total error introduced by the nonuniformity of the samples can be kept well below 0.1 %.

References

(1) R. Gunnink, J.B. Niday and P.D. Siemens, Report UCRL-51577 Pt. 1, (1974).

5.1.2 A Computerized ^{235}U Enrichment Monitor for Continuous Process Control Measurements in an LWRM Fuel Fabrication Plant*

P. Matussek and H. Allex+

A computerized ^{235}U enrichment assay system based on gamma-ray spectrometry is described. It monitors continuously the enrichment of the low enriched uranium oxide powder processed to pellet presses in an LWR fuel fabrication plant. Details of the system and first operational experiences are reported.

*Proceedings of the 1st Symposium of the European Safeguards Research and Development Association (ESARDA) on "Safeguards and Nuclear Material Management", Brussels, 25-26 April 1979.

+Reaktor-Brennelement Union GmbH, D-6450 Hanau, Germany

5.1.3 Analysis of the Uranium Concentration in Reference Solutions by K-Edge Gamma Densitometry

H. Eberle, P. Matussek, I. Michel-Piper, and H. Ottmar

The existing K-edge gamma absorptiometry system equipped with an a.c. high voltage X-ray generator (160 kV) has been used for further investigations of the K-edge densitometry technique. In particular, the linearity of the response, the influences of matrix effects, and the long-term stability behaviour have been examined in more detail. A set of 10 uranium solutions prepared by the Radiochemistry Division served as reference samples for the gamma transmission measurements. The uranium concentration values in the reference samples, which had been determined by gravimetry, ranged between 30 g/l and 260 g/l. The solutions had been filled into accurately dimensioned quartz and stainless steel cells, with effective transmission path lengths ranging between 2 cm and 15 cm. For the analysis of the gamma transmission measurements, the previously described analysis procedure /1/ has been adopted.

When the results from the K-edge absorptiometry are normalized by the method of least squares to the chemical reference values, the relative differences plotted in Fig. 1 are observed between both analyses.

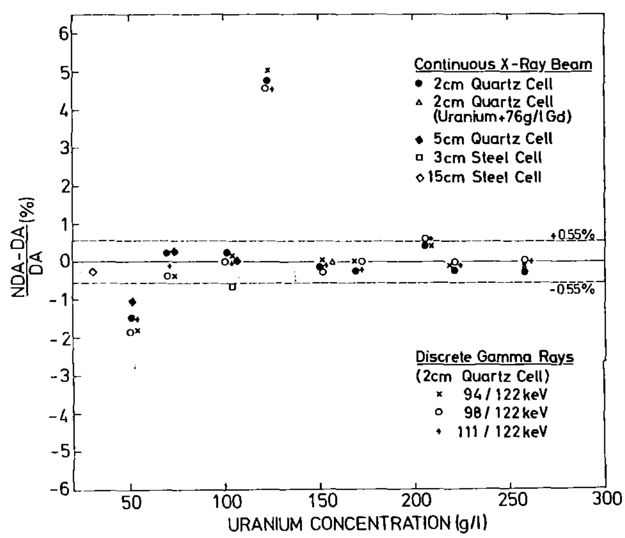

Fig. 1. Relative differences of uranium concentrations in solutions determined by K-edge absorptiometry and gravimetry. The error band of ± 0.55 %, represents the combined error from the absorptiometry measurements (0.25 %) and from the chemical analysis (0.3 %).

The error band of ± 0.55 % represents the combined error from the chemical analysis (0.3 %) and from the K-edge absorptiometry. The experimental data points are within this error band, with the exception of significantly differing results obtained for 2 out of the 10 samples. No satisfactory explanations could be found for the latter deviations.

In order to further substantiate the K-edge absorptiometry results obtained from the transmission measurements with the continuous x-ray beam, also pairs of discrete gamma lines bracketing the K-absorption edge have been employed for transmission analyses. For this purpose we used fluorescence radiation from uranium in conjunction with the 122.06 keV gamma rays from a ^{57}Co source for uranium concentration measurements. The experimental setup is shown in Fig. 2. The thickness of the fluorescent uranium foil (D = 300 μm) is chosen such that it is still transparent for the ^{57}Co gamma radiation, but also thick enough to provide sufficient fluorescent intensity. Fig. 3 shows the intensity distribution of the

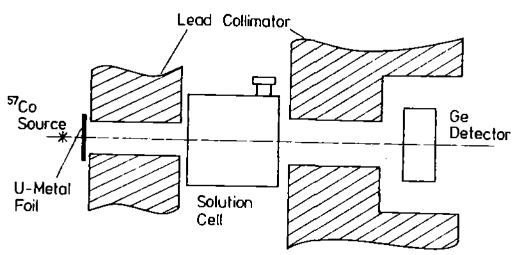

Fig. 2. Experimental set-up for K-edge densitometry using fluorescent uranium X rays and ^{57}Co gamma rays.

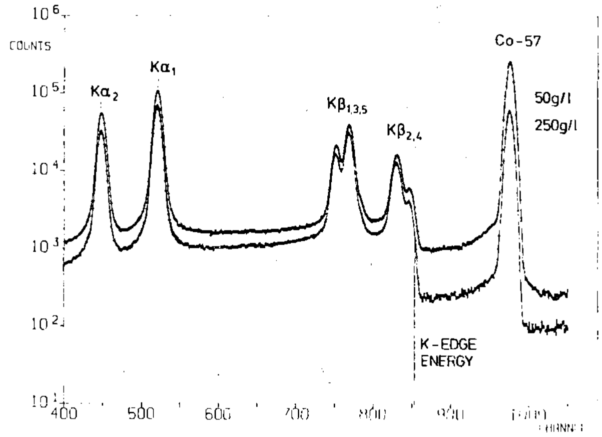

Fig. 3. Transmission spectra for different uranium concentrations in the solutions.

transmitted radiations for different uranium concentrations. The results from the transmission measurements with the uranium $K\alpha_1$, $K\alpha_2$ and $K\beta_{1,3,5}$ X rays (the $K\beta_{2,4}$ X rays have been excluded from the analysis because of the difficult background assessment near the absorption edge), and with the 122 keV ^{57}Co gamma rays are also included in Fig. 1. They are in close agreement with the results from the continuous beam measurements. Within the experimental uncertainty, the results shown in Fig. 1 do not indicate any deviation from the linear response of the transmission ratio measurements with respect to the heavy metal concentration of the solution.

Long-term measurements with the present equipment have shown a relative long-term stability and reproduceability of better than 0.3 %. A new system has now been set up including a d.c. high voltage X-ray generator which permits much faster analyses. At the same integral detector countrate, a factor of six will be gained in time in comparison to the measurements with the a.c. generator.

References

(1) P. Matussek, I. Michel-Piper, and H. Ottmar, Report KfK 2686 (1978) 85.

5.1.4 Relative Total Photon Cross Section of Uranium Near the K-Absorption Edge

P. Matussek, I. Michel-Piper, and H. Ottmar

The K- or L-edge densitometry for the determination of heavy element concentrations in solutions makes use of the discontinuity of the total absorption photon cross section at element specific energies. This technique exhibits the attractive feature that absolute concentration measurements can be performed without calibration standards, provided the difference of the total photon-cross section $\Delta\mu$ is precisely known for two energies closely bracketing the absorption edge. For uranium we measured the total photon cross section differences at selected energies and the height of the K-edge jump.

As a source of discrete gamma rays near the uranium K-absorption edge we used the fluorescence X-ray radiation from an uranium metal foil in conjunction with the 122.06 keV gamma rays from a ^{57}Co source. The transmission values were corrected for fluorescent uranium X-rays produced in the measured sample. The K- edge cross section jump was determined using a continuous energy photon beam from an X-ray generator. The experimental setup and the data evaluation procedure is described in ref. (1).

The measurements have been performed on 10 reference uranium nitrate solutions within precision quartz cells using a highly collimated narrow beam geometry. The uranium concentrations range from 30 g U/l to 260 g U/l.

Table 1 shows our measured values of the total photon cross section differences at various energies together with those obtained from compilations for photon cross sections. The data compiled by Veigele (2) are nearest to our experimental results.

Table 1. Comparison of Experimental and Theoretical Total Photon Cross Section Differences for Uranium

	Total Photon Cross Section Differences $\Delta\mu (cm^2/g)$			
Energies (keV)	Storm and Israel /3/	Veigele /2/	McMaster et al. /4/	Experimental This work
122/112	2.772	2.837	2.870	2.832 ± 0.014
122/98	2.274	2.339	2.363	2.323 ± 0.014
122/94	2.097	2.145	2.162	2.127 ± 0.012
115.61 / K-Edge Jump	3.501	3.605	3.651	3.578 ± 0.02

References

(1) P. Matussek, I. Michel-Piper, and H. Ottmar, Report KfK 2686 (1978) 85.

(2) W.M.J. Veigele, Photon Cross Sections from 0.1 keV to 1 MeV for Elements Z = 1 to Z = 94, Atomic Data Tables 5 (1973) 51-111.

(3) E. Storm, H. Israel, Photon Cross Sections from 1 keV to 100 MeV for elements Z = 1 to Z = 100, Nuclear Data Tables 7 (1970) 6.

(4) W.H. McMaster, N.K. Del Grande, J.H. Mallett, J.H. Hubbell, Compilation of X-ray Cross Sections, Rep. UCRL-50174 R, Section 2 (1969).

5.1.5 Determination of Plutonium Isotopic Composition by Gamma Spectrometry: Results from Interlaboratory Comparison Measurements Organized by ESARDA*

H. Ottmar and H. Eberle

The present status of the non-destructive plutonium isotopic analysis technique using high-resolution gamma spectrometry is evaluated in the light of results which have been obtained from interlaboratory comparison measurements initiated and organized by the ESARDA working group on NDA techniques. The analysis results provided by nine different laboratories permit a fairly accurate assessment of the present capabilities and limitations of the gamma-spectrometric plutonium isotopic analysis techniques.

*Proceedings of the 1st Symposium of the European Safeguards Research and Development Association (ESARDA) on "Safeguards and Nuclear Material Management", Brussels, 25-26 April 1979.

5.1.6 Non-Destructive Elemental and Isotopic Assay of Plutonium and Uranium in Nuclear Materials*

H. Eberle, P. Matussek, H. Ottmar, I. Michel-Piper, M.R. Iyer[+], P.P. Chakraborty[+]

Non-destructive assay techniques based on the analysis of X rays and isotopic gamma rays have been employed for elemental and isotopic analysis of uranium and plutonium materials. The selected techniques of analysis include high-resolution gamma spectrometry for plutonium isotopic analysis of small and bulk plutonium samples, energy-dispersive X ray fluorescence analysis of K X rays for plutonium enrichment measurements in mixed U-Pu fuels, and K-edge gamma densitometry for the special nuclear material assay in solutions. The intrinsic calibration approach has been adopted for the evaluation of the parameter of interest from the various measurements. The results obtained from the non-destructive intrinsic calibration measurements compare reasonably well with the known reference values from destructive analyses. Some suggestions for the proper adjustment and choice of published atomic and nuclear data entering into the procedure of intrinsic calibration are given.

*Proceedings of the International Symposium on Nuclear Material Safeguards, Vienna, 2-6 October, 1978, IAEA (1979).

+Delegates from Bhabha Atomic Research Centre, Bombay, India

5.2 ELEMENTAL ANALYSIS

5.2.1 Determination of Neptunium and Plutonium Impurities in Americium Samples by K-Edge Gamma Absorptiometry

I. Michel-Piper and H. Ottmar

At the request of our Van de Graaff group we have analyzed nondestructively two americium samples for possible contamination by plutonium. The samples which physically consisted of sintered AmO_2 sealed in stainless steel capsules had been used for neutron cross-section measurements. The suspicion existed that the samples contained some plutonium, which, of course, would have affected the fission cross-section measurements. Table 1 summarizes some characteristics of the samples.

The existing setup designed for special nuclear materials concentration measurements by K-edge gamma absorptiometry was employed for the analysis of the samples. In this setup a filtered and wellcollimated X-ray beam is extracted from a 160 kV X-ray generator for gamma transmission measurements. The americium samples was viewed by an X-ray detector through a lead collimator which had a diameter of 0.2 cm, and a length of 15 cm. A 12 cm long plug of aluminium inserted into the collimator hole both served for shaping the primary X-ray beam and for the attenuation of the gamma radiation from the samples. No problems have been experienced with the intrinsic radiation from the large americium samples.

Fig. 1 shows the continuous X-ray spectrum transmitted through one of the samples. The elements neptunium (the decay product of americium), plutonium and americium are easily identified by the discontinuities of the transmission spectrum at the respective K-absorption edges. The element ratio, N_1/N_2, of two elements directly deduces from the measured ratio of the transmissions, R, below and above the respective K-edge energies:

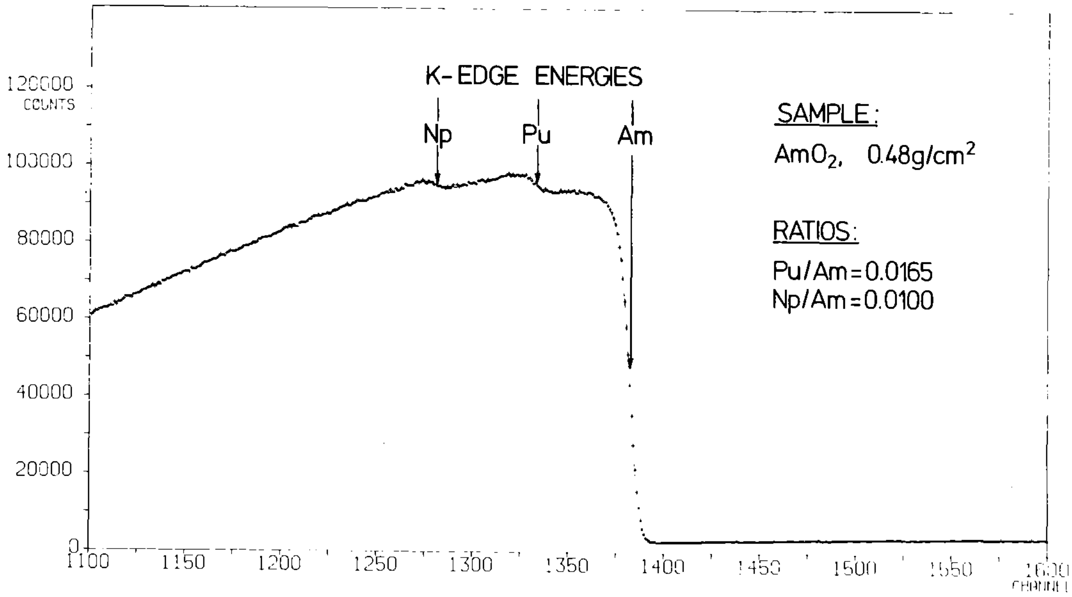

Fig. 1. Continuous X-ray beam after the transmission through sample No. 2.

$$N_1/N_2 = \frac{\ln R_1}{\ln R_2} \cdot \frac{\Delta\mu_2}{\Delta\mu_1} .$$

$\Delta\mu$ is the change of the total photon cross section at the K-absorption edge. The $\Delta\mu$ values from Ref.1 have been used for the element ratio evaluations. The results of the analysis are listed in Table 1.

Table 1. Characteristics of the Americium Samples

Physical Properties	Sample 1	Sample 2
AmO_2 Weight	3.56 g	3.24 g
Diameter	17.7 mm	30 mm
Mass per Unit Area	1.45 g/cm^2	0.46 g/cm^2
Assay Results		
Np/Am Ratio	0.0135 ± 0.0006	0.0100 ± 0.0006
Pu/Am Ratio	<0.002	0.0165 ± 0.0008

A plutonium content of 1.65 % has been determined for sample no. 2 (Fig. 1). The transmission spectrum obtained from sample no. 1 did not indicate any plutonium. If present, the plutonium content in this sample must be below the detection limit of 0.2 %.

A few months after the present analyses sample no. 2 was destroyed for chemical analysis. A plutonium content of 1.63 $\pm$ 0.03 % was obtained using the isotope dilution technique. This agrees very well with the value of 1.65 $\pm$ 0.08 % obtained from the K-edge absorptiometry.

References

(1) E. Storm and H. Israel, Nuclear Data Tables 7, 6 (1970).

5.2.2 Bulk Sample Analysis of Pd-Alloys with PIXE

D. Heck

Proton induced x-ray emission (PIXE) has been used for quantitative determination of elemental concentrations in Pd-alloy bulk samples. To get the peak area of the characteristic gamma-rays, one has to integrate the production of x-rays along the path x of the protons. The concentration c of element Z is proportional (1) to

$$c_Z \sim \int_o^R \sigma_Z(x) \cdot \exp\,(-\,\mu_{mz} \cdot \rho \cdot a \cdot x)\, dx$$

The protons are slowed down (2) and come at rest after the range R. As the production cross section σ_Z (ref. 3) is energy dependent, σ_Z varies along x. The emitted x-rays penetrate the matrix material of density ρ with the mass absorption coefficient μ_m (ref. 4). The penetration length is proportional to x for samples with a plane surface. The constant a is given by a = $\tan\alpha/\tan\beta$, where α and ß are the angles between the surface normal and the incident protons respectively emitted x-rays.

The contribution to the x-ray yield as a function of depth is drawn in fig. 1 for ferromagnetic metal contaminations in the matrix metal Pd. For matrices of Pd alloys with contents $\leq$ 10 % of Rh or Ag the changes in the curves are negligible.

Problems arise from pulse pile-up, as the K x-ray energies of the contaminant elements are just about twice the energy of the Pd_L x-rays. Filtering with 20 µm Al-foil suppresses pile-up by a factor of 10^4, while the interesting line intensities are reduced to ∿ 55-75 %. Fig. 2 shows the X-ray spectrum of a Pd + 10 % Ag alloy. The detection limit, which is given by counting statistics, is about 15 ppm for integrated charges of 15 μC.

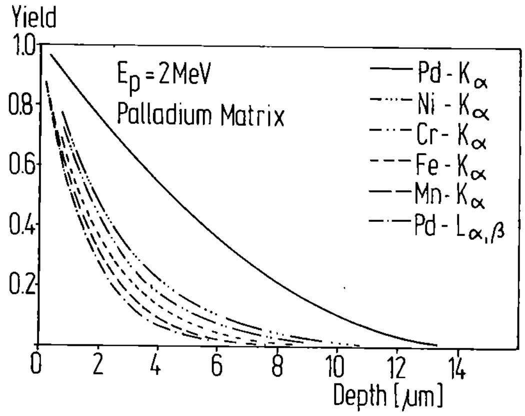

Fig. 1. Contribution to the x-ray yield as a function of depth for ferromagnetic contaminations in the matrix metal Pd (parameters α = ß = 45°).

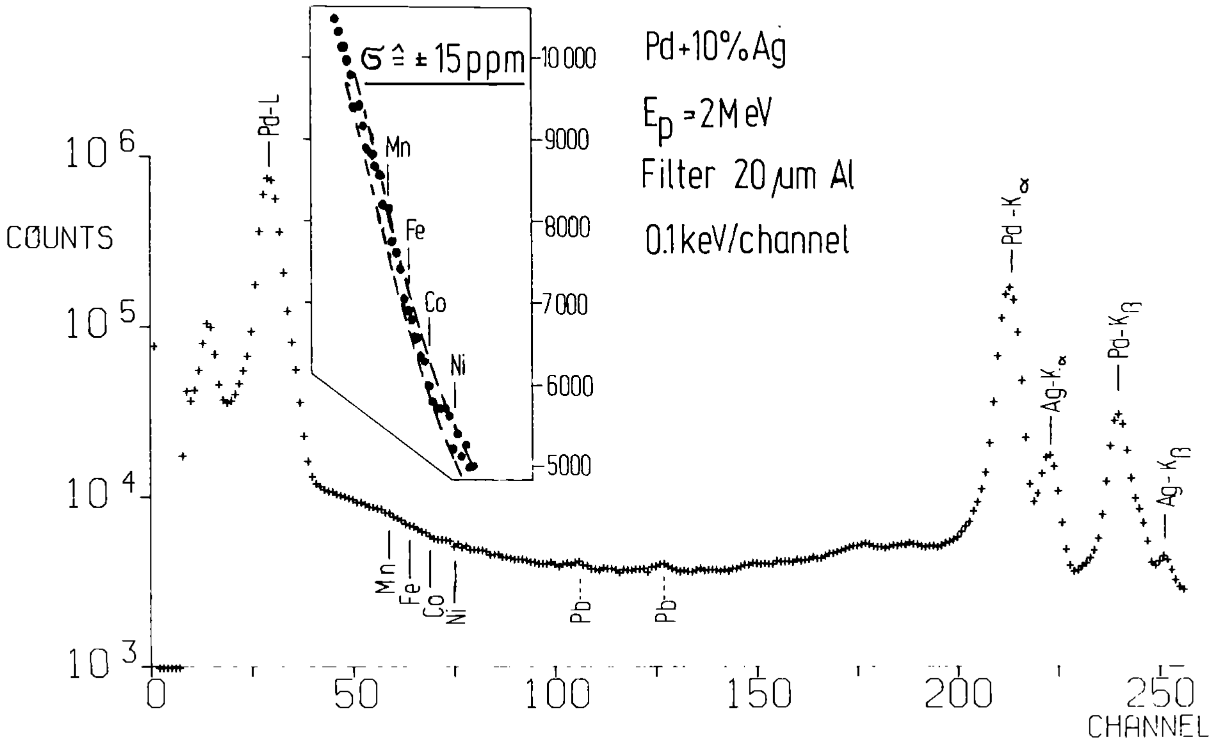

Fig. 2. X-ray spectrum of a Pd + 10 % Ag alloy. The dashed lines in the inset give the statistical uncertainty, which corresponds to 15 ppm of ferromagnetic contaminations.

References

(1) M.S. Ahlberg, Nucl. Instr. Meth. 146 (1977) 465
(2) L.C. Northcliffe and R.F. Schilling, Nucl. Data Tables A7 (1970) 233
(3) S.A.E. Johansson and T.B. Johansson, Nucl. Instr. Meth. 137 (1976) 473
(4) E. Storm and H.I. Israel, Nucl. Data Tables A7 (1970) 565

5.2.3 A Proton Microbeam Deflection System to Scan Target Surfaces*

D. Heck

A system to deflect the proton beam within the Karlsruhe microbeam setup is described. The deflection is achieved by a transverse electrical field generated between parallel electrodes. Their tension is controlled by a pattern generator, thus enabling areal and line scans with a variable number of scan points at variable scan speed. The application is demonstrated at two different examples.

*KfK 2734

6. TECHNICAL DEVELOPMENTS

6.1 CYCLOTRON

6.1.1 Operation Summary of the Karlsruhe Isochronous Cyclotron

F. Schulz and H. Schweickert

During the period of report the machine was in full operation (see Table 1).The total of available beam time of 7507 h is practically the same number as in the last year (1). Looking back to the situation during the yearly christmas shut down this number is really surprising. What happened? As described in the last report (1) we knew, that there was heavy corrosion in the inner conductor of the dees (built in 1971), and it was planned to replace them in the above mentioned shut down

CYCLOTRON OPERATIONAL	WITH INTERNAL ION SOURCES		WITH EXTERNAL ION SOURCES		TOTAL	
FOR EXPERIMENTS	5001 H	76.2 %	1369 H*	72.8 %	6370 H	75.4 %
BEAM DEVELOPMENT, TESTING NEW COMPONENTS, DEVELOPMENTS FOR ISOTOPE PRODUCTION	1023 H	15.5 %	114 H	6.0 %	1137 H	13.4 %
TOTAL TIME OF OPERATION WITH THE BEAM ON TARGETS	6024 H	91.7 %	1483 H	78.8 %	7507 H	88.9 %
SCHEDULED SHUT-DOWN FOR MAINTENANCE, REPAIR AND INSTALLATION	210 H	3.2 %	36 H	2.0 %	246 H	2.9 %
UNSCHEDULED SHUT-DOWN	336 H	5.1 %	361 H	19.2 %	697 H	8.2 %
TOTAL SHIFT TIME	6570 H	100 %	1880 H	100 %	8450 H**	100 %

* POLARIZED DEUTERONS 296 H
$^{6}Li^{3+}$-IONS (156 MEV) 1073 H

** THE REAL TIME OF 8760 H IS ACHIEVED BY ADDING A TOTAL OF 13 DAYS SHUT DOWNS 22.12.78 - 1.1.79; 3 DAYS IN JANUARY 79; 3 DAYS IN APRIL 79

Table 1: Statistics of the cyclotron from July 1978 to June 1979

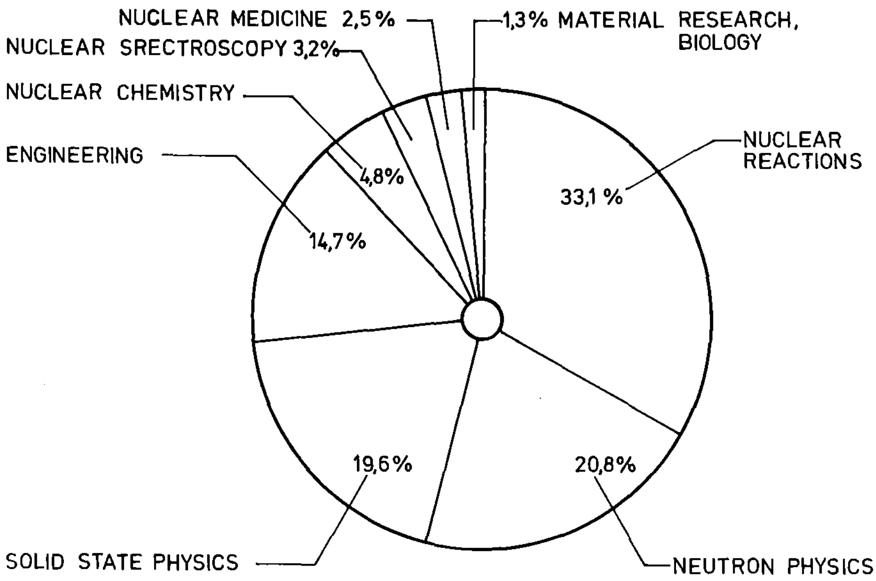

KFK-KARLSRUHE USERS

INSTITUT FÜR KERNPHYSIK	1372 H	21.5 %
INSTITUT FÜR ANGEWANDTE KERNPHYSIK	1371 H	21.5 %
LABOR FÜR ISOTOPENTECHNIK	900 H	14.1 %
INSTITUT FÜR TECHNISCHE PHYSIK	176 H	2.8 %
INSTITUT FÜR RADIOCHEMIE	103 H	1.6 %
INSTITUT FÜR HEISSE CHEMIE	43 H	0.7 %
INSTITUT FÜR GINETIK UND TOXIKOLOGIE VON SPALTSTOFFEN	2 H	0.1 %
	3967 H	62.3 %

EXTERNAL USERS

FREIE UNIVERSITÄT BERLIN	545 H	8.6 %
MAX-PLANCK-INSTITUT FÜR KERNPHYSIK HEIDELBERG	496 H	7.8 %
UNIVERSITÄT ERLANGEN	385 H	6.1 %
TECHNISCHE UNIVERSITÄT MÜNCHEN	375 H	6.0 %
TECHNISCHE HOCHSCHULE DARMSTADT	112 H	1.7 %
KERNFORSCHUNGSANLAGE JÜLICH	112 H	1.7 %
UNIVERSITÄT ULM	77 H	1.2 %
UNIVERSITÄT BONN	64 H	1.0 %
DEUTSCHES KREBSFORSCHUNGSZENTRUM HEIDELBERG	38 H	0.6 %
UNIVERSITÄT MÜNSTER	29 H	0.4 %
UNIVERSITÄT HAMBURG	23 H	0.3 %
UNIVERSITÄT FRANKFURT	8 H	0.1 %
UNIVERSITÄT GÖTTINGEN	8 H	0.1 %
HAHN MEITNER INSTITUT BERLIN	6 H	0.1 %
UNIVERSITÄT STUTTGART	6 H	0.1 %
	2284 H	35.8 %
COMMERCIAL IODINE-123 PRODUCTION	119 H	1.9 %
GRAND TOTAL	6370 H	100 %

Table 2: User statistics from July 1978 to June 1979 and the distribution of the 6591 h experimental time on the different fields of activity.

(see fig. 1). But after the withdrawal of the dee systems we observed that now also the outer conductors (exchanged in 1973) showed heavy localized corrosion on the aluminium cooling vanes. The only possible fast solution to this problem was to cover the cooling vanes with an adhesive (see fig. 1), and it worked. In the meantime we decided to replace successively all aluminium parts of our dee system by copper parts.

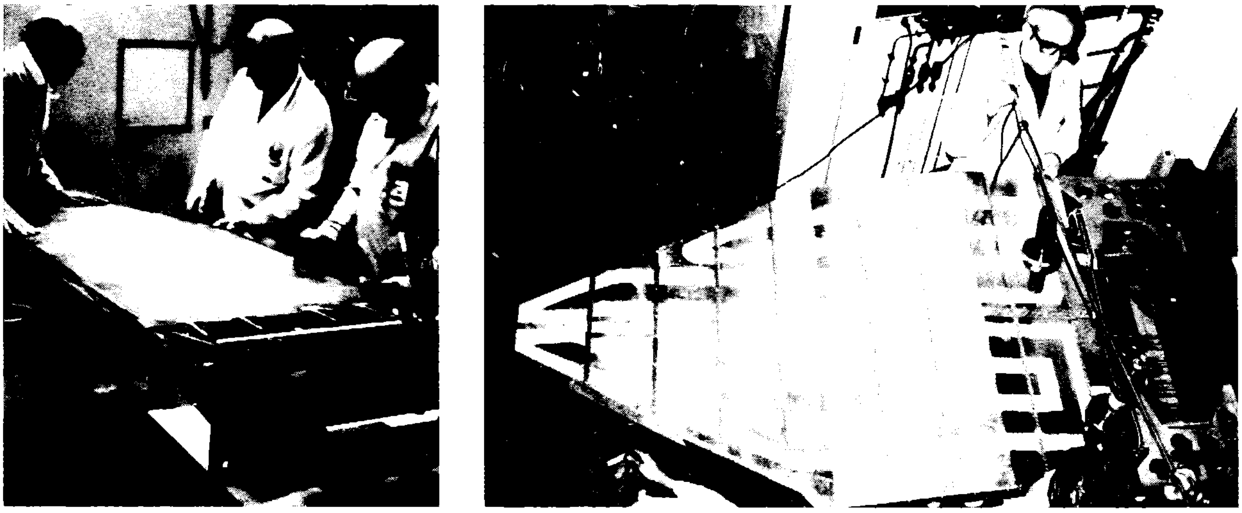

Fig. 1 Pictures taken during the christmas shut down from 22-12-1978 to 1-1-1979.
Left side: Operators exchanging the inner conductor of a dee.
Right side:In order to close the corroded holes the cooling vanes of the outer conductor of the dees were covered with an epoxy resin (UHU-plus).

The axial injection system was used very intensively for $^{6}Li^{3+}$-ions (1073 h) and polarized deuterons (296 h). The total of 1369 h in the period of report means that now more than 60 % of the experiments studying nuclear reactions with charged particles have been performed with this injected ions.

The main technical developments carried out

- Design and first tests for HISKA (Heavy Ion Source Karlsruhe), an ion source of the Electron Cyclotron Resonance (ECR), principle.
- Improvements and extension of the isotope production for medical applications.

- Extension of the computer aided operation of the cyclotron.
- Improvements of the internal pulsing systems

are described in the following contributions.

On the users side (table 2) of our machine there is one noteworthy new tendency. We observed a significant increase in the use of the cyclotron for basic research from 45 % to 55 % of the total experimental time. This is due to the fact that the large neutron time-of-flight spectrometer is now again used for basic nuclear research (in the preceding years it was mainly used for the measurement of nuclear data required for the design of fast breeder reactors). For the year 1980 a further increase in neutron physics is expected because then a new experimental area of about 200 m² especially for neutron work will be finished.

References

(1) F. Schulz and H. Schweickert, Report KfK 2686 (1978) 89.

6.1.2 Improvement of the Internal Pulsing System of the Karlsruhe Isochronous Cyclotron

G. Haushahn, K. Heidenreich, and W. Maier

The pulsing system for the internal ion beam of the cyclotron is now in use for several years (1-3). In 1978 we have changed the old system consisting of a radial and vertical deflecting plate to a system with two vertical deflecting plates (Fig. 1). The reason for this change was the installation of a new axial phase slit on the second turn in the south-east, which proved to be more efficient than the former radial phase slit on the same turn in the north dee. With this new phase slit (radial 6 mm, vertical 4 mm, transparency 10 %) 200 µA of deuterons with a phase width of <1 nsec are now produced routinely.
To find the exact position and form of the deflectors the beam position was determined by perforating a foil with the beam (fig. 2). In order to keep the deflection voltages as low as possible a small distance between the voltage carrying lower plates and the coverplate was choosen (13 mm).
In front of these deflector plates there are two tantalum bars to stop the deflected beam (fig. 3).

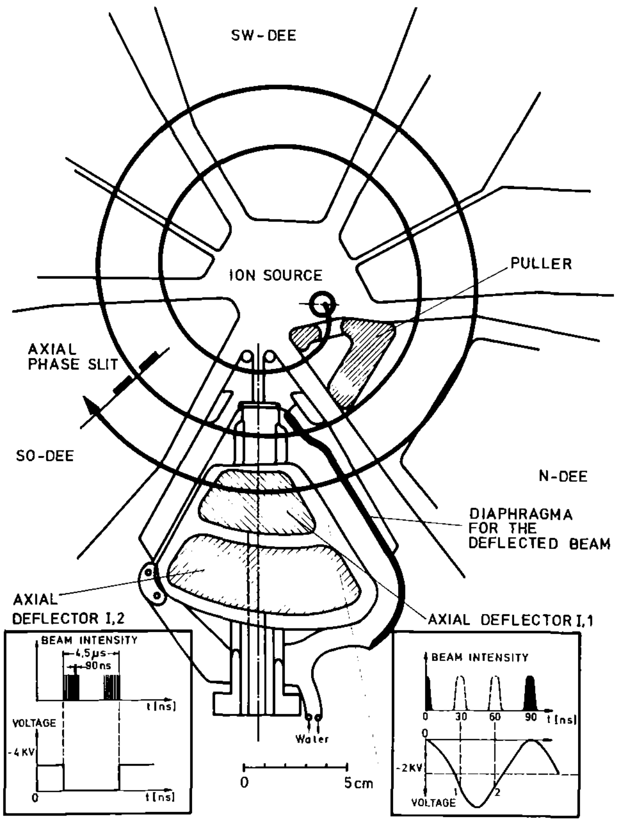

Fig. 1 Principle of the pulsing system and position of the deflector plates (I/1 and I/2) in the north east hill sector.

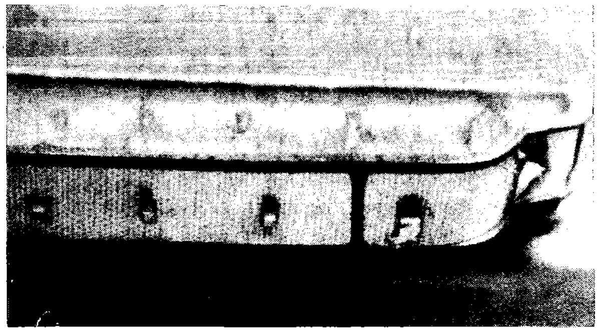

Fig. 2 Determination of the beam position by perforating a foil

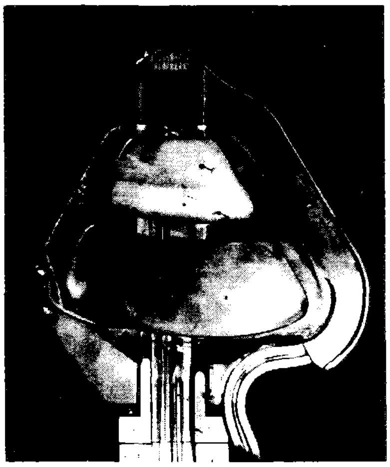

Fig. 3 Internal deflectors I,1 and I,2 with watercooled cover removed

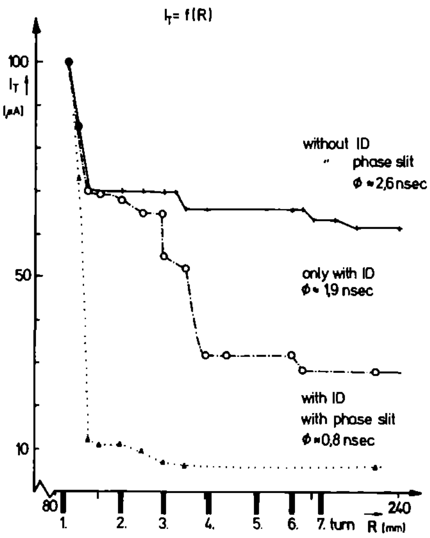

Fig. 4 Ion current as a function of the deflection voltages

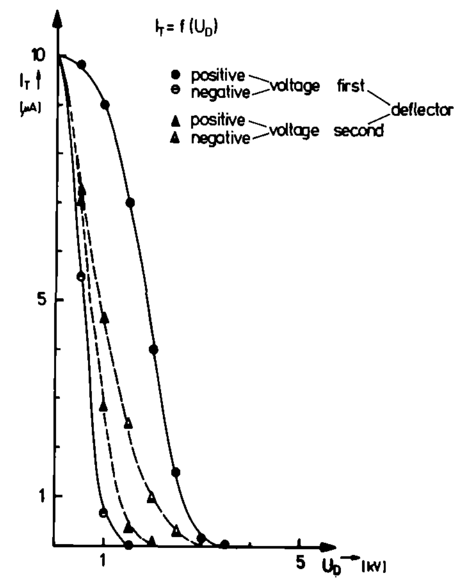

Fig. 5 Ion current as a function of radius, measured with and without internal deflector (ID) and phase slit. With the phase slit the losses at the deflector are below 5 %.

The suppression is excellent in both directions with a voltage of less than 3.5 kV as seen from fig. 4. The pulse and sine wave generators (4) therefore need small powers and sparking does not occur.
Fig. 5 shows the beam losses in the centre of the cyclotron caused by the deflector system and the phase selecting slit together with the associated phase widths.

References

(1) S. Cierjacks, B. Duelli et al., IEEE Trans. Nucl. Sci. NS-13 (1966) 353.

(2) W. Kappel, J. Möllenbeck and H. Schweickert, Proc. of the 6th Cycl. Conf. Vancouver 1972, Americ. Journ. of Phys., New York 1972, p. 368.

(3) S. Cierjacks et al. , KfK 2298 (1976) 18.

(4) E. Luft, Freie Universität Berlin, private communication.
B. Schmalz, IAK, private communication

(5) J. Biber, F. Schulz, private communication.

6.1.3 Status of the Computer Diagnostics and Control for the Karlsruhe Isochronous Cyclotron

W. Kappel, W. Kneis, B. Kögel, G. Leinweber, J. Möllenbeck, and W. Segnitz

The dual computer system (1) for diagnostics and control of the cyclotron consists of a Nova 2/10 with 96 k-Bytes of memory and a Nova 3/12 with 256 k-Bytes of memory. The Nova 3 is now in routine operation since half a year. The access of the CAMAC-branch by both computers enables the programmer to develop or test new programs on one computer without affecting the on-line machine control on the other one. Since the Nova 3 is capable to operate in a foreground/background scheme it is possible to use this computer simultaneously for off-line programming and testing. Due to the extended hardware and software facilities of the Nova 3 the available memory is used in the following way:

Operating system	56 k-Bytes
Foreground user	100 k-Bytes
Background user	100 k-Bytes

The program development under BASIC is concentrated on reorganization, improvement and modification of existing programs.

For the diagnostics and control programs a number of new hardware features have been incorporated. Among them, the lightpen, the general purpose sensor-board and the tuning board for the external beam guiding system are the most important ones concerning the use of the diagnostic system CICERO (2,3). Especially the lightpen in conjunction with the TV-monitors allows easy selection of the programs and helps the operator servicing the system.

Furthermore, due to the overlay techniques on the level of the systems software the memory space useable by the application programs has increased considerably. The available user space in BASIC on the Nova 2 is now approximately 20 k-Bytes for programs and 32 k-Bytes for data. With the space for the BASIC interpreter of about 35 K-Bytes including all additional assembler subroutines (non-overlay), the user space for BASIC programs is approximately 35 k-Bytes and the space for data is 30 k-Bytes for the Nova 3.

In addition to the development of diagnostics programs in BASIC there are programming activities in the language FORTRAN for the following reasons. Contrary to pure diagnostics, monitoring and control should be possible to proceed in parallel, say multitasking, and needs less interactivity with the operator. Since the BASIC used has no multitasking facilities, the BASIC diagnostics programs must be partly rewritten in FORTRAN to form the user dependent monitoring procedures. The modular design in FORTRAN and the higher execution speed of the same algorithms are the main advantages of using FORTRAN. Compared to a fully new FORTRAN program development, the disadvantage to rewrite parts of a known BASIC program is overcompensated by the saving in programming and testing time.

The FORTRAN multitasking system for monitoring and control actually contains the following facilities:

1. Choice of the parameters to be monitored. This is done in groups as in the BASIC status programs. The monitoring is performed by comparison with nominal parameter sets.
2. Choice of the parameters to be controlled by a simple static control routine. This control routine represents the FORTRAN equivalent of the U-mode available in the BASIC program status external beam (2).

3. Choice of monitoring the beam quality parameters such as the horizontal and vertical intensity distributions. The intensity distributions for this purpose are taken by rotating wire systems (3).

4. The execution of the different procedures is performed periodically. A detailed monitoring record can be printed out. The action taken by the individual monitoring tasks in case of unexpected disagreement with nominal values is to call for operator intervention.

References

(1) H. Heinzmann, W. Kappel, W. Kneis, B. Kögel, Ch. Lehmann, J. Möllenbeck, H. Schweickert; Report KfK 2686 (1978) 95.

(2) W. Kappel, W. Karbstein, W. Kneis, J. Möllenbeck, D. Hartwig, G. Schatz, and H. Schweickert, Proc. of the 7th Int. Conf. on Cycl. and Their Applications (Birkhäuser, Basel, 1975) p. 538-541.

(3) W. Kneis, W. Kappel, B. Kögel, Ch. Lehmann, G. Leinweber, J. Möllenbeck, W. Segnitz, and H. Schweickert, Proc. of the 8th Int. Conf. on Cyclotrons and Their Applications, Bloomington, USA, September 1978; IEEE Transactions on Nuclear Science, NS-26, 2366, No. 2 (1979).

6.1.4 Diagnostics, Control, and External Beam Optimization by Computer at the Karlsruhe Cyclotron*

W. Kneis, W. Kappel, B. Kögel, Ch. Lehmann[+], G. Leinweber[++], J. Möllenbeck, W. Segnitz, and H. Schweickert

A variety of new procedures and programs have been added to the existing diagnostic system to include new diagnostic and control hardware and to improve existing software. The CAMAC branch has been completely reorganized using a starlike arrangement. For control purposes an extendable FORTRAN multitasking system has been implemented. Actually it allows the continuous surveillance and static control of a variety of parameters for the external beam guiding system. Dynamic control of some beam properties like beam profiles is in the test phase. First results of the optimization of the external beam are available showing that it is necessary to use similar optimization strategies in on-line optimization as in the case of theoretical simulations.

*Contribution to the 8th International Cyclotron Conf., Bloomington, Indiana, USA, September 1978; IEEE Transactions on Nuclear Science, NS-26, 2366 (1979).
+Fachhochschule für Informatik, Karlsruhe, Germany
++Institut für Angewandte Informatik und formale Beschreibungsverfahren, Universität Karlsruhe, Karlsruhe, Germany

6.1.5 Computer Controlled Beam Diagnostics and Beam Optimization at the Karlsruhe Isochronous Cyclotron*

W. Kneis

The computer-controlled diagnostic and monitoring system at the Karlsruhe Isochronous Cyclotron is described and discussed. The main emphasis is on the automatic beam optimization.

For the external beam guiding system of the Karlsruhe Isochronous Cyclotron two independent procedures for the automatic beam optimization were developed. As basis for these procedures the theoretical knowledge from beam transport calculations and the methods of mathematical parameter optimization with many variables were used. It is very easy to apply both procedures to other external beam guiding systems. The methods of parameter optimization used are formulated in a way not specific to the problem so that they can be applied also to other problems like optimization of the extraction. The automatic optimization of the external beam can be performed either by using beam transport calculations (theoretical optimization) or by using the particle beam itself (experimental optimization).

*KfK-Report 2835, May 1979

6.1.6 Design of the New Trim Coils at the Karlsruhe Isochronous Cyclotron*

V. Bechtold, L. Friedrich, and L. Wiss

After the decision in 1975 to build a new set of trim coils the concept for designing the coils was such that they should give the possibility to accelerate $^{3}He^{2+}$-ions and protons, too, in addition to the e/m = 1/2-particles accessible till now. Numerical calculations were done and led to a trim coil configuration consisting of six coils per plate with summing fields. The desired field strength (1.2 kG) and a small installation height (13.5 mm) led to a high current density (122 A/mm²). The coil conductor is indirectly cooled by 3 mm copper plates which are pasted on each side of the coil which is completely filled with a special epoxy resin. To get a high accuracy in the overall height the coil was pressed during the hardening process in a special set-up which can be heated up to 90°C. The basic design of the coil and first results will be reported.

*Contribution to the 8th International Cyclotron Conf., Bloomington, Indiana, USA, September 1978; IEEE Transactions on Nuclear Science NS-26, 2016 (1979).

6.1.7 The ECR-Source HISKA for the Karlsruhe Isochronous Cyclotron

V. Bechtold, H.P. Ehret, L. Friedrich, J. Möllenbeck, H. Schweickert, and P. Ziegler

In summer 1978 a new heavy ion source development was started at the cyclotron lab. The new source is expected to deliver fully strippled light ions ($^{12}C^{6+}$ up to $^{20}Ne^{10+}$) and is based on the ECR principle which is discussed in detail by several authors (1,2).

The source is a two-stage device. The cold ion plasma, created in the first stage, diffuses slowly into a second stage. There the ionization to higher charge states takes place by collisions with high density electrons heated by microwaves at ECR-frequency confined in the magnetic field of two ring coils and a permanent hexapolar magnet.

The schematic drawing in fig. 1 gives an overview of the present design state of HISKA (Heavy Ion Source Karlsruhe). The vacuum apparatus will be made of stainless steel and consists of three parts. Part one consists of a differential pumping system which makes it feasible to produce the plasma at a pressure of 10^{-2} mbar. The second part of the source is a cylindrical vacuum tank in which the permanent hexapole is inserted. The permanent magnet slabs are fixed on three rings (11) centered in the tank. The cross section of this vacuum chamber is given in fig. 2.

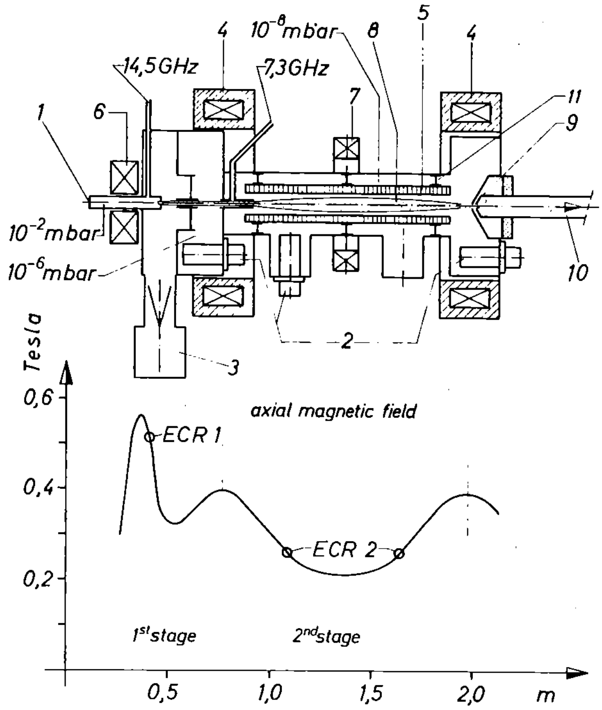

Fig. 1 Cross-section of the present design of HISKÅ. The magnetic field strength along the axis is drawn to scale below. (1) gas inlet; (2) cryo pumps; (3) turbo-pumps, (4) superconduction coils; (5) permanent hexapolar magnet; (6) (7) additional coils; (9) extraction system; (10) beam line to the cyclotron; (11) rings for fixing and centering the magnet slabs.

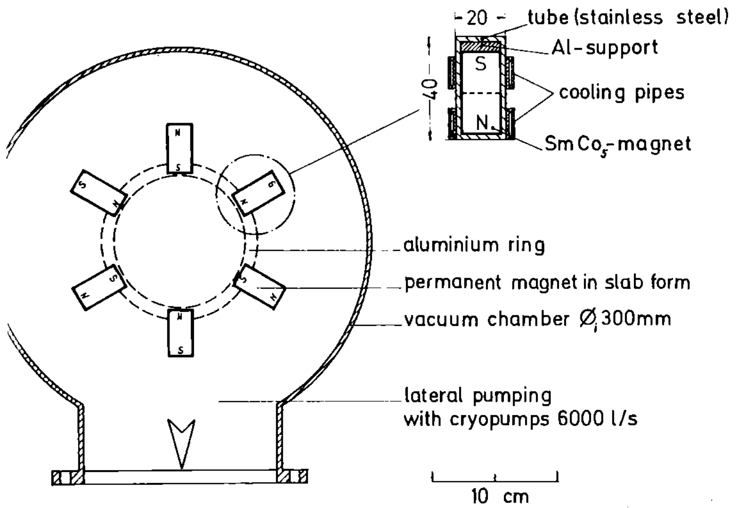

Fig. 2 Cross-section of the permanent hexapolar magnet inserted into the vacuum tube of the second stage. The $SmCo_5$ magnets are inside a rectangular tube. They are cooled since the magnets are destroyed at a temperature above 100°C.

The permanent magnets are fitted into rectangular tubes made of stainless steel which are sealed vacuum tight. The magnets are indirectly cooled because at temperatures in excess of 100°C an irreversible reduction in the magnetic flux density will occur. The arrangement of the magnetic strips in the vacuum chamber allows for lateral pumping. This lateral pumping is done by commercially available cryopumps (2) (> 12000 l/s) giving a pressure of about 10^{-8} mbar. The third part contains the extraction system (9). The whole source has to be operated at a high voltage potential of 10-20 kV.

The longitudinal mirror field will be obtained by two superconducting coils (4) at a distance of 120 cm. For further adjustment of the field gradient in the ECR-zone an additional coil (7) is provided. The field of the first superconducting coil and the field of an additional coil (6) are superimposed giving the ECR-zone (14.5 GHz) in the first stage of the source.

The transmitter for 14.5 GHz (2.5 KW) was delivered and tested in the early summer. The assembly of the microwave equipment is started and will be finished in September 1979.

This source HISKA is expected to be ready for operation at the cyclotron in 1981.

References

(1) H.C. Herbert , K. Wiesemann, GSI meeting on ion sources for highly charged heavy ions (1971), R. Geller, 13th Int. Conf. Ionized Gases, Berlin, G.D.R., September 1977.

6.1.8 Experiments with the Two Stage Source p-HISKA

V. Bechtold, H.P. Ehret, L. Friedrich, J. Möllenbeck, and H. Schweickert

In order to study an alternative first stage for the ECR-source HISKA we built up an experimental arrangement which is shown in fig. 1.

This simple setup consists of an rf-source and a mirror field. The plasma is generated in a magnetic field region where the strength is considerably lower than the maximum field of the mirror device. The plasma density for nitrogen was determined with a single probe measurement at points A and B to investigate the losses of plasma along the magnetic field.

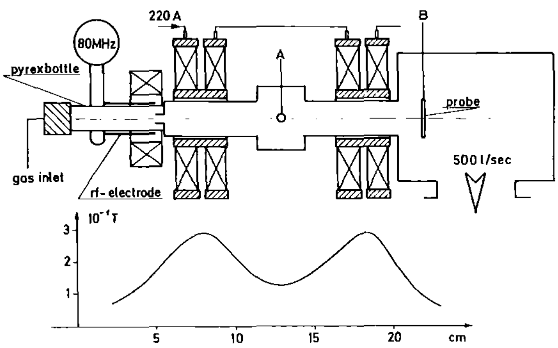

Fig. 1 Cross section of the experimental arrangement to investigate the plasma injection. A simple rf discharge delivers a plasma which is transported through the magnetic mirror to point B. With a single-probe measurement the electron temperature and the plasma density were determined. Plasma diameters and currents were measured at points A and B. The magnetic field distribution along the axis is shown below.

It turned out that a plasma produced in a magnetic field much lower than the peak field of the magnetic mirror can be injected with tolerable loss of plasma density.

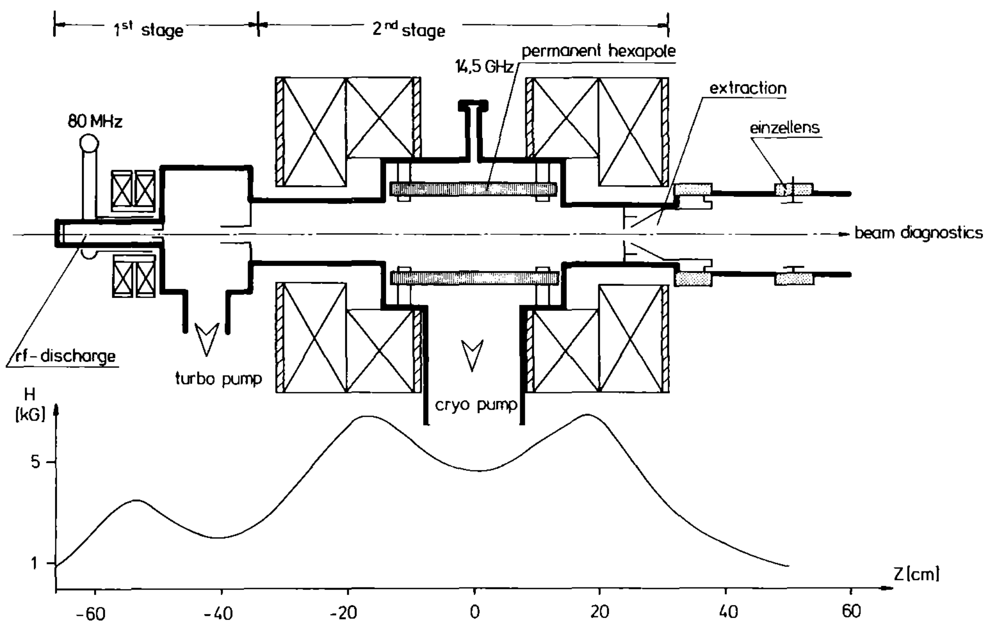

Fig. 2 Arrangement for testing: 1. Plasma injection by different plasma sources e.g. rf-discharge or duoplasmatron. 2. Permanent hexapole in high longitudinal mirror field for 14.5 GHz ECR-frequency.
3. Influence of the radial dependence of the magnetic hexapole field.
4. Efficiency of lateral pumping. 5. Various extraction configurations.

Consequently, we are now building up a small version of a two stage ECR-source, named p-HISKA, using as the first stage a rf-discharge at 80 MHz. The whole set-up is shown in fig. 2. This arrangement is used for testing plasma injection, permanent hexapole, vacuum system, and extraction configurations.

The extraction system was successfully tested. We could extract up to 60 μA Ar^{+}-ions within an emittance of 480 mm mrad at 10 keV after transporting the plasma from the rf discharge to the extraction electrode. The permanent hexapole will be delivered in August so that the assembly of the second stage can be finished. The whole setup of p-HISKA will be ready for the test bench by the end of this year.

6.1.9 An ECR-Type Light Ion Source for the Karlsruhe Isochronous Cyclotron*

V. Bechtold, H.P. Ehret, L. Friedrich, J. Möllenbeck, and H. Schweickert

An ion source for fully stripped light ions ($^{12}C^{6+}$ up to $^{20}Ne^{10+}$) is under development. In the first stage of the source a plasma is created and in the second stage ionization to high charge states takes place. The required high electron energy and density is achieved by microwave heating at the electron cyclotron resonance (ECR) frequency in the magnetic field of two superconducting solenoids and an additional permanent hexapolar magnet. Currents up to several 100 nA at 26 MeV/N are expected in the scattering chamber.

A general description of the setup with details of the magnetic field configuration and vacuum system is given.

*Proceedings of the 1979 Particle Accelerator Conference, San Francisco, USA; IEEE Transact. Nucl. Sci., to be published.

6.1.10 Production of Highest Purity ^{81}Rb for Use in Nuclear Medicine

A. Hanser and B. Feurer

$^{81}Rb(T_{1/2} = 4.6$ h) is of great importance for nuclear medicine. However, the strong contamination by other radioisotopes, especially by ^{82m}Rb ($T_{1/2} = 6.3$ h), which cannot be avoided in the usual production processes limits severely its applicability. Generally, a separation of neighbouring isotopes is performed by use of an electromagnetic mass separation, especially, if small amounts are to be separated. But for the production of radioisotopes for medical purposes such a procedure is not used to our knowledge, presumedly because of the usually low yield and of the expensive apparatus.

The use of an ion source with surface-volume ionization (1) allows electromagnetic mass separation with a very high yield (> 50 %) for a small number of elements. Rubidium is one of them. Radioactive rubidium isotopes can be well produced by irradiation of krypton with deuterons (see also ref. (2)) or protons. Electromagnetic mass separation with surface-volume ionization in connection with the irradiation of a gas target represents a practicable and fast method to produce radioisotopes of highest purity. Procedure and apparatus (see also fig. 1) are described in the previous annual report, where the case of barium isotopes produced by irradiating xenon is considered (3). The procedure results also in a purification from radioisotopes of other elements produced in the deuteron irradiation of krypton. The separated ^{81}Rb can be collected (implanted) in NaCl crystals; 10 mg are sufficient for it. Dissolving the NaCl containing the ^{81}Rb in water should give a solution ready for medical application by injection if pyrogen-free materials are used. If a mass separator is constructed only for this purpose the magnetic mass filter can be kept rather small because of the moderate mass number of Kr and because of the unweighable ion source charge which allows the formation of a very small beam cross section.

Some pilot experiments using the apparatus developed for production of single barium radioisotopes from irradiated xenon (3) have been carried out with a pressure of 6.5 bars in the target (30 mm effective length) and with a deuteron beam of 51 MeV and ≦ 13 µA. They showed that under these conditions a one-hour irradiation with 13 µA beam current leads to 3.5 mCi separated ^{81}Rb in a few milliliters of NaCl-solution two hours after the end of irradiation. The mass separation yield is 70 % so far, little im-

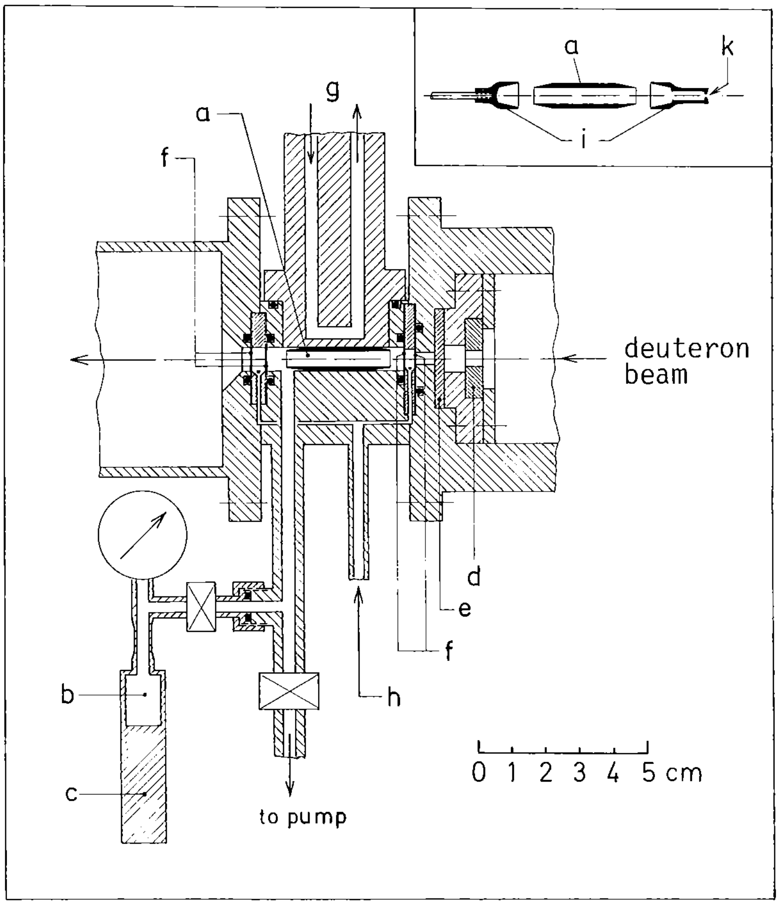

Fig. 1 Krypton gas target for production of ^{81}Rb.
a: tantalum tube surrounding the krypton and collecting the produced rubidium; b: krypton stock vessel in which the gas is stored after irradiation by liquid nitrogen cryopumping; c: cooling finger; d: diaphgragm; e: absorber (not used in this case); f: Havar foil windows; g: cooling water; h: cooling air; i: caps closing the tantalum tube (a) after irradiation, thus forming the oven ampoule of the mass separator ion source; K: ion extraction orifice.

provements should yet be possible. The irradiation yield can be increased presumedly by a factor of 5 at least by higher pressure in the target, somewhat enlarged dimensions, better cooling, and by irradiation with a somewhat higher deuteron energy (∿ 58 MeV which is not possible at the Karlsruhe Isochronous Cyclotron).

Further substantial increase is possible by irradiation of enriched ^{82}Kr with ∿ 35 MeV deuterons or ∿ 30 MeV protons. The techniques of irradiating expensive enriched rare gases without loss of target material have been demonstrated in the case of production of barium isotopes from xenon mentioned above (fig. 1).

References

(1) G. Beyer, E. Herrmann, A. Piotrowski, V.I. Raiko, and H. Tyrroff, Nucl. Instr. and Meth. 96 (1971) 437.

(2) N. Kernert, this report 5.3.2.

(3) B. Feuer and A. Hanser, KfK-Report No. 2686, p. 72 (1978).

6.1.11 A Method for the Production of ^{81}Rb for Medical Applications

G. Bauer, N. Kernert, Ch. Rämer, and H. Schweickert

Since the beginning of 1979 a method for the production of ^{81}Rb (half-life 4.65 h) for the application in nuclear medicine was developed. The reason was the increasing interest in its short-lived daughter ^{81m}Kr (half-life 13 s.) for lung ventilation studies.

At the moment there are several production methods known for this isotope (1-4) which could be used in principle also at our cyclotron. In view of the cost of routine production we have chosen the irradiation of a natural krypton gas target with the 52 MeV deuteron beam. The experimental arrangement is shown in fig. 1.

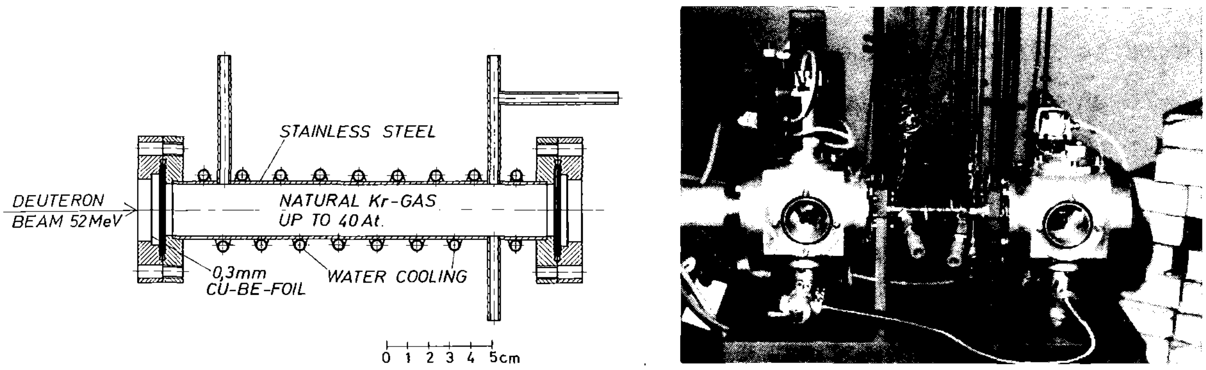

Fig. 1 Schematic view (left side) and photograph of the high pressure Krypton target used for the ^{81}Rb yield measurements. After the irradiation the Krypton gas is released into an exhaust system and the whole target volume is filled with water. It could be proved that in this way more than 90 % of the Rb-activity could be extracted from the target.

Yield measurements as a function of Krypton gas pressure have been performed for ^{81}Rb and ^{82m}Rb and are shown in Fig. 2. It should be mentioned that in order to get reliable values of the ^{81}Rb yield one has to wait at least 2 hours after the end of irradiation for the measurement because of the high yield of ^{81m}Rb which decays with a half life of 30.5 min to the groundstate. The ratio of ^{81m}Rb to ^{81}Rb (EOB) has been measured to be 2.4:1, which is understandable because at our high beam energies the production of the isomeric state with a spin value of 9/2 is preferred

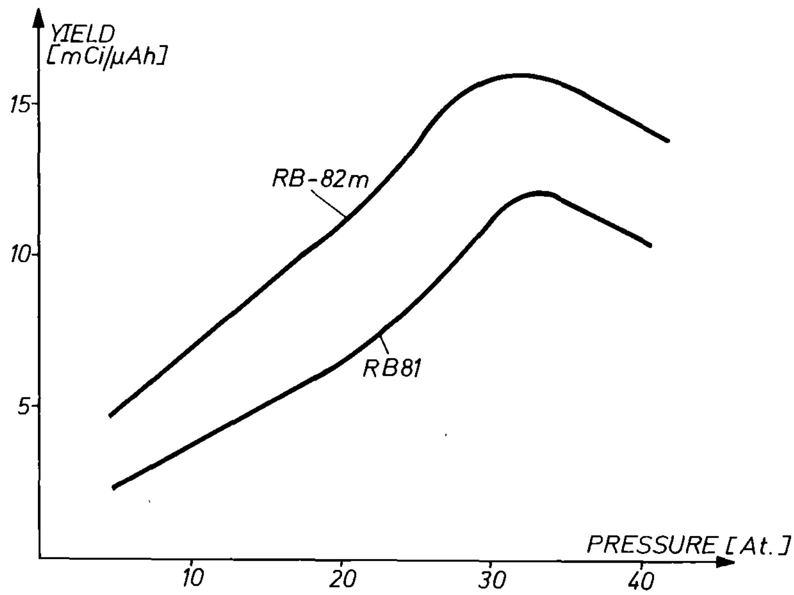

Fig. 2.
Yields for ^{81}R and ^{81m}Rb extrapolated to the end of bombardment time (EOB). For the ^{81}Kr-generator system the ^{82m}Rb impurity is only important for the design of the lead shielding around the generator because it decays to the stable ^{82}Kr.

compared to the ground state (spin 3/2). With an available beam intensity of 15-20 μA we expect from these measurements to obtain a production yield of at least 100 mCi/h of ^{81}Rb. At the moment an automatic transfer system for the produced ^{81}Rb to an ion exchanger in the generator system is built up.

References

(1) L.W. Mayron, A.M. Friedman, J.E. Gindler, Int. Journ. of Appl. Rad. and Isot. 25, 237 (1974).

(2) P.V. Harper, B. Rich, K.A. Lathrop, Dyn. Stud. with Radioisot. in Med., 133 (1974).

(3) J.E. Gindler, M.C. Oselka, A.M. Friedman, Int. Journ. of Appl. RAd. and Isot., 27, 330 (1976).

(4) W. Vaalburg, G. van Herk, A.M. Paans, Journ. of Radioanal. Chem. 35, 31 (1977).

6.1.12 Status of the Iodine-123 Production at the Karlsruhe Isochronous Cyclotron

K.H. Assmus, K. Feißt, R. Schütz, F. Schulz, and H. Schweickert

During the period of report the production method for iodine-123 (1), has been used routinely to prepare 330 batches with a total of 20 Ci of iodine-123 for application at now six hospitals in the southern part of Germany (Fig. 1). Again the production could be performed with a high reliability (95 % of the scheduled delivieries were in time). Since 1979 we have a well working collaboration in production between SIN Würenlingen and Karlsruhe. The shut down periods and times where the production cannot be performed because of a special modification of the machines (for example neutron time-of-flight experiments at Karlsruhe) were correlated at the end of 1978. Therefore iodine-123 is now available in southern part of Germany and Switzerland without intermission.

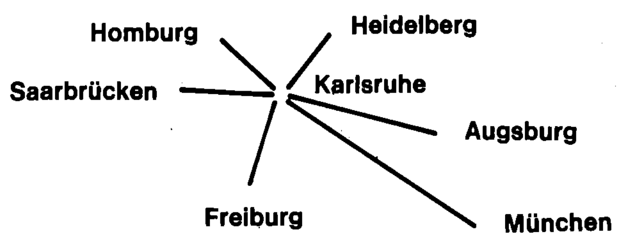

Fig. 1 Geographical situation of the hospitals delivered by iodine-123 from Karlsruhe. The longest way is to Munich (250 km).

There have been two important improvements in the target technology (1):

1. More or less by chance it was found that a small admixture of Al_2O_3 (1 %) to the TeO_2 leads to a much better target material (reduced inhomogeneity, reduced losses of target material per production cycle, reduced losses of iodine-123 to the cooling water during the irradiation). In Fig. 2 an x-ray photograph of the two different targets is shown.

2. In order to improve the cooling of our target the platinum backing (fig. 3) was provided with some checkerboardlike cooling ribs.
   By these methods the maximum beam current for the irradiations could be increased from 10 μA to 14 μA of 26 MeV protons.

Fig.2: X-ray photograph showing the effect of a small admixture of Al_2O_3 to the TeO_2.
Left side: pure TeO_2;
right side: TeO_2 with 1 % Al_2O_3

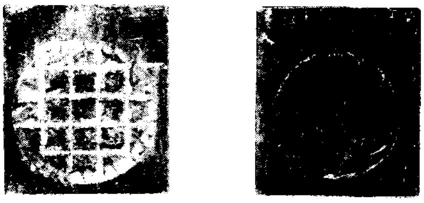

Fig.3: Photograph of the target arrangements in 1978 (right side) and 1979 (left side)
1978: Pure TeO_2
1979: TeO_2 + 1 % Al_2O_3 with checkerboardlike cooling ribs produced by spark erosion

References

(1) K.H. Assmus, K. Jäger, R. Schütz, F. Schulz, H. Schweickert
Routine Production of Iodine-123 at the Karlsruhe Isochronous Cyclotron.
8th International Conf.on Cyclotrons and Their Applications,
Bloomington, Ind., USA, September 18-21, 1978.

6.1.13 Routine Production of Iodine-123 at the Karlsruhe Isochronous Cyclotron*

K.H. Assmus, K. Jäger, R. Schütz, F. Schulz, and H. Schweickert

Routine, twice-weekly, preparation of iodine-123 with the Karlsruhe Isochronous Cyclotron is achieved by bombardment of thin highly enriched $^{124}TeO_2$ (> 96 %) targets with protons of 26 MeV incident energy. This paper describes the experimental details of the targetry and radiochemical procedures that are in routine use at Karlsruhe for production and separation of ^{123}I since two years.

*Contribution to the 8^{th} International Cyclotron Conference, Bloomington, Indiana, USA, September 18-21, 1978, IEEE Transactions on Nuclear Science NS-26, No. 2, 2265 (1979).

6.2 COMPUTER DEVELOPMENT

6.2.1 Code for "Model Independent" Analysis of Optical Potentials for Scattering of (S=0)-Particles

H.J. Gils

An optical model code for analysis of elastic scattering cross sections of spin-zero particles (1) has been extended for a versatile use of different interaction models. The main aim was to include the "model independent" description of the real optical potential in terms of the Fourier-Bessel (FB) method (2). In addition, a single folding procedure including saturation effects and using the FB-description for the target nucleus density distribution (3) is included. Special attention was paid to a user-friendly choice of the different models and for the ability to easily incorporate additional models by a modular technique of subroutines (i.e. replacement of one subroutine by another one having the same name).

Most of the possible options listed in table 1 are self-explaining, where code number 0 means "no" and 1 means "yes". For the options with an asterisk, different choices are possible in particular for the real potential and for the target density

REAL POTENTIAL = 1 Saxon-Woods form (SW)
2 SW squared
3 SW + FB
4 SW squared + FB
5 Gaussian folding
6 Folding with arbitrary interaction

TARGET DENSITY = 1 3-parameter Fermi form (F3) with $\frac{N}{A}\rho_n \equiv \frac{Z}{A}\rho_p \equiv \rho_m$

2 F3; $\frac{N}{A}\rho_n \neq \frac{Z}{A}\rho_p$; ρ_p fixed, ρ_n varied

3 F3 + FB series; $\frac{N}{A}\rho_n \equiv \frac{Z}{A}\rho_p \equiv \rho_m$

4 F3 + FB series; $\frac{N}{A}\rho_n = \frac{Z}{A}\rho_p$; ρ_p fixed; ρ_m varied

For the imaginary potential the Saxon-Woods form and the Saxon-Woods form squared with and without surface term are available and can be combined with an arbitrary real potential. A flexible print-out of the results is possible, and graphs of experimental and theoretical angular distributions ready for publication can be prepared by the included plotter-software.

The CPU-time for calculating one theoretical angular distribution (i.e. one iteration in fit-calculations) depends on the number of radial integration steps, the number of partial waves, and on the number of data points. On the IBM 3033 computer of KfK the code needs about 1.5 sec (CPU) when using a phenomenological potential and 2.3 sec when using a folded potential (with 60 partial waves, a suitable radial step size, and 100 cross sections to be calculated).

Table 1: Standard Options of the Optical Model Code

NUMBER OF INDEPENDENT CALCULATIONS	1
PRINT CPU-TIME	0
CM-DATA	1
PRINT INPUT	1
GRID CALCULATIONS	0
PRINT CROSS SECTIONS	0
PRINT CROSS SECTIONS/RUTHERFORD	0
PRINT SCATTERING AMPLITUDES	0
PRINT POTENTIALS	1
PRINT DENSITIES	0
PRINT VOLUME-INTEGRAL	2
PRINT MOMENTA	2
PRINT ERRORS (ONLY AT FB)	1
PUNCH POTENTIALS OR DENSITIES	0
FOLDED COULOMB POTENTIAL	1
REAL POTENTIAL	4
TARGET DENSITY (FOLDING)	0
IMAGINARY POTENTIAL	1
CONSERVE VOLUME-INTEGRAL	0
KE(20-28) : FREE	
PLOTTER TYPE	0
PLOT CROSS SECTIONS	0
PLOT CS/RUTHERFORD	0
PLOT POTENTIALS	0
PLOT DENSITIES	0
LIN-LOG PLOT	0
KE(35-42) : FREE	

References

(1) G.W. Schweimer, unpublished results.
(2) E. Friedman and C.J. Batty; Phys. Rev. C17 (1978) 34.
(3) E. Friedman, H.J. Gils, H. Rebel, and Z. Majka, Phys. Rev. Lett. 41 (1978) 1220.

6.2.2 User Supplied Functions for the Graphics System GS

J. Buschmann, K. Gogg[+], and W. Olbrich[++]

The "Graphics System" (1), supported by FORTRAN, PL/1, and TSO, allows the interactive handling and external storage of pictures including the definition and manipulation of parts and the generation of "user function objects", "UFOs". These capabilities make GS a powerful tool in the whole field of scientific and technical applications.

The elementary GS-functions, however, generate only standard objects like centered point symbols, characters, strings, vectors and lines. In order to facilitate the use of GS, these primitive objects should be supplemented by more sophisticated objects like filled point symbols, lower case letters, Greek letters, dotted lines, smooth interpolation curves, axes, and grids. The corresponding generator programs should be available not only at UFOs, but also as subroutines which can be nested. Moreover, some shortcomings of GS could be eliminated by introducing, e.g., the possibility of rotating characters and strings, equalization of character appearance and character width on different plotters, transforming the whole pictures including symbols and strings by rotating and scaling, and combining the line thickness attribute and the colour attribute for XYNETICS-Plots. In addition, some service subprograms are desirable for, e.g., conversion of the GS attribute values into numerical values and viceversa, decoding the contents of the GS error variable, determining the number of actual arguments of a subprogram, and free format numeric input as well as "axis" alphameric input for FORTRAN programs running in the TSO foreground. Some of these service programs may be of general interest. Last, universal interactive programs guiding the user without the necessity of knowledge of the special GS syntax seemed to be attractive.

Some of the programs realized so far are summarized in ref. (2) and briefly described in ref. (1), chapter 4. More detailed program descriptions are contained in ref. (3).

+ Abteilung Datenverarbeitung und Instrumentierung, KfK Karlsruhe, Germany
++ Institut für Reaktorentwicklung, KfK Karlsruhe, Germany

References

(1) GS-Manual

(2) J. Buschmann, H. Rebel; unpublished results.

(3) W. Olbrich; unpublished results.

6.2.3 Further Developments of the Data Analysis System on the Experiment Computer NOVA-2 at the Cyclotron

S. Zagromski

For nuclear reaction measurements using the Nova-2 data acquisition system of the cyclotron laboratory some new programs have been developed in order to improve and speed up the evalution and analysis of the measured data:

TSL2: Reading of presorted listmode-data from magnetic tape and calculation of particle identified spectra, based on the Goulding-Method. For addition of the signals of two detectors, two calibration-tables of each 8192 (Energy = f (Channel))-values are used. Energy and particle-identifier windows can be set. Spectra are shown twodimensional on TV-display and particle-identified on x-y-display. The particle-identified spectra are stored together with pre-records, containing the acquisition parameters, to magnetic tape or magnetic disc.

LISTSE: Generation of calibration-tables for the use in Program TSL2 and storage on magnetic disc.

LISTBE: Reading of calibration-tables with each 20 supporting points from pre-records of presorted data and conversion to tables with 8192 values by interpolation.

BLIST: Printing of significant values of normalized pre-records and listing of the number of following data-records, respectively filemarks.

BLESE: Printing of the contents of preselected magnetic tape records of any length and any part of them in different format.

6.2.4 Standard Subroutines for CAMAC

W. Kneis

During the last years the Software Working Group (NSWG) of the U.S. NIM Committee+ and the Subroutines Study Group (ESSG) of the ESONE Committee++ of European Laboratories developed in collaboration a recommended set of subroutines (1) for use with the CAMAC+++ modular instrumentation and interface system of IEEE Standard 583-1975. These subroutines provide a general capability for communication with CAMAC systems. They will be of primary interest for all applications using procedure oriented high-level programming languages such as FORTRAN or ALGOL.

The present approach (1) contains the explicit description of these subroutines for FORTRAN implementations. It is based largely on IML (2) representing the recommendations to communicate with the CAMAC system in a macro-assembler environment. A distinction is made between "declarations" and "actions". "Declarations" are used to specify computer and CAMAC entities. This allows the user to separate the definition or inititation part from the execution part of a program. "Actions" are used to perform the various data movements and condition tests between the computer and the CAMAC system. The subroutines have been grouped into three subsets in order to provide different standard levels of implementation. The lowest level requiring only two subroutines enables most of the facilities which can be found in CAMAC systems. The next higher level contains procedures to provide better handling of LAM's (interrupts from the CAMAC system) and to be independent of the type of CAMAC highway used, e.g. parallel or serial system. In the third level of implementation subroutines are added to use the full capability of the CAMAC system by providing efficient block-transfer modes.

The lowest level of implementation is called level A and contains the primary subroutines which are required in all implementations. The first one, CDREG, allows to define the address of a CAMAC register and provides access to it. The second one, CFSA, is used to perform CAMAC operations or "single action" on the register defined by CDREG. In FORTRAN the reference for these two subroutines is:

CALL CDREG (ext, b, c, n, a)

- ext - integer used as an identifier of an external CAMAC address
- b - integer representing the branch number
- c - integer representing the crate number
- n - integer representing the station number
- a - integer representing the subaddress

CALL CFSA (f, ext, int, q)

- f - integer representing the function code
- ext - see above
- int - represents a CAMAC data word stored in computer memory; the form is not specified
- q - contains information on the CAMAC Q-response.

In developing this standard subroutines for CAMAC by the working groups NSWG and ESSG it was very helpful for the author to check the current results by appropriate test implementations. This gave the possibility to detect errors and inconsistencies in the definition and to see the specific problems of implementation. The CAMAC subroutines for FORTRAN actually used in our institute contain the two primary subroutines CDREG and CFSA. Some subroutines of the next higher level are already available. As far as possible all subroutines strictly remain within the frame of the recommendations for standard subroutines for CAMAC.

+ NIM - National Instrumentation Methods

++ ESONE - European Standards on Nuclear Electronics

+++ CAMAC - Computer Automated Measurement and Control

References
(1) U.S. NIM and ESONE, Subroutines for CAMAC, ESONE(SR/01, CEC, CGR-BCMN, B-2440 Geel, Belgium (1978).
(2) U.S. NIM and ESONE, The Definition of IML - A Language for Use in CAMAC systems, ESONE/IML/01, CEC, CGR-BCMN, B-2440 Geel, Belgium (1976).

6.2.5 New Developments on Data Acquisition and On-line Analysis for the Experiment Computer Nova-2 at the Cyclotron

J. Bialy, B. Kögel, W. Kneis, and W. Segnitz

In the programming language FORTRAN a data acquisition and on-line analysis program has already been developed for high data rates (1). This program has been extended with respect to multitasking and overlay structure. Due to the simple and memory saving facilities of the newly developed load-on-call managers (2) the complete disk and tape file handling and the on-line data analysis could be incorporated into one program.

The file handling has been modified to include the complete information on the stored data. The on-line data analysis comprises the evaluation and storage of a 200 x 200 channel matrix of the list data input (fig. 1). Furthermore, an extension of the user control functions allows a variety of new control possibilities, i.e. it allows to combine an adjusting phase with a calibration phase. This flexible user control is possible by using the newly developed 24-bit sensor board (3) and the lightpen in conjunction with the TV-display.

The control is divided into two groups of functions, the execution control of the program and the control of the visualization of the data gathered. The program flow control functions are solely accessible via sensor board, whereas the display control functions are mainly acces-

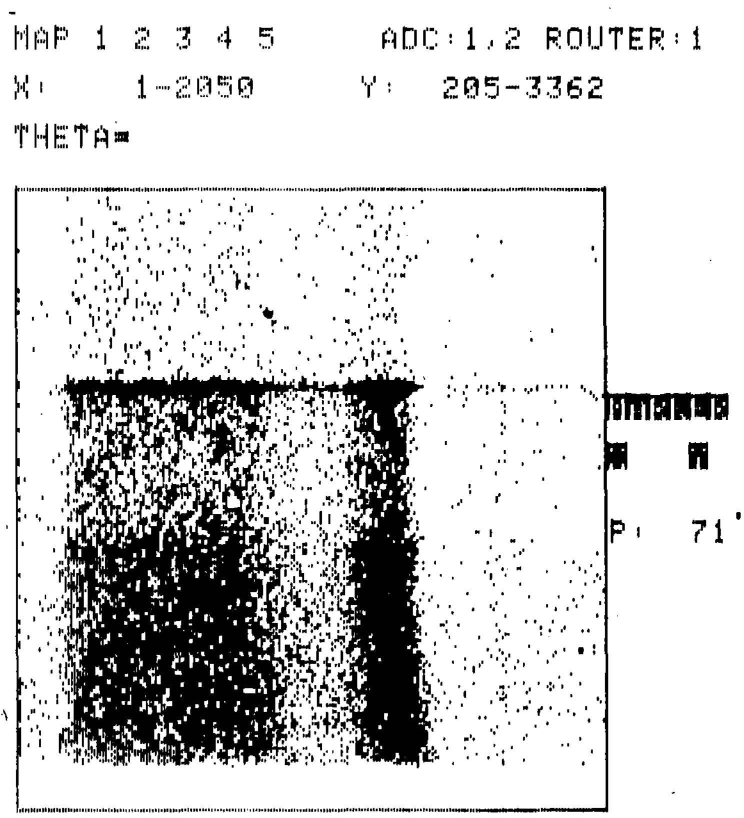

Fig. 1
Two dimensional display of test data in a 200x200 channel matrix.

sible via the appropriate choice by light pen. The latter e.g. includes spectrum definition, fixing of peak windows and choice of the map-display windows.

The execution of tasks with low priority, i.e. printing of the different experiment parameters or finishing the program, is furthermore controlled via the main console. These functions, however, are only available if there is no data acquisition in execution.

References

(1) J. Bialy, B. Kögel, W. Kneis, and W. Segnitz, Report KfK 2686 (1978)120.
(2) H. Sobiesiak, Report KfK 2686 (1978) 136.
(3) W. Kneis, Report KfK 2835.

6.2.6 A New Colour TV-Board

J. Bialy, W. Kneis, B. Kögel, and W. Segnitz

A new colour TV-board has been developed for the Nova 2 and 3 computers of Data General. The purpose of this development was to design a stand-alone interface board with a proper 32 k 16 bit words memory where a region of 12 k words (4 k words for each colour) is reserved for the TV display. An integrated Fairchild's microprocessor of the type 9440 microflame makes possible to use the remaining 20 k words as program memory. The microflame microprocessor was chosen because it offers comparable performance and executes the same instruction sets as the Nova 2 and 3 computers (1).

The communication between the Nova 2 and 3 computer and the microprocessor on the TV board can be ensued by a block transfer on the computer bus. The block transfer between the memories of the two computers can be controlled either by the main processor's or the microprocessor's CPU, whereby that one which is not carrying out the block transfer can write into the register file of the colour TV board at every time.

Reference

(1) Preliminary Data Sheet 9440 Microflame, Fairchild, July 1978.

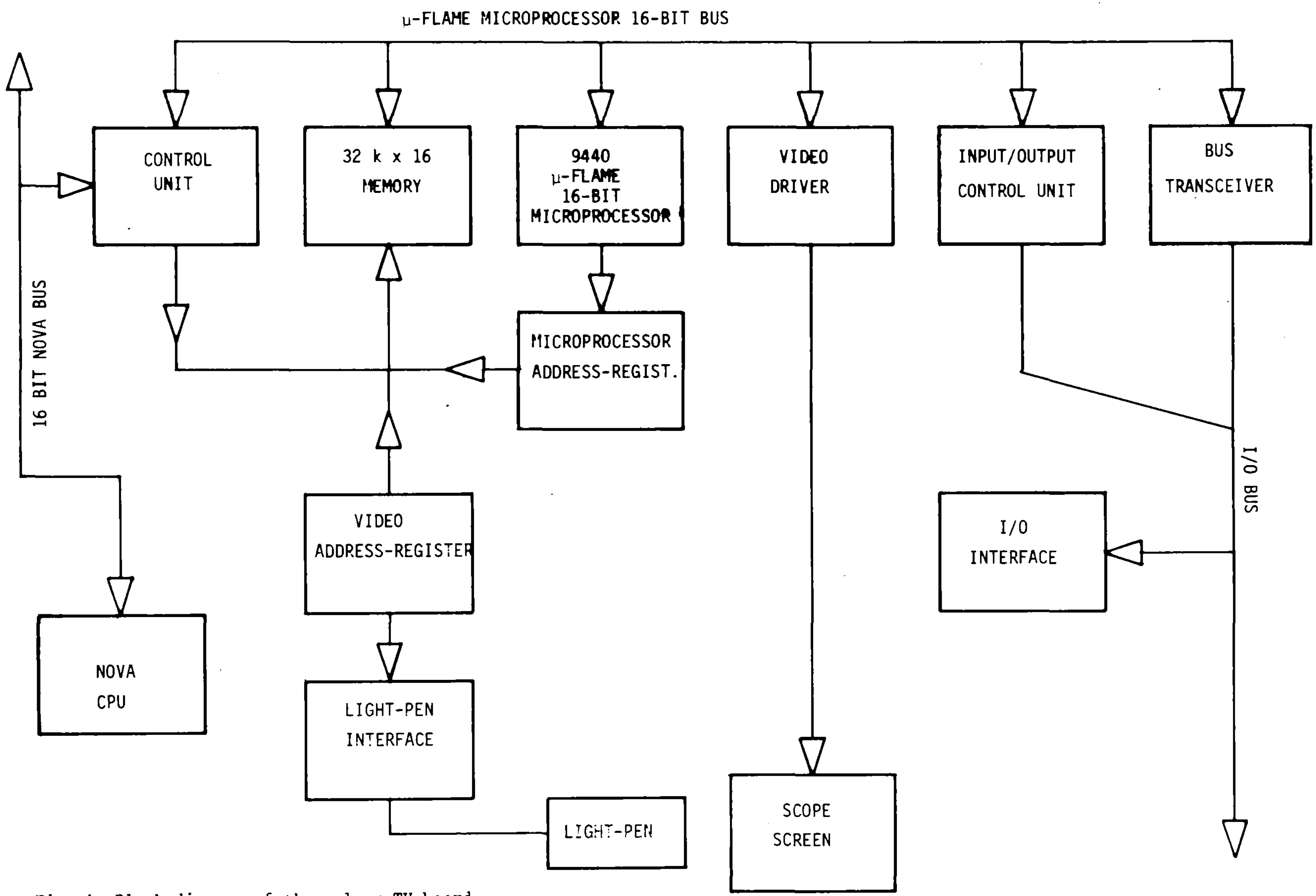

Fig. 1 Block diagram of the colour TV board

6.2.7 The Adaption of Basic System Driver to the NOVA 3 Computer

H. Sobiesiak and G. Ehret

In order to participate from the extended possibilities of mapped NOVA 3 computers over those of NOVA 2's, several extensions have been made in the driver programs. The goal of the work was an absolutely compatible set of routine on all machines from the user's point of view.

Three different problems had to be solved to adapt the existing software to mapped NOVA 3 computers.

a) user device drivers for data channel devices had to be modified to account for the different advers-calculations in mapped systems. Up to now the drivers for the TV-display and the add-one-interface have been modified.

b) The modular memory switch suited for the NOVA 2 had to be simulated via system calls like REMAP.

c) The programming language most frequently used in our institute (BASIC, Ref. 3.6) is, because of its age, available only for unmapped systems or mapped NOVA 820.An easy way has been found to modify the software for the mapped NOVA 820 according to the different instruction set of a mapped NOVA 3.

7. SEMINARS

11.8.78	K. Grotowski, University of Cracow Some Problems of Scattering of Heavy Ions
4.10.78	J.C. Brown, Lawrence Livermore Laboratory Neutron Capture Cross Sections for ^{186}Os and ^{187}Os and the Age of the Universe
6.10.78	F. Hansen, Lawrence Livermore Laboratory Proton and Neutron Induced Reaction Studies in the Lawrence Livermore Laboratory
18.10.78	C. Wagemans, S.C.K. - C.E.N., Mol Fission Fragment Mass and Energy Distributions for Low Energy Neutron Induced Fission of Actinide Isotopes
8.11.78	W. Scheid, Universität Giessen Theorie der Massenfragmentation in Spaltung, Fusion und Schwerionenstreuung
29.11.78	A. Weiguny, Universität Münster Effekte des Pauli-Prinzips in der Schwerionenstreuung
6.12.78	J. Meyer-ter-Vehn, KFA Jülich Die Struktur von Übergangsatomkernen im Gebiet $50 < N,Z < 82$
24.1.79	S.M. Quaim, KFA Jülich Anwendung der Aktivierungstechnik für kurze Halbwertszeiten und kleine Querschnitte
26.1.79	F. Hinterberger, Universität Bonn Untersuchung der T = 3/2 Resonanzen in den Systemen $^{16}O + n$ und $^{12}C + n$
16.5.79	C. Rolfs, Universität Münster Die Reaktion $^{3}He(\alpha,\gamma)^{7}Be$ und das solare Neutrino Problem
23.5.79	G. Reffo, C.N.E.N. Bologna Statistical Model Calculations of Neutron Capture Cross Sections for the S-Process Isotopes of Se, Br and Kr
25.5.79	J. Walker, University of Birmingham Current Research at the Birmingham Radiation Centre

6.6.79	G.B. Plattner, Universität Basel Kernstruktur aus anomaler α-Streuung ?
9.7.79	R.C. Thompson, Clarendon Laboratory Oxford Experimental Studies of Resonance Broadening in Neon
11.7.79	W. Baran, Krupp Forschungslabor Moderne Magnetwerkstoffe und ihre Anwendungen unter besonderer Berücksichtigung der Samarium-Kobalt-5-Materialien
18.7.79	D. Olsen, Oak Ridge National Laboratory A Measurement of the Gamma Ray Production Cross Sections $^{238}U(n,n'\gamma)$ and $^{7}Li(n,n'\gamma)$
26.7.79	P. Kirsten, MPI für Kernphysik, Heidelberg Isotopische Inhomogenitäten in Meteoriten

8. PUBLICATIONS AND CONFERENCE CONTRIBUTIONS

8.1 PUBLICATIONS

Beer, H.

Investigation of the Validity of the Valence Model for Neutron Capture in the Mass Range 40<A<70
J. de Physique 40 (1979) 339

Beer, H., Bröders, C., Bröders, I., Cierjacks, S., Fröhner, F.H., Goel, B., Jahn, H., Käppeler, F., Kiefhaber, E., Krieg, B., Küsters, H., Stein, E., Wiese, H.W., Wisshak, K.

Die kernphysikalische Datenbasis der Berechnung Schneller Reaktoren
KfK-Nachrichten 10 (1978) No. 3/4

Beer, H., Cierjacks, S., Erbe, D., Gupta, S.K.,Hage, W., Hensley, F., Hettinger, H., Hinterberger, F., Käppeler, F., Kari, K., Kazerouni, M.A., Kumpf, S., Leugers, B., Hong, L.D., Rossen, P. von, Schmalz, G., Schouky, I., Voss, F., Wisshak, K.

Nuclear Data Research in the Institut für Angewandte Kernphysik, Kernforschungszentrum Karlsruhe,
In: NEANDC(E)-192 U Vol. 5 (April 78) Progress Report on Nuclear Data Research in the Federal Republic of Germany for the Period April 1, 1977 to March 31, 1978. S. 1-32

Beer, H., Hong, L.D., Käppeler, F.
A Measurement of the Total Neutron Cross Section of Iron-58 in the Energy Range from 7 to 325 keV
Nuclear Science and Engineering 67 (1978) S. 184-89

Beer, H., Spencer,

The Total Neutron Cross Section of Boron-10 between 90 and 420 keV
Nuclear Science and Engineering 70 (1979) S. 98-101

Bekk, K.

Hochauflösende Laserspektroskopie zur Untersuchung von Kernladungsradien und Kernmomenten neutronenarmer Ba-Isotope
Dissertation, Universität Heidelberg; 1979
KfK-2793 (Mai 79)

Bekk, K., Andl, A., Göring, S., Hanser, A., Nowicki, G., Rebel, H., Schatz, G.

Laserspectroscopic Studies of Collective Properties of Neutron Deficient Ba Nuclei
Zeitschrift für Physik A 291 (1979) S. 219-230

Bernhardt, H., Beyrich, W., Brandalise, B., Chakraborty, P.P., Choithramani, S.J., Cördt, W., Deutsch, H., Eberle, H., Gantner E., Iyer, M.R., Koch, L., König, W., Mainka, E., Matussek, P., Michel-Piper, I., Müller, H.G., Ottmar, H., Ruf, H., Schoof, S., Spannagel, G.

Entwicklung und Erprobung von Verfahren und Komponenten im Zusammenhang mit der Kernmaterialüberwachung
In: Projekt Spaltstoffflusskontrolle, Jahresbericht 1977
KfK-2681 (Oktober 78) S. 3/1-3/46

Bork, G., Braun, R., Brückner, Chr., Buttler, R., Eberle, H., Engelhardt, H., Eyrich, W., Flach, S., Hagenberg, W., Küchle, M., Matussek, R., Neuber, J., Ottmar, H., Pfeffer, K.H., Raschendorfer, V., Stein, G.

Implementierung von Überwachungssystemen
In: Projekt Spaltstoffflusskontrolle, Jahresbericht 1977
KfK-2681 (Oktober 78) S. 2/1-2/30

Cierjacks, S., Sowerby, M.G.

Eighth BI-Meeting Report on the Activities of the NEA-NDC
NEANDC 198 'U'

Friedmann, E., Gils, H.J., Rebel, H., Majka, Z.
^{48}Ca-^{40}Ca Radius Difference from Elastic Scattering of 104 MeV α-Particles
Physical Review Letters 41 (1978) S. 1220-24

Haushahn, G., Wisshak, K.,

Annual Report. Teilinstitut Kernphysik (July 1, 1977 - June 30, 1978)
KfK-2686 (Oktober 78)

Heck, D.

A Proton Microbeam Deflection System to Scan Target Surfaces
KfK-2734 (Dezember 78)

Heck, D., Pinston, J.A.

Tables of Gamma-Rays Observed After Thermal Neutron Capture in ^{99}Tc
KfK-2693 (Septmeber 78)

Kari, K.

Messung der Spaltquerschnitte von ^{239}Pu und ^{240}Pu relativ zum Spaltquerschnitt von ^{235}U und Streuquerschnitt H(n,p) in dem Neutronenenergiebereich zwischen 0,5 - 20 MeV
Dissertation, Universität Karlsruhe 1978
KfK-2673 (Juli 78)

Majka, Z., Gils, H.J., Rebel, H.

104 MeV Alpha Particle and 156 MeV ^{6}Li Scattering and the Validity of Refined Folding Model Approaches for Light Complex Projectile Scattering
KfK-2622 (Juli 78)
Z. Physik A 288 (1978) 139-152

Neumann, B., Buschmann, J., Klewe-Nebenius, H., Rebel, H., Gils, H.J.

Transfer of ^{6}Li Break-up Fragments at ^{6}Li Projectile Energies Far Above the Coulomb Barrier
KfK-2819 (Mai 79)

Nowicki, G., Bekk, K., Göring, S., Hanser, A., Rebel, H., Schatz, G.

Nuclear Charge Radii and Nuclear Moments of Neutron Deficient Ba Isotopes from High Resolution Laser Spectroscopy
Physical Review C 18 (1978) S. 2369-2379
KfK-2464 (Juli 78)

Schulz, F., Schütz, R.

Verfahren und Vorrichtung zur Erzeugung des Isotopes Jod-123
DE-OS 27 07 390 (24.8.78) (PLA 77/11)

Schweickert, H.

Produktion von Jod-123 für die Nuklearmedizin am Karlsruher Isochronzyklotron
KfK-Nachrichten 10 (1978) No. 1, S. 19-24

Wisshak, K., Käppeler, F.

Neutron Capture Cross-Section Ratios of Plutonium-240 and Plutonium-242 Versus Gold-197 in the Energy Range from 50 to 250 keV
Nuclear Science and Engineering 69 (1979) H.1, S. 39-46

Wisshak, K., Käppeler, F.

A Measurement of the Subthreshold Neutron Fission Cross-Section of Plutonium-240 in the Energy Range from 10 to 250 keV
Nuclear Science and Engineering 69 (1979) H.1, S. 47-54

8.2 CONFERENCE CONTRIBUTIONS

10. Conference on Atomic Spectroscopy, EGAS München, July 10-14, 1978

Bekk, K., Göring, S., Hanser, A., Nowicki, G., Rebel, H., Schatz, G.

Nuclear Charge Radii and Moments of Neutron Deficient Ba-Isotopes by High Resolution Laser Spectroscopy

International School in Physics, Predeal, September 10-22, 1978

Gils, H.J., Rebel, H., Buschmann, J., Klewe-Nebenius, H., Majka, Z., Neumann, B., Zagromski, S.

Nuclear Reactions Induced by 156 MeV ^{6}Li-Projectiles

Rebel, H.

High Resolution Laser Spectroscopy of Short-Lived Nuclides

Stach, W., Kretschmer, W., Rebel, H.

Nuclear Shape Effects in Scattering of Alpha-Particles and Polarized Deuterons

8. International Conference on Cyclotrons and their Applications, Bloomington, Ind., September 18-21, 1978

Assmus, K.H., Jäger, K., Schütz, R., Schulz, F., Schweickert, H.

Routine Production of Iodine-123 at the Karlsruhe Isochronous Cyclotron

Bechtold, V., Friedrich, L., Wiss, L.

Design of the New Trim Coils at the Karlsruhe Isochronous Cyclotron

Kappel, W., Kneis, W., Kögel, B., Lehmann, Ch., Leinweber, G., Möllenbeck, J., Segnitz, W., Schweickert, H.

Diagnostics, Control and External Beam Optimization by Computer at the Karlsruhe Cyclotron

Workshop on Microscopic Optical Potentials, Hamburg, September 25-27, 1978

Gils, H.J., Friedman, E., Rebel, H., Majka, Z.,

Fourier-Bessel-Analysis of α-Particle Scattering Optical Potentials and Nuclear Matter Densities

Majka, Z., Gils, H.J., Rebel, H.

Validity of Refined Folding Model Approaches for Light Projectile Scattering

International Conference on Neutron Physics and Nuclear Data for Reactors and Other Applied Purposes, Harwell, September 25-29, 1978

Käppeler, F.

Counter Techniques for Highly Radioactive Samples

Kari, K., Cierjacks, S.

Absolute Fast Neutron Fission Cross Sections of ^{239}Pu and ^{240}Pu

Schouky, I., Cierjacks, S.

Measurement of the Differential Elastic Neutron Scattering Cross Section of Fe between 0.5 and 3 MeV

Wisshak, K., Käppeler, F., Hage, W.

Measurement of the Subthresold Fission Cross-Section of ^{240}Pu and ^{241}Am

International Symposium on Nuclear Materials Safeguards, Wien, October 2-6, 1978

Eberle, H., Matussek, P., Ottmar H., Michel-Piper, I., Iyer, M.R., Chakraborty, P.P.

Non-Destructive Elemental and Isotopic Assay of Plutonium and Uranium in Nuclear Materials

NEA Specialists Meeting on the Nuclear Data of Higher Plutonium and Americium Isotopes for Reactor Applications, Brookhaven, November 20-22, 1978

Käppeler, F., Hong, L.D., Beer, H.

Neutron Total Cross Sections of ^{240}Pu and ^{242}Pu in the Energy Range from 10 to 375 keV

Kari, W., Cierjacks, S.

Measurement of the Fast Neutron Fission Cross Section of ^{240}Pu Relative to σ_f of ^{235}U and to the H(n,p) Cross Section

Wisshak, K., Käppeler, F., Hage, W.

Measurements of Fast Neutron Capture and Fission Cross Sections of Minor Actinide Isotopes

Conference on High Resolution Spectroscopy, Faraday Division of the Chemical Society, Bristol, December 19-20, 1978

Baird, P.E.G., Hunt, H.G., Nowicki, G., Roberts, G.J., Sandars, P.G.H., Selby, D.R., Stacey, D.N.

Parity Non-Conversation in Atomic Bismuth: Progress Report

Gross Properties of Nuclei and Nuclear Excitations, International Workshop VII, Hirschegg, January, 15-27, 1979

Andl, A., Bekk, K., Göring, S., Hanser, A., Nowicki, G., Rebel, H., Schatz, G.

Nuclear Charge Radii and Moments of Neutron Deficient Ba Isotopes from High Resolution Laser Spectroscopy

17. International Winter Meeting on Nuclear Physics, Bormio, January, 22-27, 1979

Andl, A., Bekk, K., Göring, S., Hanser, A., Nowicki, G., Rebel, H., Schatz, G.

Nuclear Charge Radii and Moments of Neutron Deficient Ba Isotopes from High Resolution Laser Spectroscopy

Neumann, B., Buschmann, J., Klewe-Nebenius, H., Rebel, H., Gils, H.J.

Transfer of ^{6}Li-Break-up Fragments, a Special Feature of ^{6}Li Induced Reactions Far Above the Coulomb Barrier

Frühjahrstagung DPG, Atomphysik, Berlin 5.-9. März 1979

Bekk, K., Andl, A., Göring, S., Hanser, A., Nowicki, G., Rebel, H., Schatz, G.

Laserspektroskopische Messungen von Isotopieverschiebung und Hyperfeinstruktur neutronenarmer Ba Isotope von A = 126 bis A = 138

Particle Accelerator Conference, San Francisco, March 12-14, 1979

Bechtold, V., Ehret, H.P., Friedrich, L., Möllenbeck, J., Schweickert, H.

An ECR-Type Light Ion Source for the Karlsruhe Isochronous Cyclotron

Spring Meeting DPG, NNV, DFS, ENV-SBP, Nuclear Physics, Gent, March 26-30, 1979

Abdel-Wahab, M.S., Schmidt, F.K., Bechtold, V., Bialy, J., Friedrich, L.

Measurement of the Vector Analyzing Power in d-^{4}He Elastic Scattering at 52 MeV

Andl, A., Bekk, K., Göring, S., Hanser, A., Nowicki, G., Rebel, H., Schatz, G.

Nuclear Charge Radii and Moments of Neutron Deficient Ba Isotopes from High Resolution Laser Spectroscopy

Faust, H., Rebel, H.

Evidence for Hexadecapole Deformation in the Transitional Region of the Rare Earths from the Structure of the h 11/2 Bands

Gils, H.J., Buschmann, J., Rebel, H., Bechtold G., Klewe-Nebenius, H., Neumann, B., Pesl, R., Zagromski, S., Friedman, E.

Radius Differences of ^{40,42,44,48}Ca Investigated by Elastic Scattering of 104 MeV α-Particles

Bechtold, V., Bialy, J., Friedrich, L., Knöpfle, K.T., Mairle, G., Riedesel, H., Schindler, K., Wagner, G.J.

The Investigation of Selected Spectroscopic Problems with 52 MeV Vectorpolarized Neuterons

Bechtold, V., Ehret, H.P., Friedrich, L., Möllenbeck, J., Schweickert, H.

An ECR-Type Light Ion Source for the Karlsruhe Isochronous Cyclotron

Beer, H.

Investigation of the ^{176}Lu Cosmochronometer

Dobiasch, B., Häsner, B., Heeringa, W., Klages, H.O., Schwarz, P., Zeitnitz, B., Erbe, D., Käppeler, F., Leugers, B., Schmalz, G.

Neutron Total Cross Section of the He-Isotopes in the Energy Range from 1 to 40 MeV

Eyrich, W., Hofmann, A., Rebel, H., Rost, H., Scheib, U., Schneider, S., Vogler, F.

A Study of the Isoscalar Giant Resonances in ^{208}Pb and ^{40}Ca

Gils, H.J., Rebel, H.

Fourier-Bessel-Analyses of α-^{12}C and ^{6}Li-^{12}C Optical Potentials at E_{proj} = 26 MeV/N

Leugers, B.

Neutron Capture and Total Cross-Sections of Krypton Isotopes and their Astrophysical Implications

Naqvi, A., Käppeler, F., Müller, R., Gönnenwein, F.

Fragment Mass and Kinetic Energy Distributions in Neutron Induced Fission of ^{237}Np Above the Barrier

Neumann, B., Buschmann, J., Klewe-Nebenius, H., Rebel, H., Gils, H.J.

Experimental Studies of a Particular Reaction Type-Transfer of ^{6}Li-Break-up Fragments

Safeguards and Nuclear Material Management, ESARDA, 1. Symposium, Brussels, April 25-26, 1979

Matussek, P., Allex, H.

A Computerized ^{235}U Enrichment Monitor for Continous Process Control Measurements in a DWR Fuel Fabrication Plant

Ottmar, H., Eberle, H.

Determination of Plutonium Isotopic Composition by Gamma-Spectrometry: Results from Interlaboratory Comparison Measurements Organized by ESARDA

What Do We Know about the Radial Shape of Nuclei in the Ca-Region ?, International Discussion Meeting, Karlsruhe, May 2-4, 1979

Gils, H.J.

Alpha-Particle Scattering from Ca-Nuclei

Majka, Z., Gils, H.J., Rebel, H.

Saturation Effect and Determination of Nuclear Matter Density Distribution from Optical Potential

Physics and Chemistry of Fission, International Symposium, Jülich, May 14-18, 1979

Dickmann, F.

Dynamics of the Late Stages in Fission

Nuclear Physics with Electromagnetic Interactions, International Conference, Mainz, June 5-9, 1979

Schumacher, M., Rullhusen, P., Smend, F., Mückenheim, W., Hanser, A., Börner, H.

QED Effects in Elastic Photon Scattering Investigated at Energies between 1 and 5 MeV

4. International Conference on Laser Spectroscopy, Rottach-Egern, June 11-15, 1979

Schatz, G.

Atomic Beam Laser Spectroscopy of Radioactive Ba Atoms

Nuclear Reaction Mechanism Confernece, Varenna, June 18-22, 1979

Leugers, B., Käppeler, F., Reffo, G., Fabbri, F.

The s-Process Branch at ^{79}Se

16. European Cyclotron Progress Meeting, Villigen, June 21-22, 1979

Bechtold, V., Ehret, H.P., Friedrich, L., Möllenbeck, J., Schweickert, H.

Status of the ECR Source HISKA for the Karlsruhe Cyclotron

Biber, J., Haushahn, G., Heidenreich, K., Maier, W., Schmalz, G., Schulz, F., Schweickert, H.

Improved Fast Neutron Time-of-Flight Spectrometer at the Karlsruhe Isochronous Cyclotron

NEUTRON INTERLAB SEMINAR, PARIS, JUNE 25-27, 1979

Beer, H., Käppeler, F.

Capture Cross Section Measurements at 30 keV Neutron Energy for ^{138}Ba, ^{140}Ce, ^{170}Yb, $^{175,176}Lu$ and ^{184}W to Investigate the ^{176}Lu Cosmochronometer

Käppeler, F.

Activities in the Field of Differential Neutron Data at Various Laboratories in the Federal Republic of Germany

Wisshak, K., Käppeler, F.

Determination of the Capture Width of the 27.7 keV s-Wave Resonance in ^{56}Fe

Wisshak, K., Käppeler, F., Hage, W.

Determination of the Capture and Subthreshold Fission Cross-Section of ^{241}Am in the Energy Range from 10 to 250 keV

8.3 LECTURES AND SEMINARS

Schatz, G.

Laserspektroskopie an radioaktiven Ba-Atomen
Universität Darmstadt, 14. Juli 1978

Kappel, W., Kneis, W., Kögel, B., Lehmann, Ch., Leinweber, G., Möllenbeck, J., Segnitz, W., Schweickert, H.

Strahldiagnose, -überwachung und -kontrolle am Karlsruher Isochronzyklotron
Institut für Kernphysik der KFA Jülich, 25. Oktober 1978

Schatz, G.

Ladungsradien und Kernmomente neutronenarmer Ba-Nuklide aus der hochauflösenden Laser-Spektroskopie
Institut für Angewandte Kernphysik, Univ. Bonn, 9. Januar 1979

Cierjacks, S.

Fast Neutron Fission Cross Section Measurements of Some Uranium and Plutonium Isotopes
CEA (Commissariat a l'energie atomique), Paris, 15. Januar 1979

Rebel, H.

Hochauflösende Laserspektroskopie an kurzlebigen Nukliden
Universität Giessen, 28. Mai 1979

9. PERSONNEL

Head of the Teilinstitut Kernphysik: Prof. Dr. G. Schatz

Scientific and technical staff:

Bechtold, G., Mrs.
Beck, R., Dr.
Beer, H., Dr.
Bekk, K., Dr.
Buschmann, J., Dr.
Cierjacks, S., Dr.
Dickmann, F., Dr.
Dohrmann, H., Ing.
Eberle, H., Ing.
Erbe, D.
Feurer, B.
Gils, H.J., Dr.
Göring, S., Dipl.-Phys.
Hanser, A., Dr.
Heck, D., Dr.
Hong, L.D., Dipl.-Phys.
Käppeler, F., Dr.
Leugers, B., Dipl.-Phys.
Matussek, P., Dipl.-Phys.
Michel-Piper, I., Mrs., Ing.
Nowicki, G., Dr,
Ottmar, H., Dr.
Rebel, H.G., Prof., Dr.
Rupp, G.
Schmalz, G., Dipl.-Ing.
Schmidt, K.A., Dipl.-Phys.
Wisshak, K., Dr.
Zagromski, S., Ing.

Guests and research students:

Almeida, J., Dipl.-Phys.
Andl, A., Dipl.-Phys.
Hensley, F., Dipl.-Phys.
Kazerouni, M.A., Dipl.-Phys.
Majka, Z., Dr.
Naqvi, S.A.A., Dipl. Phys.
Neumann, B., Dipl.-Phys.
Pesl, R., Dipl.-Phys.

Secretarial staff: Mrs. H.M. Friederich, Mrs. E. Maaß

Head of the Cyclotron Laboratory: Dr. H. Schweickert

Scientific and technical staff of the Cyclotron Laboratory:

Assmus, K.H.
Bauer, G.
Bechtold. V., Dr.
Bialy, J., Dipl.-Phys.
Biber, J.
Depta, A.
Ehret, H.P.
Erdel, E.
Feisst, K., Mrs.
Franz, J.
Friedrich, L., Dr.
Günther, O.
Haushahn, G., Dipl.-Phys.
Heidenreich, K.
Hirth, W.
Kappel, W.-R., Ing.
Kauther, P.
Kessel, M.
Kneis, W., Dr.
Kögel, B.
Kuhn, H.
Mangold, D.
Möllenbeck, J., Ing.
Radtke, G., Ing.
Rämer, Ch., Miss, Ing.
Röhrl, E.

Schimpf, P.	Seidel, H.	Walter, A., Miss
Schulz, F., Ing.	Seitz, J.	Wiss, L.
Segnitz, W.	Seufert, H.	

Workshop of the Cyclotron Laboratory:

Bleier, W.	Maier, W.	Schönstein, E.
Ernst, R.	Möck, W.	Schütz, R.
Hauer, W.	Ripp, H.	Würges, J.
Klinger, G.	Schlenker, G.	

Secretarial staff: Mrs. E. Kirste